UNIVERSIDADE DA BEIRA INTERIOR
Engenharia Aeronáutica

Automatic engine and propeller selection for mission and performance optimization

(versão corrigida após defesa)

Nídia Salvador Ribau

Dissertação para obtenção do Grau de Mestre em
Engenharia Aeronáutica
(ciclo de estudos integrado)

Orientador: Prof. Doutor Pedro Vieira Gamboa

Covilhã, fevereiro de 2019

To my dear family.

Acknowledgements

Throughout the course of this dissertation I was blessed to have the help and support of a faithful amount of people, which gave me motivation and focus to finish and deliver an honest work to be proud of.

Without further delays, I would like to thank my advisor, Professor Pedro Vieira Gamboa, for his precise and utmost needed guidance, which enabled me to complete this thesis.

I would also like to thank from the bottom of my heart to my big little family, which always encouraged me to finish my studies and helped me financially in all matters. Without them I could not have completed this stage.

At last, I would like to thank all my dear and close friends which accompanied me through all these college years and with whom I had the pleasure to share astonishing moments.

Resumo

Nesta dissertação, um programa de otimização já existente foi empregue de modo a minimizar a energia consumida durante uma dada missão. Inicialmente, o algoritmo de otimização apenas devolve os valores otimizados das variáveis de projeto referentes à hélice, e nenhum constrangimento no desempenho da missão pode ser imposto. Assim sendo, dois principais objetivos são estipulados nesta tese. Primeiramente, permitir a otimização de variáveis de projeto referentes ao sistema propulsivo, de modo a efetuar a correspondência adequada com a hélice. Por conseguinte, é necessário criar duas bases de dados, uma com as especificações do motor elétrico e outra com as especificações do motor a combustão, de modo a desenvolver modelos empíricos dependentes the certas variáveis de projeto. Estas variáveis são então introduzidas no algoritmo de optimização, para que sejam otimizadas em conjunto com os parametros de projeto da hélice. O segundo objetivo estabelecido é adicionar certos constrangimentos relativos ao desempenho da missão, para possibilitar ao utilizador o constrangimento de certos parâmetros dentro de cada iteração do algoritmo.

Ambas as bases de dados foram criadas com sucesso, obtendo-se assim os modelos empíricos desejados, apesar de estes possuirem um determinado erro associado aos coeficientes das funções. As variáveis de projeto selecionadas para serem introduzidas no algoritmo foram a potência útil máxima e a velocidade do motor máxima no caso dos motores a combustão, e a corrente máxima e a constante de velocidade do motor no caso do motor eléctrico. Os constrangimentos da missão foram também calculados e introduzidos dentro do algoritmo, sendo que este otimiza de acordo com o espaço viável definido pelo utilizador.

O programa atualizado devolve, para um dado conjunto de constrangimentos relativos ao desempenho da missão, a solução do motor que corresponde às variáveis de projeto otimizadas da hélice, e seleciona um motor real a partir da base de dados criada. Os resultados obtidos confirmam que os modelos empiricos dos motores revelam-se bastante pragmáticos, possibilitanto boas correspondências para com a solução ótima, apesar de não serem perfeitas. As variáveis de projeto e a função objetivo convergem corretamente para uma solução estável, de acordo com o espaço viável que o utilizador pode optar por definir.

Palavras-chave

Algoritmo de otimização, modelos empíricos, desempenho da missão, minimização da energia

Abstract

In this dissertation, an already existing optimization software is employed to minimize the total energy consumed at a certain given mission. Initially, the optimization algorithm only returns the optimized design variables for the propeller specifications, and no mission performance constraints can be defined. Hence, on this thesis, two main objectives are stipulated. One is to enable the optimization of certain engine/motor design parameters to match the propeller. Thus it is required to create two data bases, one with the IC engine specifications and another with the electric motor specifications, in order to develop empirical models as functions of certain design variables. These engine design variables are then inputted into the optimization algorithm, to be optimized alongside the propeller parameters. The second objective established is to add certain mission performance constraints, to enable the user to constrain certain parameters inside the algorithm iterations.

Both data bases were successfully created, and all empirical models obtained, although with a certain error associated with the coefficients of the functions. The design variables selected to be introduced in the algorithm, which are the inputs of the empirical models, were rated power and rated engine speed for the IC engine, and maximum allowed current and the motor speed constant for the electric motor. The mission constrains are also calculated and inputted inside the algorithm, optimizing according to the feasible space defined by the user.

The updated software now returns, for a given set of mission constraints, the engine solution which matches the optimized propeller parameters, and selects a real engine from the database created. The results obtained confirmed the practicality of the engine empirical models, given good matches, although not perfect, to the optimum solution reached. The design variables and the objective function are converging correctly to a stabilized solution, according to the feasible space the user may choose to define.

Keywords

Optimization algorithm, empirical models, mission performance, energy minimization

Contents

List of Figures

List of Tables

Acronyms

UAV	Unmanned Aerial Vehicle
IC	Internal Combustion
EC	External Combustion
MBT	Maximum Brake Torque
SI	Spark Ignition
CI	Compression Ignition
CG	Conjugate Gradient
RC	Radio Controlled
FFSQP	FORTRAN Feasible Sequential Quadratic Programming
SQP	Sequential Quadratic Programming

Nomenclature

a	Acceleration	$[\,m/s^2]$
$bsfc_{0_{data}}$	Data Value for Brake Specific Fuel Consumption at $\delta = 1$	$[kg/Ws]$
$bsfc_0$	Brake Specific Fuel Consumption at $\delta = 1$	$[\,kg/W.s\,]$
bp_{min}	Minimum brake power (idle)	$[\,W\,]$
bp_{SL}	Brake Power at Sea Level	$[\,W\,]$
bp	Brake Power	$[\,W\,]$
$bsfc$	Brake Specific Fuel Consumption	$[kg/W.s]$
C_{D_i}	Drag Coefficient Vector	
C_D	Drag Coefficient	
$C_{L_{TO}}$	Takeoff Lift Coefficient	
C_L	Lift Coefficient	
C_{P_0}	Propeller Power Coefficient at Null Advance Ratio	
C_p	Propeller Power Coefficient	
C_t	Propeller Thrust Coefficient	
D_i	Updated Propeller Diameter	$[m]$
$D_{original}$	Original Propeller Diameter	$[m]$
D_{TO}	Takeoff Drag Force	$[N]$
D	Propeller Diameter	$[m]$
D	Drag Force	$[N]$
dT	Temperature Deviation from T_0	$[K]$
E_m	Total Mission Energy	$[J]$
F_R	Resulting Force	$[N]$
fc_0	Maximum Fuel Consumption	$[kg/s]$
fc	Fuel Consumption	$[kg/s]$
g	Gravity acceleration constant	$[\,m/s^2\,]$
h_{RC}	Defined altitude to calculate RC_{max}	$[m]$
h_{turn}	Defined altitude to calculate δ_{turn}	$[m]$
$h_{V_{max}}$	Defined altitude to calculate V_{max}	$[m]$
h_γ	Defined altitude to calculate $\theta\gamma_{max}$	$[m]$
h	Altitude	$[m]$
$I_{max}{}'$	Mission Maximum Required Current	$[A]$
$I_{0_{data}}$	Data Value for No Load Current	$[A]$
$I_{\substack{max \\ data}}$	Data Value for Maximum Current	$[A]$
I_0	No load Current	$[A]$
I_{eff}	Motor Effective Current	$[A]$

I	Input Current	$[A]$
i	Current value	
$i+1$	Following value	
ip	Indicated Power	$[\,W\,]$
J_{max}	Maximum Propeller Advance Ratio	
J	Propeller Advance Ratio	
K_t	Motor Torque Constant	$[\,Nm/A\,]$
Kv	Motor speed constant	$[\,rpm/V\,]$
L	Lift Force	$[N]$
$\dot{m}_f$	Fuel flow per unit of time	$[\,kg/s\,]$
M_{engine_i}	Updated Engine Mass	$[kg]$
M_{prop_i}	Updated Propeller Mass	$[kg]$
$M_{aircraft}$	Aircraft Mass	$[kg]$
M_{data}	Data Value for Engine Mass	$[kg]$
M_{energy}	Energy Mass	$[kg]$
$M_{original\ engines}$	Original Engine Mass	$[kg]$
$M_{original\ prop}$	Original Propeller Mass	$[kg]$
$M_{payload}$	Payload Mass	$[kg]$
$M_{structure}$	Aircraft Structure Mass	$[kg]$
$M_{systems}$	Aircraft Systems Mass	$[kg]$
M	Mass	$[kg]$
$N_{max}{}'$	Mission Maximum Required Engine Speed	$[rpm]$
$N_{\substack{max \\ data}}$	Data Value for Maximum Engine Speed	$[rpm]$
N_{min}	Minimum Engine Speed	$[rpm]$
n_{engine}	Number of engines	
n_{limit}	Limit Load Factor	
n_{load}	Load Factor	
$n_{ultimate}$	Ultimate Load Factor	
N	Rotational Speed	$[\,rpm\,]$
N	Normal Reaction Force	$[N]$
P_{shaft}	Motor Shaft power	$[\,W\,]$
p_i	SQP algorithm step direction	
p	Propeller Blade Pitch	$[m]$
Q	Engine Torque	$[\,Nm\,]$
$RC_{max_{ref}}$	Constraint Reference for Maximum Rate of Climb	$[\,m/s\,]$
$RC_{sc_{min}}$	Constraint Reference for Maximum Rate of Climb at h_{sc}	$[\,m/s\,]$
R_{data}	Data Value for Electric Resistance	$[\Omega]$
R_{gear}	Engine Gear Ratio	

R_U	Battery Internal Resistance	$[\Omega]$
R_Ω	Motor Speed Controller Resistance	$[\Omega]$
R	Motor Resistance	$[\Omega]$
R	Universal Gas Constant	$[J/kg.K]$
R	Friction Force	$[N]$
RC	Rate of Climb	$[m/s]$
rc	Compression Ratio	
$S_{TO_{ref}}$	Constraint Reference for Ground Roll	$[m]$
S_g	Ground Roll	$[m]$
S	Wing Surface Wet Area	$[m^2]$
sfc	Specific Fuel Consumption	$[kg/W.s]$
$T_{R_{min}}$	Minimum Required Thrust	$[N]$
T_0	Standard Sea Level Temperature	$[K]$
T_A	Propeller Available Thrust	$[N]$
T_R	Required Thrust	$[N]$
T_{TO}	Takeoff Thrust	$[N]$
t_{TO}	Takeoff Time	$[s]$
T	Air Temperature	$[K]$
t	Time	$[s]$
U_{eff}	Back Electromotive Voltage	$[V]$
U	Input Voltage	$[V]$
$V_{S_{turn}}$	Stall Speed at Level Turn	$[m/s]$
V^*	Maneuver Speed	$[m/s]$
V_{BC}	Best Rate of Climb Speed	$[m/s]$
V_D	Dive Speed	$[m/s]$
V_H	Horizontal Component of Speed	$[m/s]$
V_S	Stall Speed	$[m/s]$
V_{TO}	Takeoff Speed	$[m/s]$
V_d	Displacement Volume	$[m^3]$
$V_{max_{ref}}$	Constraint Reference for Maximum Allowed Speed	$[m/s]$
V_{max}	Maximum Allowed Speed	$[m/s]$
V_{min}	Minimum Allowed Speed	$[m/s]$
V_{turn}	Air Speed at Level Turn	$[m/s]$
V	Air speed	$[m/s]$
$W_{aircraft_i}$	Updated Aircraft Weight	$[N]$
W_{fuel}	Fuel Weight Consumed	$[N]$
W_{turn}	Aircraft Weight at Level Turn	$[N]$
W	Aircraft Weight	$[N]$
ΔP	Available Excess Power	$[W]$

Δt_i	Mission Segment Duration	$[s]$
Φ	Rolling Angle	[°]
Ω	Motor Speed	$[rpm]$
$\bar{\alpha}$	Coefficient Vector of the C_p Equation	
α_i	SQP algorithm step length	
α	Temperature Increment per Meter Climbed Below Tropopause	$[℃/m]$
$\bar{\beta}$	Coefficient Vector of the η_p Equation	
$\bar{\gamma}$	Coefficient Vector of the J_{max} Equation	
$\gamma_{max_{ref}}$	Maximum Rate of Climb Angle Constraint Reference	[°]
γ_{max}	Maximum Rate of Climb Angle	[°]
γ	Rate of Climb Angle	[°]
δ'_{max}	Mission Required Throttle	
δ_{turn}	Engine Throttle for a Sustained Turn	
δ	Engine Throttle	
$\bar{\varepsilon}$	Coefficient Vector of the C_{p_0} Equation	
ε	SQP Algorithm Tolerance Error	
$\bar{\zeta}$	Coefficient Vector of the η_{max} Equation	
η_{max}	Maximum Propeller Efficiency	
η_p	Propeller Efficiency	
η	Motor Efficiency	
θ_{pitch}	Blade Chord Angle	[°]
μ	Friction Coefficient	
ρ_0	Air density at Sea Level	$[kg/m^3]$
ρ	Air density	$[kg/m^3]$
ω	Angular Velocity	$[\,rad/s\,]$

1 Introduction

1.1 Motivation and Focus

Since the beginning of the 20th century, when the first developments in aeronautical sciences started and the first airplanes were constructed, engineers have always tried to improve aircraft performance, while simultaneously diminishing its energy consumption. This is a continuous aim throughout history, as men possess a need to improve and perfect any scientific work which may be useful, serviceable and profitable to the overall community. Hence aircraft optimization is a highly studied field, in order to find the best design conditions which grant the best possible outcome.

However, optimizing the innumerous design variables which condition an aircraft, no matter its size, proves to be quite challenging. At a designing phase, all parameters interrelate, having oftentimes inverse relations with each another. This means changing a variable at a certain field may considerably affect another at a seemingly unrelated section. Thus optimizing an aircraft design parameters requires a multi-disciplinary optimization which takes into account various different dependent variables.

Aircraft optimization may prove very costly in terms of time and calculations, but in the last decades it has been specially improved, due mostly to the improved technology and resources provided by many different computer simulators. Therefore, after the creation of optimization algorithms which facilitated immensely the analysis between the various relations of the design variables, in relation to a certain objective function, many optimization softwares were created. Still, the majority of them only consider one simple condition, like one fixed altitude, or one single stage of flight. Optimizing an aircraft for an entire operating mission which considers the whole flight envelope is a much more ambitious goal. Mission optimization softwares are not so easily available and are much scarcer. Henceforward, in this dissertation the performance of an aircraft will be optimized for a full operating mission, and for the resulting optimized solution it will be found the most suitable propulsion system in order to minimize the total energy spent.

1.2 Objectives

In this dissertation, an already existing optimization software was used to minimize the total energy consumed during a given mission, for two types of aircraft. One is powered by an electric motor, and another by an internal combustion engine. In order to do so, several modifications and additions must be introduced in the program. It is necessary to match a suitable propulsion system to the optimum solution given by the software. This optimum solution is the minimization of the objective function, i.e. the total mission energy consumed. The software

returns the optimized design values for the propeller diameter and pitch, but only for a fixed engine.

Since the optimization algorithm has the ability to optimize the design variables that the user chooses to input, in this thesis the engine design parameters are added into the algorithm, and the resulting solution returns not only the optimized propeller diameter and pitch, but also the matching engine parameters.

Therefore, it is necessary to create two data bases, one for the electric motor and another for the internal combustion engine, with a large number of data elements. Then, the relations between all the engine/motor variables are analyzed and investigated, in order to obtain certain empirical functions. These functions should return the engine specifications, dependent on one or more parameters. These parameters would then become the design variables, or in other terms the abscissas of the objective function, and all engine related calculations inside each iteration of the algorithm use these empirical models.

When the algorithm displays the final solution for a minimum value of the objective function, it returns also the optimized design specifications of the engine, and so the engine selection will be made from the database created. The engine selected is the one most similar to the empirical models solution.

Another addition to the program is the calculation of the mission performance variables inside the algorithm, to enable the user to constrain mission parameters (such at maximum speed or takeoff runway distance) and still obtain the intended minimum solution inside the feasible space.

To summarize, there are two main objectives in this dissertation, in order to fully improve the intended mission performance:

- To create two data bases, one for electric motors and another for internal combustion engines, in order to obtain the empirical engine models and verify if these models present satisfactory matches with the optimum solution.

- To add the performance mission parameters calculations into the algorithm, to enable the user to constrain them.

All programing procedures are written in FORTRAN.

1.3 Dissertation Layout

This dissertation consists of five main parts. The first chapter introduces the focus and the objective of the thesis, and presents a very brief literature review concerning optimization algorithms and some concepts related to the combustion engine and the electric motor.

The second chapter presents an overview on aircraft performance theory. More precisely, it presents the engine and propeller performance mathematical models which are used in the software calculations, and the mission performance model that is to be added.

The third chapter presents the methodology concerning the programing procedures applied. In further sections, it presents the engine data bases created and the empirical models obtained, which were then introduced in the software. The mission performance calculations and constraints added to the program are also discriminated in the final section of this chapter.

Chapter four presents the optimized results for two different cases of study, by applying the engine empirical models obtained for certain mission restrictions imposed, and verifying if the models present satisfactory matches. One case of study is analyzed for an UAV powered by an electric motor, and the other for an UAV powered by an IC engine.

Chapter five presents the conclusions of the overall analysis and reflects if the objectives defined in section 1.3 were met, presenting some considerations regarding future works.

1.4 Literature Review

The invention of the engine was one of the most noteworthy events in history, as it improved significantly the distance in which vehicles could travel with much less effort and much more convenience. It is defined as a mechanical engineering device that converts one form of energy into a mechanical work, which is used to produce a pushing force called thrust [1]. Thus the engine propels a certain vehicle into movement, whether it is an automobile, a ship, a space shuttle or an aircraft. Among the many types of engines used in aircraft propulsion systems, two of the most relevant are the internal combustion engine and the electric motor.

Since the performance of the engine/motor greatly influences the overall performance of the mission, properly selecting an engine to match a certain airframe and propeller is vital to an optimized flight performance. Hence, and taking advantage of the nowadays technology, many computational optimization procedures and analysis software are used to improve aircraft design. Optimizing the performance of an aircraft requires the use of intense computational simulation, in order to design and analyze complex systems that interact with one another. Consequently, it is essential to understand what optimization is, as well as what types of different computational methods were developed. Thus below follows a brief summary on the state of computational simulation in aircraft design, an overview on different types of optimization algorithms and lastly, some concepts and classifications regarding the IC engine and the electric motor.

1.4.1 Brief summary on modeling and aircraft design optimization

Before 1960, the development and analysis of aerodynamic configurations relied mostly on practical experiments and wind tunnel tests. As technology improved, computational methods provided better numerical algorithms, capable of performing faster and improved optimization techniques. These were, from there on, applied frequently to aircraft design optimization problems [2], since many formed a system too costly in time and means to analyze without the aid of computer processing. Researchers were then allowed to analyze phenomena which were before too complex to model. Exemplifying, in 1978, Raymond M. Hicks and C. A. Szelazek [3] were able to optimize an airfoil through a numerical optimization using a minicomputer. Later in the 1980s, Gary B. Cosentino and Terry L. Holst [4] performed a study on transonic wing configurations, using, likewise, a numerical optimization process through computational simulation. Computational science started then to become indispensable for the aircraft industry, and was greatly developed in multidisciplinary optimization in the 1990s [5].

When defining design optimization problems, it is important to properly select the objective function in order to achieve the intended performance [2]. Many objective functions were analyzed in previous works. For instance, reducing the maximum takeoff weight or reducing the aircraft operation costs [6, 7] are two examples. However, finding an optimization which considers the entire mission and flight envelope is indeed quite difficult. Most optimizations

are performed at a single flight condition. However, aircrafts are designed to fly different missions at different flight circumstances, such as altitude, speed and available throttle. Hence, it is essential to optimize the performance of an aircraft under multiple mission flight conditions. An efficient and accurate mission analysis procedure is therefore required to realistically model aircraft performance in optimization problems [2]. When formulating a problem, it must always be taken into consideration the decision variables, the restrictions and the objective function. Modeling the objective function in order to maximize it or minimize it is very complex, as the many parameters affecting the performance present interdependencies between them. Hence there must always exist a balance between the various input parameters.

1.4.2 Overview on optimization algorithms

Optimization has a wide variety of applications and it is implemented in almost every scientific field, such as engineering, physics, management and design. Such wide scope of uses exists due to the need of obtaining the best solution for a given problem, without wasting more than the necessary means and time [8]. This makes optimization much more important in the resolution of practical procedures rather than theoretical problems [9]. In some fields, the main goal may be to minimize the cost of a certain product, the fuel consumption of a vehicle or the energy consumption of an equipment. Else it may be to maximize a certain characteristic like the profit of a company.

However determining the optimal use of the available resources may prove a challenge, since real world issues present complex parameters and technical features which are too elaborate to formulate. With the amount of complexity and variables that can be presented at a stated problem, computational calculations is almost always required, since it efficiently allows the analysis of more complex and apparently aleatory problems. Therefore in the last century, computational optimization algorithms have been developed and studied [10].

To start the resolution of the problem in study, an optimal procedure is employed, which consists of three main parts: modeling, choosing the algorithm and running the simulator. The representation of the physical problem through a set of mathematical equations, which can be solved numerically, is the modeling phase of the problem. Then, at a later stage, it is necessary to select the appropriate algorithm according to the mathematical characteristics of the problem. Finally, it is selected a computational simulator capable of performing the calculation and evaluating if the proposed solution is optimal and doable [10]. Fig. 1.1 represents a graphical scheme of an optimization procedure.

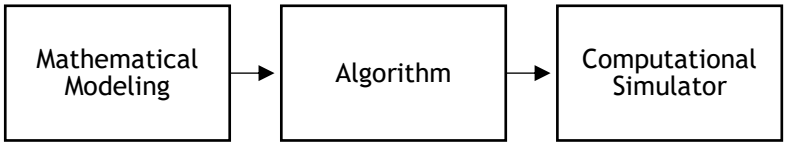

Figure 1.1 Optimization Process

Although there are several ways to formulate the problem in the modeling phase, the most widely method used is to write it as a minimization of a function or a set of functions, subject to a series of constraints [10], in a manner such as

$$Minimize\ f_i(x_n), (i = 1,2, \dots, M)$$

subject to a set of constraints like, for example,

$$h_j(x_n) = 0, (j = 1,2, \dots., J)$$

$$g_k(x_n) \leq 0, (k = 1,2, \dots, K)$$

where $f_i(x)$, $h_j(x)$ and $g_k(x)$ are in general nonlinear functions and the vector $(x_1, x_2, \dots, x_n)$ can be continuous or discrete. The function $f_i(x_n)$ is called the objective or cost function, since it is the property that one wants to optimize. This formulation can also be written as a maximization by simply replacing $f_i(x_n)$, with $-f_i(x_n)$ [10]. Thus, this allows the simplification of a physical attribute, translating it into a set of numerical equations. The objectives, variables and restrictions are all identified in this phase, and the choice of the most effective algorithm depends on a good and efficient mathematical formulation, in order to ensure the minimized solutions are reachable.

There is no universal algorithm which can solve every problem. Finding the correct one depends on the properties of the problem which is being analyzed [11]. Optimization algorithms can be classified in many different ways. They may depend on the type of function (linear, nonlinear, restricted or unrestricted), the type of variables (continuous or discrete), the techniques employed (deterministic, hybrid or stochastic), the solution desired (global or local optimization) or if the minimization relies or not in the knowledge of derivatives/gradients [12].

Gradient-based algorithms, like the Gauss-Newton method [10], use the derivative information. Generally the most common used method, since it requires a lower number of evaluations of the objective function, and therefore a low computational cost. In contrast, gradient-free based algorithms, like the downhill simplex method [13], do not use the derivative information which will result in more complex calculations and a higher number of evaluations. It has a high computational cost and is used when the objective function is non-differentiable or it is trapped in a local minimum.

Deterministic algorithms work in a mechanical and deterministic manner, without any random nature. Downhill simplex and hill climbing methods are good examples of deterministic algorithms that will reach the same final solution if they start with the same initial point.

However, if every time the algorithm runs with the same starting point, it presents a different solution, it means there is some randomness to its nature. Genetic algorithms or hill climbing with random restart are classified as stochastic algorithms, due to the random nature associated with the results they generate [14].

Some problems require mixed-type or hybrid algorithms. They use the combination of deterministic methods and randomness, in order to achieve a more suitable solution to the case in study. Genetic algorithms may be hybridized with others, modifying some components of the other algorithm and creating a more efficient method to the specific problem.

From another perspective, if the algorithm converges to a local optimum and not the global one, it is classified as a local search algorithm. Most deterministic methods like hill climbing are also local methods since it is sometimes very hard to determine the global optimum and instead, given a set of constraints, it is possible to achieve a satisfying local optimum for a particular case. If, however, some random restart is inserted to a hill climbing algorithm, it changes from a local to a global search algorithm. This means randomness is a crucial factor in global search methods [14].

Another important matter to focus upon is the complexity that some objective functions may present. Non-differentiable functions that many times are generated from computer simulations, present a very high computational cost and difficult calculations. In this cases straightforward optimization of the cost function is not advisable. Hence, it is better to construct from the sample data of the objective function a mathematical model which substitutes the original one, being the most similar as possible and yet simpler. This new model is easier to optimize, but it must still be reasonably accurate so it can produce predictions and solutions like the original objective function. This is the surrogate based algorithm [15].

There is indeed a wide variety of optimization methods to be selected, and sometimes a combination of various algorithms may prove the best option. This highly depends on the restrictions and mathematical properties of the problem, so the selection of the algorithm is a significant phase that must be carefully weighted.

1.4.2.1 Conjugated gradient algorithm

Derivative-based or gradient-based algorithms use the information of the function derivatives. Such algorithms should not be selected if there is discontinuity in the objective function, which makes it a non-differentiable equation and therefore, may render such methods unsuitable [10]. The most well-known classical methods are the Newton's Method and Hill-Climbing, while more modern approaches use algorithms like the conjugate gradient (CG) method, the steepest descent method or the Broyden–Fletcher–Goldfarb–Shanno (BFGS) method. Gradient-based algorithms are therefore widely used in discrete modelling [10, 16]. Since detailed

mathematical explanation about gradient-based algorithms is not the main focus of this dissertation, only a brief account on its particulars is presented below.

Gradient based methods use the gradient vector of the objective function, which gives the partial derivatives with respect to each of the independent input parameters. In a sense it is the slope of the tangent line to the objective function at a certain point (design parameter value), and equals zero at the minimum of the objective function, which is the desired solution. The derivative of a function also indicates in which direction the function is decreasing or increasing. A partial derivative (gradient) less than zero corresponds to a decrease in the objective function, and therefore the algorithm has the direction in which to search for the minimum. However, the objective function must be non-convex or else the algorithm would be trapped in a local minimum [17], as illustrated below.

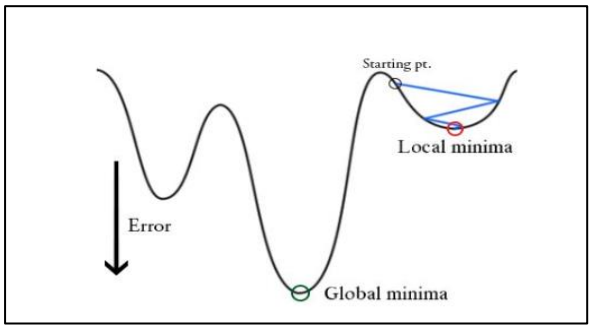

Figure 1.2 Non-convex function [18]

A gradient measures how much the output of a function changes if one changes the inputs in small proportions. The higher the gradient, the higher and steeper the slope is in the objective function. One common analogy used for better understanding is a descent into the bottom of a valley. Exemplifying, the objective is to be exactly at the bottom point of a valley in the minimum amount of time possible, without knowing, however, its exact location. In the starting point of the valley descent, one would start taking larger portions of the steepest path towards the bottom to save time, and as it approaches the final objective it would take less steep paths as it would slowly search and converge into the lowest point. A similar process occurs with gradient based algorithms. The higher the slope value, or in better terms the gradient value, the faster the algorithm learns and progresses rapidly, and as it goes nearer to the intended optimum point it assumes smaller gradient values, as it converges to zero and therefore to the solution. Henceforth, the gradient vector takes a descendent path towards the solution, assuming smaller and smaller values. This phenomenon is also designated as the gradient descent, which can prove to be quite slow in many occasions. Gradient descent is a minimization process that minimizes the Hessian matrix (matrix which contains all gradients) of the objective function, $\nabla f_i(x_n)$. Both the steepest descent method and the conjugate gradient method (CG) present this gradient descent. The difference is that the CG based method in particular, takes into account the history of the gradients to move more directly

towards the optimum. Each descent direction is modified by adding a contribution from the previous direction/gradient [17]. The figures below better clarify the process, assuming an objective function $f(x_1, x_2)$ with the input parameters defined as x_1 and x_2.

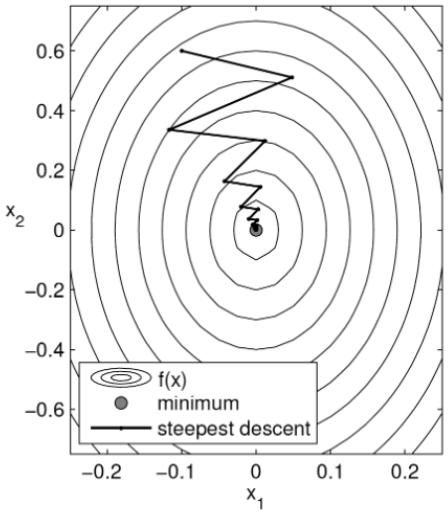

Figure 1.3 2D representantion of the solution path of the steepest descent method [19]

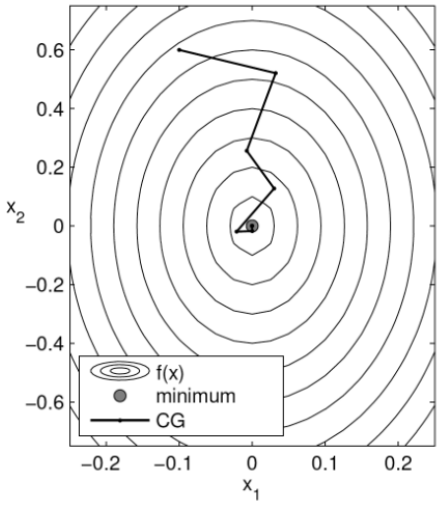

Figure 1.4 2D representation of the solution path of the conjugate gradient method [19]

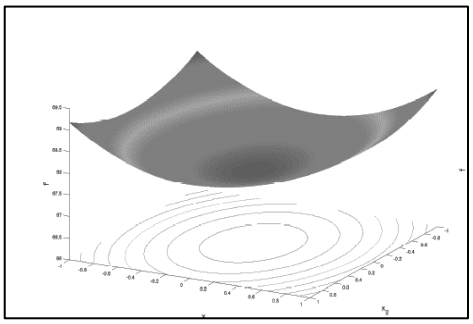

Figure 1.5 3D representation of $f(x_1, x_2)$ [19]

Note that in this graphical representations, the parameter variables x_1 and x_2 are not subjected to any constraints, so there is not a feasible space defined. A feasible space is a space where the independent variables are defined within certain constraints [20]. So if there is no local minimum inside this space, the solution is not feasible and there would not exit a feasible region for the minimum desired. Additionally, if there is indeed a local minimum, the gradients of the function would not converge to zero (since it is not the global minimum) but to the minimum solution possible given the constraints applied. Thus, it is important to consider what constraints values to apply to the problem and avoid design requirement bounds which impose too tight limits for the feasible space.

Defining the feasible space within reasonable values, given the context of the problem to optimize, is an important step towards an efficient optimization process. Conclusively, a

gradient based algorithm will begin at certain starting design values, x_n. Then it searches for the minimum solution desired between a set of x_n values defined by an upper boundary and a lower boundary, i.e. $lower \leq x_n \leq upper$. Lastly, the optimum solution is then achieved if the gradients of the objective function, i.e. $\nabla f_i(x_n)$, converge to zero or to a very small tolerance error, ε, near zero.

1.4.3 Internal combustion engine: concepts and classifications

According to Williard W. Pulkrabek [1], the internal combustion engine is a heat engine that converts chemical energy in a fuel into mechanical energy, usually made available on a rotating output shaft. The chemical energy of the fuel is first converted to thermal energy, by means of a combustion process or oxidation, with air inside the engine. This thermal energy raises the temperature and pressures of the gases within, and the high pressure gas then expands against the mechanical mechanism of the engine. This expansion is converted by the linkages of the engine to a rotating crankshaft. The crankshaft, in turn, is connected to a transmission which transmits the mechanical output work to the desired final use. This will often mean the propulsion of a vehicle, such as automobiles, marine vessels or aircrafts [1].

A combustion that takes place inside the engine system is designated as internal combustion (IC) engine. Early in the latter half of the 1700s, heat engines, including external combustion and internal combustion engines, suffered major developments due to the emerging of the railroad locomotive. However, drastically improvements of the IC engine occurred only in the latter half of the 1800s, with the invention of the automobile. Nowadays, different manufactures have produced many distinct IC engines which vary in size, geometry, style and operating properties. Most IC engines are reciprocating engines, due to the reciprocating motion of the pistons within the cylinders, which can be arranged in many different configurations. Reciprocating engines are classified depending on different criteria. Commonly, they are more frequently differentiated depending on the type of ignition and the type of engine cycle. Thus, they may be classified as spark ignition engines (SI) or as compression ignition engines (CI), and either of these two types may be classified as a two stroke engine or a four stroke engine [21].

In SI engines the combustion process of the fuel, at each cycle, occurs by a spark generated by the spark plug, located in the cylinder head of the engine. The fuel used is gasoline or petrol. The engine works on the basis of a constant volume heat addition cycle, also known as Otto cycle [21]. Not only an ignition system is necessary, but also a carburetor responsible for mixing the air and fuel that is afterwards introduce in the cylinder through the suction stroke.

In CI engines, the combustion process of the fuel starts when the air fuel mixture self-ignites due to high temperature in the combustion chamber, caused by high compression [1]. The fuel used is Diesel, since it has a low self-ignition temperature when compared to gasoline.

Important to note that CI engines are also comparatively heavier due to higher peak pressures required [22]. The engine works therefore on a basis of a constant pressure heat addition cycle, also known as Diesel cycle. CI engines have a fuel injector and a fuel pump, since fuel is injected directly into the combustion chamber at high pressure.

SI and CI engines are either two stroke or four stroke engines. In four stroke engines the thermodynamic cycle, in order to produce one power stroke, is completed in four strokes of the piston or two revolutions of the shaft. In two stroke engines the thermodynamic cycle, in order to produce one power stroke, is completed in two strokes of the piston or one revolution of the shaft [22]. Comparing the two, four stroke engines have higher efficiencies for every cycled completed. Two stroke engines tend to produce more power for the same size of engine, or rather the same amount of power for lighter and more compact engines [22].

1.4.4 Electric motor: concepts and classifications

Electric motors are being used more frequently, since they are overall more reliable and require less maintenance cares. An electric motor is a device which converts electric energy shaft power. They operate according to the interaction between the motors magnetic field and current, in order to generate a rotational force. The link between electricity, magnetism, and movement was originally discovered in 1820 by French physicist André-Marie Ampère (1775–1867) and later developed by Englishmen Michael Faraday (1791–1867). When an electric current flows through a wire, it creates a certain magnetic field. If the wire is near a permanent magnet, which has its own magnetic field, the two fields will interact with each other and create a repelling or attracting motion [23]. The direction of the motion is generated according to Fleming's Left-Hand Rule [24], where the second finger is the direction of the current, the first finger the direction of the magnetic field and the thumb the direction of the force.

Furthermore, if a wire with a current flowing in one direction, is shaped like an U, then theoretically there are two parallel wires running through the magnetic field of the permanent magnet, each with current flowing in different directions. Then according to Fleming's Left-Hand Rule the two wires will move in opposite directions, one upward and the other downward, and a turning motion, i.e. torque, is thus created [23]. However, the coil of wire will not fully rotate. Once the coil reaches the vertical position and flips, the electric current would be flowing in the opposite direction, so the forces would also reverse. Instead of rotating continuously in the same direction it would move back and forward. Thus, for every half a turn of the coil, the direction of the electric current through the windings must be reversed.

To overcome this problem, electric motors present different operating mechanism and are classified according to its component parts, connections and type of current. In brief, electric motors can be classified between AC motors and DC motors. Although AC and DC motors serve the same function of converting electrical energy into mechanical energy, they are powered,

constructed and controlled differently. AC motors use alternating current, i.e. a current which periodically reverses direction, and motor speed is controlled by frequency. DC motors operate with direct current and are powered by ion batteries. Motor speed is controlled by varying the current flux, which can be controlled by altering the applied voltage or resistance (through a speed controller resistance). DC motors are additionally classified as brushed or brushless. A brushed motor uses a direct current together with a component, named a commutator, placed in the ends of the coil, which is responsible for reversing the electric current each time the coil rotates through half a turn. Electric power is delivered from the battery into the commutator through a pair of loose connectors called brushes, and thus the coil will rotate continuously in the same direction. However, the commutator presents many disadvantages. Power losses occur due to friction between the brushes and the commutator, which wears down the soft brush material. This adds to maintenance costs and reduces the motor life expectancy, which justifies a decline in the use of brushed DC motors. With the development of electronics, brushless DC motors without a commutator or brushes were created. Contrarily to a brushed motor, the coils do not rotate and remain static, surrounding a permanent magnet. Since the coils do not move, there is no need for a commutator or brushes. Instead, by changing the direction of the magnetic fields generated by the stationary coils, the permanent magnet rotates. The rotation is controlled by adjusting the magnitude and direction of the current. Hence, brushless DC motors present increased reliability, life expectancy, efficiency and torque to weight ratio, and have therefore become a popular motor choice for RC aircraft models.

2 Performance Models

It is important to note that the electric motor and the internal combustion engines present very different performance parameters and mathematical models. A parameter is a numerical or other measurable factor, forming one of a set that defines a system and sets the conditions of its operation. Therefore the efficiency of the engine is restricted by certain performance parameters. Before analyzing the optimization procedure applied, a brief summary on the mathematical performance models already being used in the software for these two types of engines and for the propeller is presented below. Furthermore, the mission performance model which was added to the software is also latter presented.

2.1 Internal combustion engine performance model

Internal combustion engines typically work within a useful range of speed. The overall performance of the engine depends on the relation between the power developed, the engine rotational speed, N, and the specific fuel consumption at each operating condition, sfc, as depicted in the figure below [22].

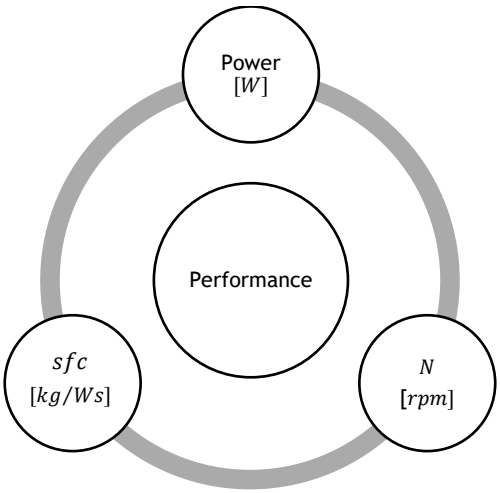

Figure 2.1 Relation between IC engine performance parameters

In general, the energy that flows through the engine can be summarized in two different terms. They are the indicated power, ip, and brake power, bp. ip is the theoretical maximum output power of the engine, available from the expansion of the gases in the cylinders without taking into account any friction losses, heat losses or entropy within the system [22]. bp is the actual power available at the delivery point, the engine crankshaft, after taking into account energy losses in friction, pumping, and various other factors. It presents a more practical interest as it is responsible for delivering the rotational speed to the propeller. Fig. 2.2 presents graphical representation of the energy distribution inside the engine, for a better understanding.

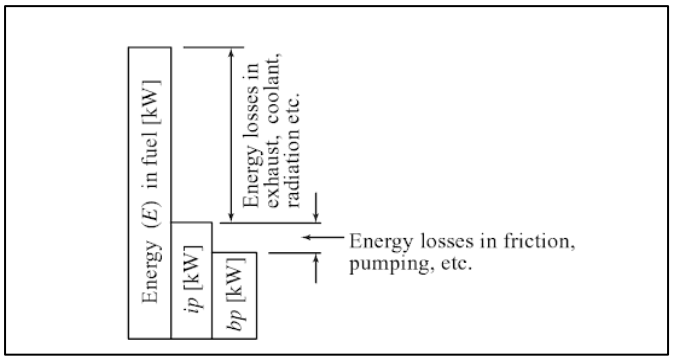

Figure 2.2 Energy Distribution in the IC Engine [22]

Indicated power, ip, is thus a measure of the forces that are developed within the cylinder. The actual useful power delivered by the engine, bp, is a measure of the remaining power that effectively contributes to the rotational force at the shaft. [22].

Engine performance can be better analyzed through a set of operating charts which illustrate the performance of the engine, as well as its rating operating characteristics. Engine rating usually indicates the highest power at which the engine delivers a reasonably good performance. Generally, the factors evaluated are satisfactory economy, reliability, maximum power (bp_{max}) and durability under service conditions [22]. Since IC engines generally operate within a useful range of speed, N, there are various operating circumstances which should be considered, namely if it is a maximum or normal rated operation, or if it is a full load operation. Commonly normal rated power designates the highest power an engine is allowed to develop during continuous operation, and it is achieved at a wide-open throttle regime. As for maximum rated power, it is defined as the highest power an engine is allowed to develop during specific short periods of time, like the takeoff segment. Fig. 2.3 represents the dependence of brake power, bp, torque, Q, and $bsfc$ as a function of engine speed, N.

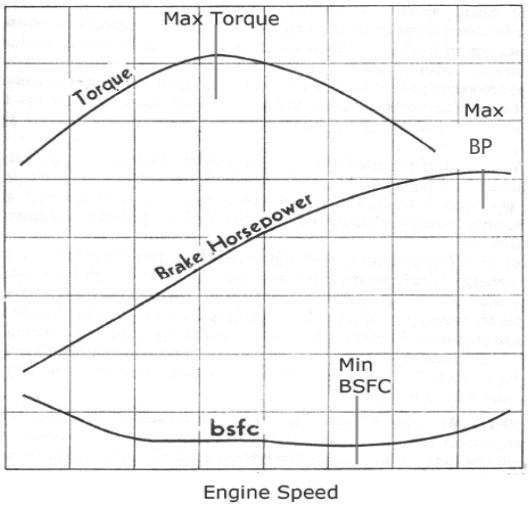

Figure 2.3 Torque, brake power and brake specific fuel consumption as a function of engine speed [25]

Within the useful range of speed, power has a maximum usable value. The ratio between power available at a certain speed, N, to the maximum output power at this same speed is called load, bp/bp_{max}, or in other terms, engine throttle, δ.

Another operating circumstance also frequently considered is the mission duration. For long periods of operation, the ideal parameter to optimize, instead of the bp and Q, would be the engine brake specific fuel consumption, $bsfc$. This would provide a greater operation time for the aircraft, since energy consumptions would be minimized. Analyzing Fig. 2.3, $bsfc$ initially decreases with engine speed, N, since at this stage there is a shorter time period for heat losses to occur. Hence the fuel energy is more efficiently harnessed. However, for a higher N, $bsfc$ again increases due to the increase in friction losses associated with high speeds.

The available engine throttle, δ, also compromises $bsfc$. The wider open the engine throttle is, the greater becomes the brake power available and thus $bsfc$ will decrease, due to pumping losses for SI engines and constant friction losses that subtract from the indicated power, since $isfc$ remains fairly constant. This decrease in $bsfc$ is illustrated in Fig. 2.4 [26].

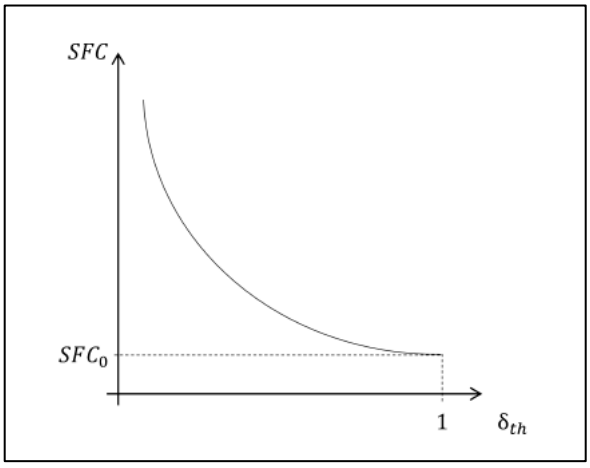

Figure 2.4 Brake specific fuel consumption as a function of engine throttle [26]

All these graphical representations of engine performance are generally obtained through two different methods, whether by using experimental results obtained from engine experimental tests, or by analytical calculation based on theoretical data. Ultimately, the internal combustion engine performance can be described through a mathematical model. The equations used in this dissertation are thus presented below.

bp is formulated through an approximated model translated by the linear regression illustrated in Fig. 2.5.

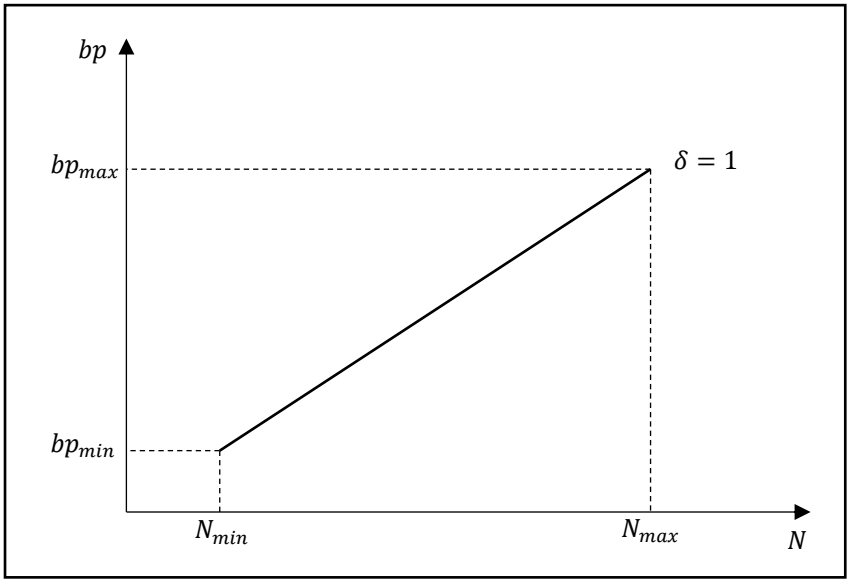

Figure 2.5 Approximated linear regression for bp, at sea level and full load

Fig. 2.5 illustrates brake power at sea level conditions for wide-open throttle, $\delta = 1$. Thus, the resulting linear equation for the presented model is given by

$$bp(N)\ [W] = bp_{min} + \left(\frac{bp_{max} - bp_{min}}{N_{max} - N_{min}}\right) \times (N - N_{min}) \quad (2.1)$$

and since brake power is also a function of the available throttle, δ, then at sea level bp is formulated as

$$bp_{SL}(N, \delta)\ [W] = \delta \times\ bp(N) \quad (2.2)$$

Altitude effects should also be taken into consideration. Mass flow into the engine is affected by the outside air density, which varies significantly with altitude. Thus, equation 2.4 accounts for the air density effects upon brake power according to reference [27], and is given by

$$bp\ (N, \delta, \rho) = bp_{SL}(N, \delta) \times \left(\frac{\rho}{\rho_0} - \frac{1 - \rho/\rho_0}{7.55}\right) \quad (2.3)$$

where ρ is the air density in $[kg/m^3]$ and ρ_0 the air density at sea level.

After calculating brake power, bp, it is possible to obtain the available torque at the rotational shaft, Q, knowing that

$$Q(N, \delta, \rho)\ [Nm] = \frac{bp(N, \delta, \rho)}{\omega} \quad (2.4)$$

where ω is the angular velocity in $[rad/s]$, formulated as

$$\omega\ [rad/s] = \frac{2\pi N}{60} \quad (2.5)$$

Hence,

$$Q(N, \delta, \rho)\ [Nm] = \frac{60bp(N, \delta, \rho)}{2\pi N} \quad (2.6)$$

Another significant parameter when evaluating the performance of an IC engine is the specific fuel consumption, sfc. It represents the mass of fuel that is consumed by an engine per unit of time, $\dot{m}_f$, in order to produce 1 W of power. In other words, is the fuel flow rate per unit of power output [22], and it measures how efficiently an engine is using the fuel supplied to produce a certain amount of work. The specific fuel consumption related to brake power, $bsfc$, is given by

$$bsfc\ \left[{}^{kg}/_{W.s}\right] = \frac{fuel\ consumption\ per\ unit\ time}{brake\ power} = \frac{\dot{m}_f}{bp} \quad (2.7)$$

In this dissertation, $bsfc$ was represented as a function of the brake specific fuel consumption at full throttle, $bsfc_0$, and engine throttle, δ, presented as

$$bsfc(\delta)\ \left[{}^{kg}/_{W.s}\right] = \frac{bsfc_0}{\delta^{0.35}} \quad (2.8)$$

The fuel consumption per unit of time, fc, is then obtained through

$$fc(\delta)\ \left[{}^{kg}/_{s}\right] = bsfc(\delta) \times bp(N, \delta, \rho) \quad (2.9)$$

2.2 Electric motor performance model

Electric motors can be characterized by several parameters, which determine how efficiency, torque and power vary with motor current, I, and motor speed, N. The motor absorbs the electric energy generated from the power supply, transforming it into mechanical energy available at the end of the shaft [28]. Figure 2.6 is a graphical depiction of the overall energy losses, resultant from this conversion process. Motor losses are the difference between the input and output power. Once the motor efficiency is determined and the input power is known, it is possible to calculate the output power and proceed to the propeller matching process.

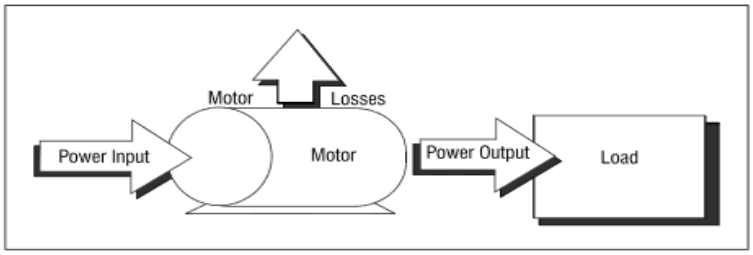

Figure 2.6 Depiction of motor losses [29]

Given the low specific energy of batteries compared with fuel, maximizing the engine efficiency becomes a priority. However, contrarily to an IC engine, an electric motor torque and speed are inversely proportional, which highly affects efficiency. Hence the inter-relations between the inputs parameters considerably affect the final performance, and are represented in Fig. 2.7 below.

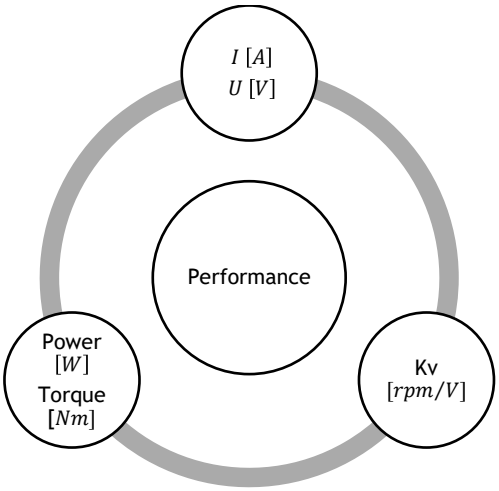

Figure 2.7 Relation between the electric motor performance parameters

The electric motor performance parameters, specified usually by the manufacturer, define the motor operating properties. All parameters can be formulated in a mathematical set of equations [24].

Kv is the motor speed constant, in rpm/V, which represents the number of revolutions per minute that the motor can perform, when one volt is applied and no load is attached to the motor. K_t is the motor torque constant that represents the ratio of torque output to current input, measured in Nm/A . The electric current is defined as I and measured in ampere, A. I_0 is the no load current, which is an electric current that also occurs when there is no load attached to the motor. In other words, it is the amount of initial current required to overcome the internal friction. R is the electrical resistance, defined as the opposition of the material to

the flow of electric current, in Ω (ohm). U_{eff} is the back electromotive voltage, measured in volts, V, that remains after energy losses occur due to internal resistance and friction. The relationship between these motor performance parameters can be illustrated through operating charts.

Considering motor speed (in revolutions per second) as a reference parameter, it is possible to evaluate the evolution of one particular output variable. In order to effectively design an electric motor, it is essential to understand the variation of torque, Q_m, and output power, P_{eff}, in relation to angular speed. Power is the rate at which the work is applied to the output shaft. In other words, it represents how fast the shaft can spin. Torque is, in another perspective, a measure of the force a motor can develop in order to rotate the shaft. In an electric motor, with fixed operating voltage, torque is inversely proportional to motor speed, as it is illustrated in Fig. 2.8.

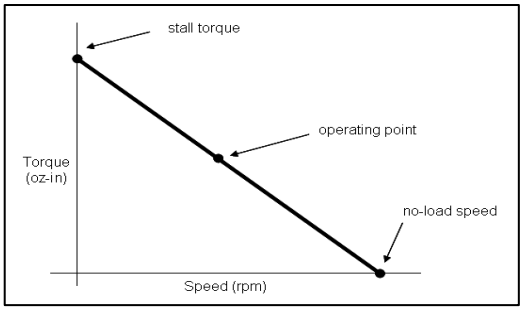

Figure 2.8 Relation between motor torque and speed [30]

Therefore and considering equation 2.21, the output power will be affected and thus there must be a compromise between Q_m and P_{eff}. Illustrated in the chart is the stall torque and the no load speed. For a fixed input voltage from a battery, the motor speed reduces as it is loaded. When there is no load on the shaft, the motor runs at its maximum rated speed, with no torque available. Further up the curve, the torque and speed of the motor correspond to a certain operating load. As the load changes, so does the operating point along the curve. When the shaft is fully loaded and not allowed to move, the speed is equal to zero and the motor is producing its stall torque, the maximum output torque.

At this stage, the current drawn out of the battery is at its maximum, since torque and current present a proportional relation, represented in Fig.2.9. Motors should be operated at stall only for brief periods of time to save battery energy and to preserve the motor from overheating.

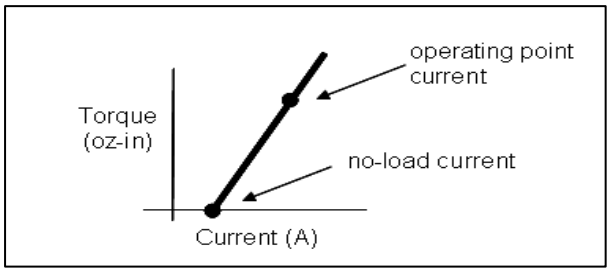

Figure 2.9 Relation between motor torque and current [30]

The slope of the curve represents the motor torque constant, K_t. It is also interesting to note that, as it was stated before, the initial current value is greater than zero as it represents the no load current I_0, which is the amount of current required to overcome internal motor friction and resistance.

Since P_{eff} is defined in equation 2.21 as the product of Q_m and N, an additional analysis to Fig. 2.8 demonstrates that the output power corresponds to the area of the rectangle below the curve, with one vertex at the origin and the other at the operating point. The area is at its maximum at $1/2$ of the no load speed and $1/2$ of the stall torque. If the operating point moves to another direction in the curve, the area mandatorily decreases. Therefore, shaft power as a function of speed assumes a parabolic curve with a maximum at half of the stall torque of the motor, as it is represented in Fig. 2.10. The figure illustrates the relation between various parameters to torque.

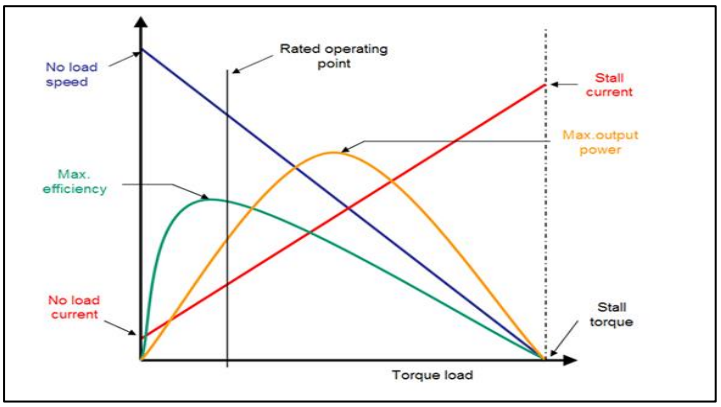

Figure 2.10 Relations between motor parameters to motor torque [31]

The maximum efficiency point appears quite early in the chart at low torque values, as speed, N, is always decreasing in relation to torque, Q_m, and P_{eff} increases only until $1/2$ of the torque load. Thus there must exists a proper compromise between the various parameters in order to optimize performance and increase efficiency.

Conclusively, achieving the optimal performance at the best efficiency value relies on a balance between motor speed, current and torque. The electrical motor performance can therefore be described as a mathematical model, which is thus presented below.

In this dissertation U_{eff} was calculated by

$$U_{eff}\ [V] = \ U - RI \quad (2.10)$$

and when multiplied by the motor velocity constant, Kv, it results in the motor angular speed in revolutions per minute, N, given by

$$N\ [rpm] = Kv\ U_{eff} \quad (2.11)$$

Thus it is also possible to represent the back electromotive voltage as a function of angular speed by

$$U_{eff}(N)\ \ [V] = \frac{N}{Kv} \quad (2.12)$$

However, the actual input motor voltage, U, which is the overall voltage without considering losses due to resistance and friction, is represented as a function of motor speed and input current, I, according to

$$U\ (N, I)\ \ [V] = \ U_{eff}(N) + IR = \frac{N}{Kv} + IR \quad (2.13)$$

Equally to the induced voltage, not all of the total current input is actually used in useful power. The no load current, I_0, does not contribute to the actual useful current which is used by the motor shaft power. Hence the effective current, I_{eff} is defined as

$$I_{eff}\ [A] = I - I_0 \quad (2.14)$$

Similarly to the input voltage, the input current, I, is the overall current without considering resistance losses. Likewise, it is formulated as a function of the motor speed, N, and input voltage, U, according to

$$I(N, U)\ [A] = \frac{1}{R}\left(U - \frac{N}{Kv}\right) \quad (2.15)$$

Hence electric current is inversely proportional to resistance, and directly proportional to voltage. Finally, with the input current and voltage values, I and U, it is possible to calculate the total electric power consumed, P_{ele}, as

$$P_{ele}\,[W] = UI \quad (2.16)$$

Following the same reasoning and considering I_{eff} and U_{eff}, the useful electric power, P_{eff}, which remains after power losses throughout the motor, can be calculated as

$$P_{eff}\,[W] = U_{eff}\,I_{eff} \quad (2.17)$$

Since power and torque are related as specified in section 2.1, the available torque at the shaft, Q_m, is defined by

$$Q_m\,[Nm] = \frac{60P_{eff}}{2\pi N} \quad (2.18)$$

Furthermore, since the input current, I, may be formulated considering the motor torque constant, Kt, as

$$I\,[A] = I_0 + Q_m\left(\frac{1}{Kt}\right) \quad (2.19)$$

then Q_m may also be described as a function of the input current, I, according to

$$Q_m(I)\,[Nm] = (I - I_0) \times K_t \quad (2.20)$$

Henceforth, with Q_m, the actual useful power available at the shaft may be obtained. The motor effective power is defined as a function of the motor speed and input voltage, U, by

$$P_{eff}\,(N,U)\;\;[W] = Q_m(\mathrm{I}) \times \frac{2\pi N}{60} \quad (2.21)$$

Power losses occur in gear box systems, and are associated primarily with tooth friction and lubrication churning losses. Thus the output shaft power must take into account the motor gear efficiency (if there is one present), and can also be defined as

$$P_{shaft}\,[W] = P_{eff} \times gear\ efficiency \quad (2.22)$$

Last of all, the motor efficiency, η, is the ratio between the shaft power and the overall power converted, since efficiency is the ratio of the useful work performed by a machine or by a

process to the total energy expended taken in. η is defined as a function of the motor speed, N, and input voltage, U according to

$$\eta\,(N,U) = \frac{P_{eff}}{P} = \frac{P_{eff}(N,U)}{I(N,U) \times\ U(N,I)} \quad (2.23)$$

2.3 Propeller performance model

A propeller is a propulsion device that converts engine power to axial thrust via torque transfer, by means of a set of rotating blades mounted in a shaft driven by an engine. Thrust occurs as the rotating propeller captures air, a fluid, and expels it out backwards. A pressure difference is produced between the forward and rear surfaces of the airfoil shaped blades, producing the thrust that is transmitted from the blades to the shaft, and finally to the airframe. The more air it expels per unit of time, the more power is converted and the greater is the thrust available. While a propeller may appear to be a simple device, its performance parameters relations are complex. Below follows a general overview on the normalized relations between propeller parameters and their importance for the performance, as well as their respective mathematical formulations [26, 24, 32].

The geometry of a propeller is defined by a set of parameters, namely the propeller tip diameter, represented as D, the blade pitch, p, and also the number of propeller blades, N_B. D is the diameter of the circle swept by the blade tips. p refers to pitch, often described in terms of units of distance that theoretically the propeller would move forward in one full rotation. Blade pitch can therefore be described as

$$p\,[m] = \frac{3}{4}\pi D arctan\theta_{pitch} \quad (2.24)$$

being θ_{pitch} the blade chord angle and $3/4 \times D$ the reference radial distance along the blade axis to define blade chord and blade pitch. Also, for a propeller with fixed geometry, it is important to take into account the propeller speed in revolutions per second $(N/60)$ and the advance speed, V, in m/s, which is defined as the forward velocity of the propeller. With these two operational parameters, a non-dimensional parameter named advance ratio, J, is defined. The advance ratio is the distance advanced by the propeller in one revolution, made dimensionless with propeller diameter. Hence J is formulated as

$$J = \frac{V}{{}^{N}/_{60} \times D} \quad (2.25)$$

Due to the complexity of the propeller performance parameters of thrust and power, efficiency and power are usually defined in terms of the dimensionless advance ratio, J. The propeller power may be defined through a power coefficient represented by C_p. In this dissertation, since the propeller diameter, D, and pitch, p, are not parameters but rather optimization variables, it was necessary to express C_p and propeller efficiency, η_p, by an estimate model dependent on D, p and J so as to optimize pitch and diameter through a sequence of algorithm iterations. This model, presented in reference [26], uses a polynomial approximation defined by

$$C_p(D,p,J) = C_{p_0} \times \left[\alpha_0 + \sum_{i=1}^{4} \alpha_i \times \left(\frac{J}{J_{max}}\right)^i\right] \quad (2.26)$$

$$\eta_p(D,p,J) = \eta_{p_{max}} \times \left[\beta_0 + \sum_{i=1}^{6} \beta_1 \times \left(\frac{J}{J_{max}}\right)^i\right] \quad (2.27)$$

where C_{p_0} is the power coefficient at a null advance ratio, $\eta_{p_{max}}$ the maximum propeller efficiency, J_{max} the maximum advance ratio and lastly $\bar{\alpha}$ and $\bar{\beta}$ the coefficient vectors obtained in the polynomial approximation [26]. The coefficients used in the model are given by

$$\bar{\alpha} = \begin{Bmatrix} 0.9999747473830 \\ 0.0026886303943 \\ -0.0542821394531 \\ -0.8141198610786 \\ 0.2382888347204 \\ -0.1060271581734 \\ 0.0222789611099 \end{Bmatrix} \quad (2.28)$$

$$\bar{\beta} = \begin{Bmatrix} 0.0000000000000 \\ 2.8358158896651 \\ -4.6740787983266 \\ 17.2094772778345 \\ -45.734194221401 \\ 55.789219497612 \\ -25.395785093511 \end{Bmatrix} \quad (2.29)$$

and J_{max}, $\eta_{p_{max}}$ and C_{p_0} are formulated as [26]

$$J_{max}(D,p) = \gamma_1 D + \gamma_2 p + \gamma_3 D^2 + \gamma_4 Dp + \gamma_5 p^2 + \gamma_6 D^3 + \gamma_7 D^2 p + \gamma_8 Dp^2 + \gamma_9 p^3 \quad (2.30)$$

$$C_{p_0}(D,p) = \varepsilon_1 D + \varepsilon_2 p + \varepsilon_3 D^2 + \varepsilon_4 Dp + \varepsilon_5 p^2 + \varepsilon_6 D^3 + \varepsilon_7 D^2 p + \varepsilon_8 Dp^2 + \varepsilon_9 p^3 \quad (2.31)$$

$$\eta_{max}(D,p) = \zeta_1 D + \zeta_2 p + \zeta_3 D^2 + \zeta_4 Dp + \zeta_5 p^2 + \zeta_6 D^3 + \zeta D^2 p + \zeta_8 Dp^2 + \zeta_9 p^3 \quad (2.32)$$

where D and p are limited, in inches, by $4 < p < 101$, $11 < D < 74$ and $0.27 < p/D < 1.47$. The coefficient vectors $\bar{\gamma}$, $\bar{\varepsilon}$ and $\bar{\zeta}$ are equal to

$$\bar{\gamma} = \begin{Bmatrix} 0.706462000000 \\ -0.046405100000 \\ 0.074350100000 \\ 0.001069860000 \\ -0.001664110000 \\ -0.000007715000 \\ -0.000006521000 \\ 0.000008688670 \\ 0.000002563530 \\ -0.000000703183 \end{Bmatrix} \quad (2.33)$$

$$\bar{\varepsilon} = \begin{Bmatrix} 0.050916200000 \\ -0.005511640000 \\ 0.007489280000 \\ 0.000144156000 \\ -0.000239091000 \\ 0.000065509200 \\ -0.000002407300 \\ 0.000005544700 \\ -0.000003824100 \\ 0.000000875200 \end{Bmatrix} \quad (2.34)$$

$$\bar{\zeta} = \begin{Bmatrix} 0.375474000000 \\ 0.013321100000 \\ 0.014884800000 \\ -0.000358479000 \\ 0.000020627100 \\ -0.000189967000 \\ 0.000003644830 \\ -0.000004047110 \\ 0.000004028760 \\ -0.000000467311 \end{Bmatrix} \quad (2.35)$$

With the power coefficient, $C_P(D,p,J)$, and the propeller efficiency, $\eta_P(D,p,J)$ it is possible to calculate the overall power available during flight operation, P_A, according to [26]

$$P_A(D,p,J,N,\rho)\ [W] = C_P(D,p,J) \times \rho \left(\frac{N}{60}\right)^3 D^5 \quad (2.36)$$

where ρ is the air density at a certain altitude. Consequently, the available propeller thrust, T_A, is given by

$$T_A(D,p,J,N,\rho,V)\ \ [N] = \frac{P_A(D,p,J,N,\rho)}{V} \quad (2.37)$$

Another important subject, which is essential to understand, is that aerodynamic effects cause the propeller to advance at a speed that is lower than the theoretically calculated advance

speed. This means it is lower than the product of the propeller speed, N, and pitch, p. This condition, $V < p\,{}^{N}/_{60}$, represents the difference between the calculated air speed and the actual real speed. If the pitch value, p, increases, so does the limit $p\,{}^{N}/_{60}$, and therefore the propeller is allowed to achieve greater values of V [33]. Therefore, the pitch parameter influences speed and consequently the propeller efficiency.

Shaft power is also influenced by pitch. This occurs since P_A is proportional to pitch, propeller speed and diameter, in a manner such as $P_A \propto \theta_{pitch}\,{}^{N}/_{60}{}^{3}\,D^5$. This relation demonstrates the importance of D and ${}^{N}/_{60}$. The higher the diameter value is, the better, although it is limited by available space and by maximum blade tip speed. However, diameter is a fixed parameter for a given propeller, and the revolutions rate can only vary a little for optimum performances during flight operations. Therefore pitch angle is commonly the variable used to control outputs like shaft power (and hence propeller thrust) and advanced speed (by the condition stated above $V < p\,{}^{N}/_{60}$), so as to achieve the maximum efficiency.

Fig. 2.11 better clarifies the influence of pitch in the power coefficient function, $C_p(D,p,J)$, whereas Fig. 2.12 illustrates the influence of pitch on the propeller efficiency, $\eta_p(D,p,J)$ [26].

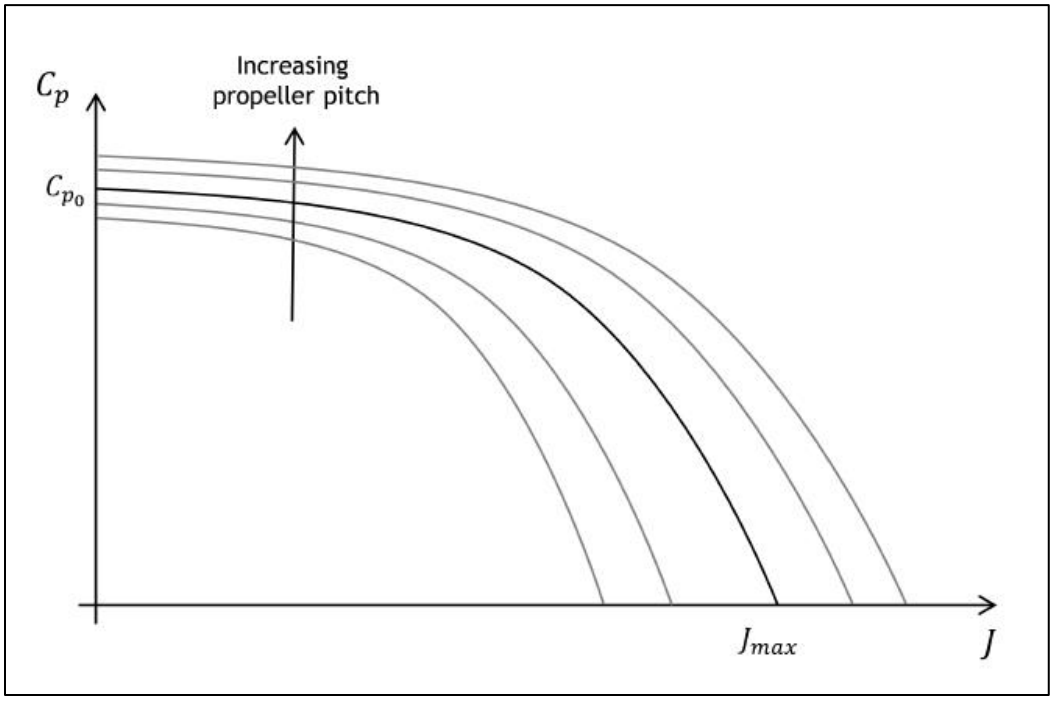

Figure 2.11 Propeller $C_p(D,p,J)$ for various pitch [26]

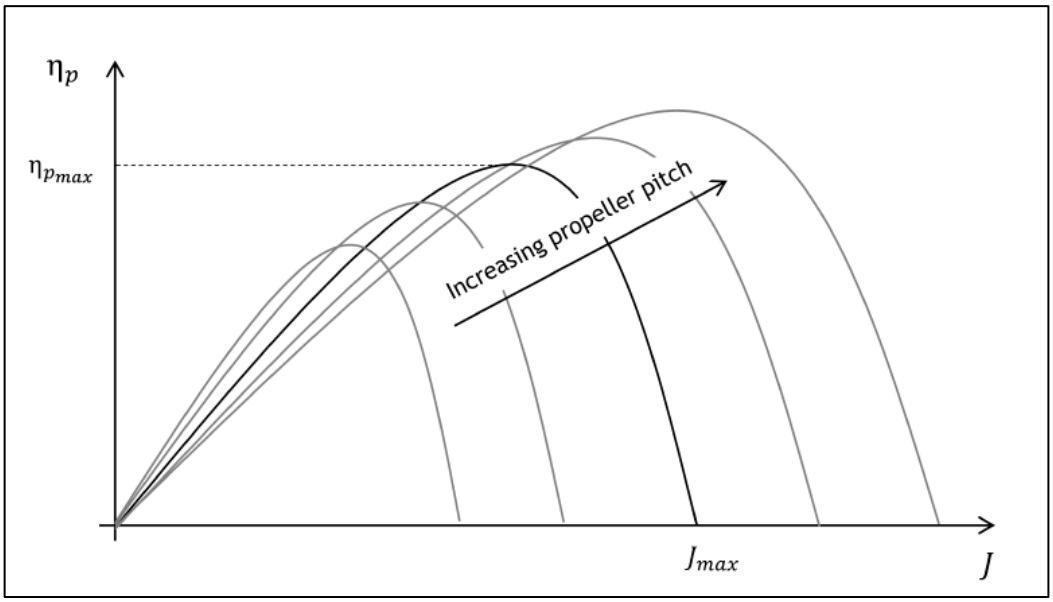

Figure 2.12 Propeller $\eta_p(D,p,J)$ for various pitch [26]

As pitch increases in relation to the propeller diameter (i.e. as p/D increases), C_{p_0}, η_P and J_{max} increase. Hence pitch may be adjusted depending on the flight phase in order to achieve the maximum possible efficiency. However this is only affordable for variable pitch propellers that adjust the blade angle to its optimum value for each flight stage, be it takeoff, climb or cruise. Low pitch, also called fine pitch, yield best for low speed accelerations (like takeoff and climb phase), as the blades deliver higher efficiency, η_p, for the smaller J condition.

Contrarily, a fixed pitch propeller (which was used in this dissertation) is the simplest propeller design, as the pitch angle is set at installation and cannot be changed during flight. Blade angle is, therefore, a compromise between the optimum pitch for takeoff, climb and cruise. Fixed pitch propeller cost less and are more affordable.
There also exist constant speed propellers that are designed to automatically change its blade pitch to allow it to maintain a constant rate of revolution, N. Otherwise, depending on the amount of engine torque being produced or the airspeed and altitude at which the aircraft is flying, the propeller speed will normally vary.

Last of all, one other design parameter to be considered is the number of blades of the propeller, N_B. It has not such a great influence as other parameters do. However it is also considered at the designing phase. Two or three blades are the best compromise between aerodynamic and structural concerns in low-speed applications.

In order to achieve a good performance, a proper initial design of propeller diameter and pitch is extremely important, as they drastically influence all the performance parameters related to the propeller efficiency.

2.4 Mission performance model

The performance of an aircraft is characterized by a great number of variables. However, for simplification purposes, below follows only the presentation of some of the parameters, the most relevant to this dissertation and related to the restrictions applied to the software. Altitude has a significant impact on the aircraft performance, since air density, $\boldsymbol{\rho}$, affects the available thrust produced by the propeller, and in the case of an IC engine the changes in density of the intake air compromise shaft power. Thus initially determining the air density for a specific altitude is mandatory, and ρ can be obtained according to the perfect gas equation by [34].

$$\rho = \frac{P}{RT} \quad (2.38)$$

where R is the universal gas constant ($287.053\ J/kg.K$), T the air temperature in Kelvin and P the air pressure, in Pascal, which below the tropopause can be calculated by

$$P = P_0(1 - \frac{\alpha}{T_0 + dT}h)^{\frac{g}{\alpha R}} \quad (2.39)$$

P_0 stands for the standard pressure at sea level ($1013.25\ hPa$), α the increment on temperature for each meter climbed below tropopause ($0.0065°C/m$), g the gravity constant, h the altitude in meters an T_0 is the standard temperature at sea level ($288.15\ K = 15°C$). Commonly temperature at sea level not always assumes the standard value, so adding the deviation of temperature, dT, to T_0 is essential.

By definition, a level flight is a flight condition in which the climb angle and the roll angle of the aircraft are null. A steady flight is a flight with no acceleration [35]. For a steady level flight the forces operating on the aircraft are balanced, as illustrated in figure 2.13.

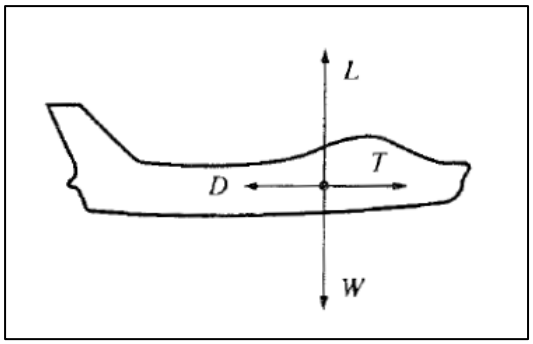

Figure 2.13 Force diagram for steady, level flight [35]

Thus in the equilibrium condition for steady level flight, weight is balanced by the lift produced, and the drag force is balanced by the thrust generated [36]. Hence, the governing equations of motion for steady level flight can be obtained from

$$T_R = D \quad (2.40)$$

$$L = W \quad (2.41)$$

where L represents the lift provided by the pressure differential between the upper and bottom surface of the wing, W stand for the weight of the aircraft, D for the drag force which opposes movement, and T_R is the required thrust in order to overcome drag. Furthermore, drag, D, and therefore thrust required, T_R, for steady, level flight can be written as

$$D = T_R = \frac{1}{2}\rho V^2 S C_D \quad (2.42)$$

being ρ the air density in kg/m^3, which varies with altitude, V the air speed in m/s and S the total wing area in m^2 [35]. The drag coefficient, C_D, is obtain by the drag polar. The drag polar expresses the dependence of the drag coefficient as a function of the lift coefficient, or in other words, the relation between the lift on an aircraft and its drag [35]. It is generally displayed on a graphical representation or by an equation. In this dissertation, C_D is calculated by an approximated polynomial model. Hence C_D is given by

$$C_D(C_L) = \sum_{i=1}^{n} C_{D_i} \times C_L^i \quad (2.43)$$

where C_{Di} are the polynomial coefficients of the drag polar, and C_L^i is the independent variable. C_{D_i} is a vector given in the form

$$C_{D_i} = \left(C_{D_1}, C_{D_2}, \dots, C_{D_i}\right) \quad (2.44)$$

and C_L is obtained through [36]

$$C_L = \frac{2L}{\rho V^2 S} = \frac{2W}{\rho V^2 S} \quad (2.45)$$

This allows the calculation of the drag force, D, which is obtained from equation 2.42. In other words, D is mainly dependent on speed, altitude (influenced by the air density, ρ) and weight [35], according to

$$D(\rho, V, W) = T_R (2.46)$$

Fig. 2.14 is an example of a graphical representation of the total drag resulting from the sum of parasite drag and induced drag, as a function of air speed, V.

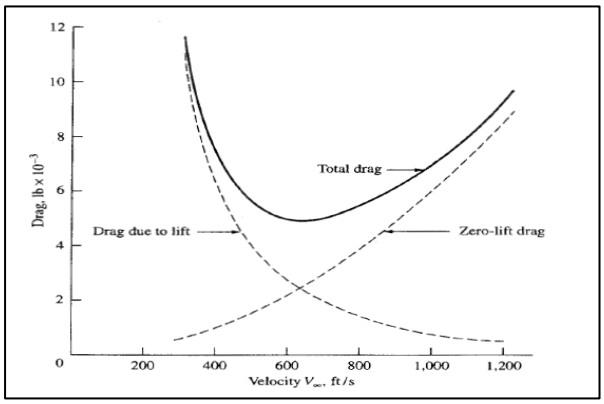

Figure 2.14 Total drag versus air speed [35]

The total drag curve assumes this shape since the induced drag decreases with air speed whereas parasite drag increases.

Looking more closely to equation 2.42, it is possible to observe that the air density ρ, which decreases with altitude, has a significant impact on the required thrust. For a higher altitude, the decreasing air density causes the value of speed at which the minimum required thrust occurs to increase [35]. Also, for decreasing values of air density, the propeller is less capable of producing thrust compared to the thrust at sea level, so as altitude increases, the available thrust, T_A, decreases. Fig.2.15 and 2.16 represent the effect of altitude on required thrust and available thrust.

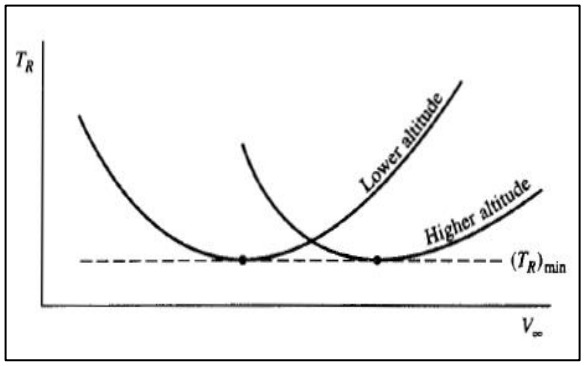

Figure 2.15 Effect of altitude on required power [35]

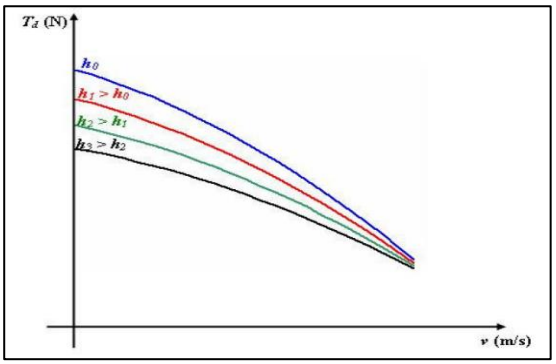

Figure 2.16 Effect of altitude on available thrust of a propeller driven aircraft [36]

However, in the case of a propeller driven aircraft, the curves for required and available power are also often used, as they allow a better evaluation of the overall endurance and maximum rate of climb and climbing conditions. Since power is obtained as the product of force and velocity, then

$$P_R = T_R V = DV \quad (2.47)$$

$$P_A = \eta_P V \quad (2.48)$$

where η_p is the propeller efficiency and P_A the power delivered by the engine at the shaft. Plotting the two curves of power as a function of air speed allows a more detailed analysis of significant performance speeds, such as the maximum allowed speed, V_{max}, the stall speed, V_s and the best rate of climb speed, V_{BC}, for a propeller driven aircraft.

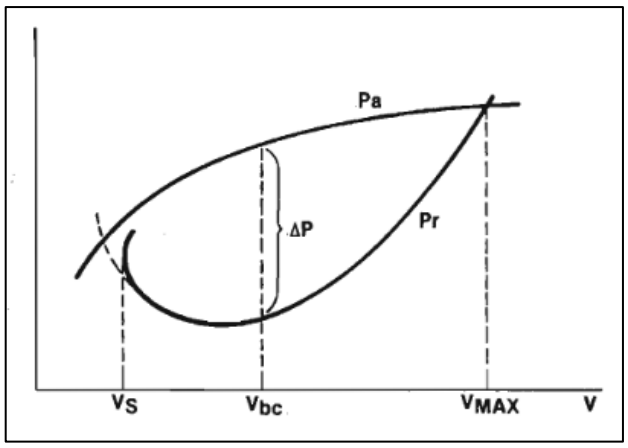

Figure 2.17 Power available and power required as a function of air speed [37]

For throttle full forward, the maximum speed which the aircraft can achieved, V_{max}, is determined by the high speed intersection of the P_A and P_R curves. If the required power increases due to an increase of the parasite and induced drag, the P_A and P_R intersection will occur earlier and the allowed V_{max} decreases [35]. Furthermore, since increasing altitude means $T_{R_{min}}$ will match higher speeds, then the P_A and P_R intersection will now occur later. Hence V_{max} will increase for higher heights, below Mach 1 (for propeller driven aircrafts only) [35].

The stall speed, V_s, is the minimum steady flight speed at which the aircraft is controllable. In aerodynamic terms, it is the speed below which the stall condition will occur, since there is a critical angle of attack beyond which no extra lift can be generated, due to an air flow detachment from the upper surface of the wing. This sets a limit on the minimum airspeed at which lift can be sustained, i.e. the stall speed, V_s. According to equation 2.45, the lift coefficient is inversely proportional to V^2. Thus the maximum lift coefficient, $C_{L_{max}}$, will occur at the minimum allowed speed, V_s. Since V equals to

$$V = \sqrt{\frac{2W}{\rho S C_L}} \quad (2.49)$$

then V_S is likewise obtained from

$$V_S = \sqrt{\frac{2W}{\rho S C_{L_{max}}}} \quad (2.50)$$

These were all parameters considering a level flight operation. However, regarding a steady, non-accelerated climbing flight, it is now important to maximize the rate of climb, RC, since it is the vertical speed of an aircraft, which translates into the rate of positive altitude change per time, expressed in m/s.

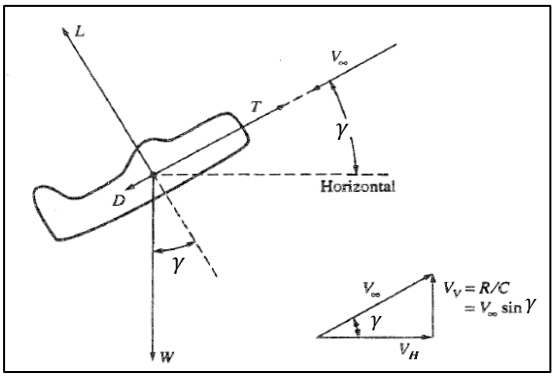

Figure 2.18 Force and speed diagram for climbing flight [35]

Considering Fig. 2.18, the rate of climb can be calculated considering the angle between the horizontal component of air speed and the actual air speed. Contrarily to a steady, level flight, thrust is not only balanced through drag force but also by the component of weight in the plane of thrust. Hence

$$T_A = D + W sen\gamma \quad (2.51)$$

where γ, in degrees, is the angle between the horizontal component of air speed, V_H, and the actual air speed V. Similarly, lift is balanced by the component of weight in the plane of lift by

$$L = W sen\gamma \quad (2.52)$$

Since the rate of climb is the vertical component of the air speed, it can be obtain from

$$RC = V sen\gamma \quad (2.53)$$

Additionally, and according to equation 2.51, $sen\gamma$ is defined as

$$sen\gamma = \frac{T_A - D}{W} \quad (2.54)$$

Thus, the rate of climb which equals $Vsen\gamma$ can be reformulated as

$$RC = Vsen\gamma = \frac{VT_A - VD}{W} = \frac{P_A - P_R}{W} = \frac{excess\ of\ power}{W} = \frac{\Delta P}{W} \quad (2.55)$$

Therefore the maximum rate of climb, RC_{max}, occurs when the maximum excess of power condition represented in Fig. 2.17 as ΔP is achieved [36]. The variation of RC with air speed is illustrated in the Fig. 2.19 below. The rate of climb angle, γ, displays the same parabolic curve when plotted as a function of V.

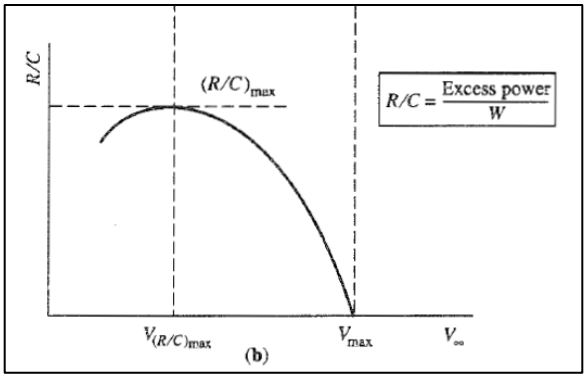

Figure 2.19 Rate of climb as a function of air speed [35]

Interesting to note that if the excess of power, ΔP, is null, the aircraft is unable to climb any further. This condition happens because the required and available power are dependent on altitude.

For higher altitudes, the available thrust the propeller is able to produce will decrease, i.e. P_A decreases. Furthermore, the minimum required thrust, $T_{R_{min}}$, will occur at higher speeds. Since $P_R = T_R V$, this demonstrates that the required power, P_R, will increase for higher altitudes, as V must assume higher values to produce the same amount of thrust.

Hence, at a certain altitude the available excess power, ΔP, and consequently RC will be null, as represented below in point A of Fig 2.20. The maximum altitude at which this occurs is designated as the absolute ceiling represented in point 2 of Fig. 2.21 [35, 36].

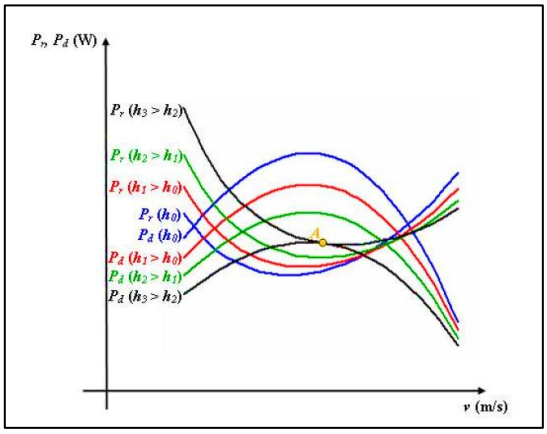

Figure 2.20 Point of null excess of power available, at the service ceiling altitude [36]

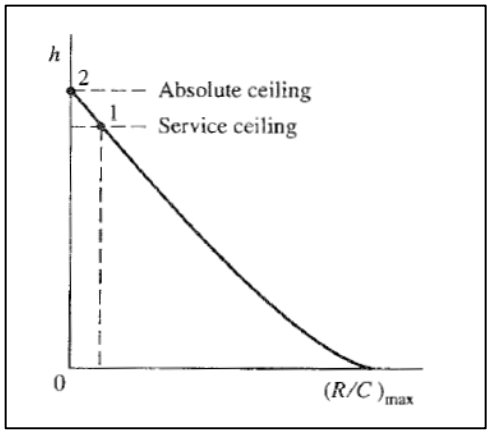

Figure 2.21 Variation of maximum rate of climb with altitude [35]

Another relevant flight condition beyond rectilinear motion is the level turn, one in which the curved flight path is in a horizontal plane, parallel to the plane of the ground (the altitude remains constant) [35]. The balance of the forces acting on the aircraft at level turn condition for a certain altitude are represented below.

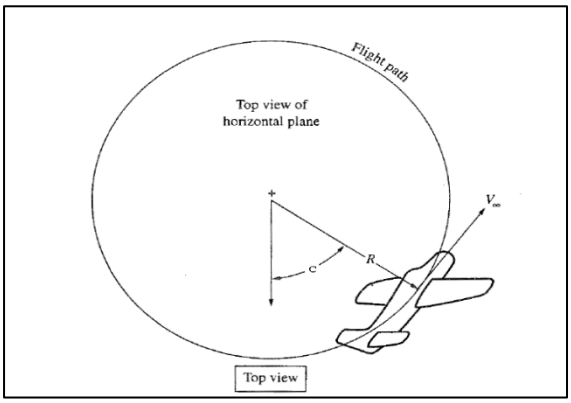

Figure 2.22 Top view of a level turn [35]

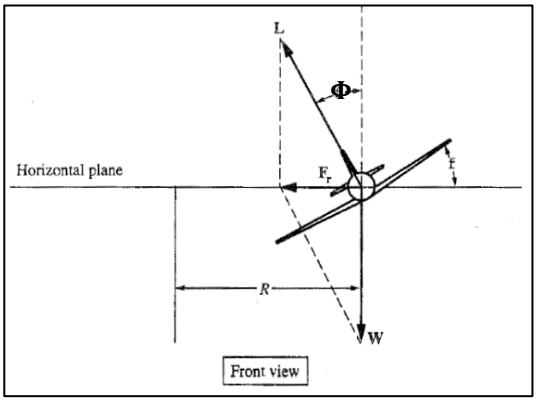

Figure 2.23 Balance of the acting forces on a level turn [35]

Hence, analyzing Fig. 2.23, on a level turn performance the aircraft is inclined in relation to the vertical plane according to the angle Φ. Weight is therefore balanced by the vertical component of lift, formulated as

$$W_{turn} = L\,cos\phi \quad (2.56)$$

Under this condition, the vertical forces acting on the aircraft are balanced. As for the horizontal plane, the forces are balanced through the component specified in Fig. 2.23 as F_R, the resulting force of the vector sum of lift, L, and weight, W. The magnitude and direction of L are adjusted, so that the vector sum of L and W results in F_R always being in the horizontal

plane [35]. The larger this resulting force, the tighter and faster the turn will be. Equation 2.56 may also be reformulated as

$$cos\phi = \frac{W}{L} = \frac{1}{L/W} \quad (2.57)$$

The ratio L/W is a fundamental parameter in turning performance, known as the load factor, n_{load}. The load factor is commonly represented according to the acceleration of gravity constants, i.e. it is expressed in $g's$. Essentially a load factor of $2\ g's$ imposes that for a given flight condition, the aircraft structure is submitted to a lift force twice the given weight [36]. n_{load} can be obtained from

$$n_{load} = \frac{L}{W} \quad (2.58)$$

Moreover, lift can be obtain by reformulated the equation to

$$L_{turn} = n_{load}\, W \quad (2.59)$$

which substituting in equation 2.45 of the lift coefficient becomes, for a level turn performance

$$C_{L_{turn}} = \frac{2L}{\rho V^2 S} = \frac{2n_{load}\, W}{\rho V^2 S} \quad (2.60)$$

Hence, reformulating equation 2.60 in order to V, is it possible to observe that the load factor affects not only the lift coefficient, but also the stall speed by means of

$$V_{turn} = \sqrt{\frac{2n_{load}W}{\rho S C_L}} \quad (2.61)$$

and thus the stall speed, V_S, for a level turn condition is obtained by

$$V_{S_{turn}} = \sqrt{\frac{2n_{load}W}{\rho S C_{L_{max}}}} \quad (2.62)$$

Therefore, when the airplane is in a level turn, the a load factor is a constraint on the stall speed, which increases proportionally to $\sqrt{n_{load}}$.

One of the most practical approaches when considering load factor analysis is translated by the elaboration of a flight envelope diagram, also called $v-n$ diagram, which represents the

structural limits for n_{load} regarding air speed. The load factor is a variable that directly reflects in the structural sizing of the aircraft, since it is a representation of the load the aircraft structure is subjected to [36]. Therefore, there are two structural limitation categories which must be taken into account at the design phase of the aircraft. First is the limit load factor, n_{limit}, which is associated with permanent deformations on the aircraft, although without rupture. The limit load factor n_{limit} is a fixed parameter defined at the designing phase. Second is the ultimate load factor, $n_{ultimate}$, which is associated with structural failure and rupture. Normally for safety cautions, it is recommended that $n_{ultimate}$ is 50% higher than n_{limit} [36], which is given by

$$n_{ultimate} = 1.5\, n_{limit} \quad (2.63)$$

Fig. 2.24 represents an example of a typical flight envelope range and it structural limits as a function of air speed, V.

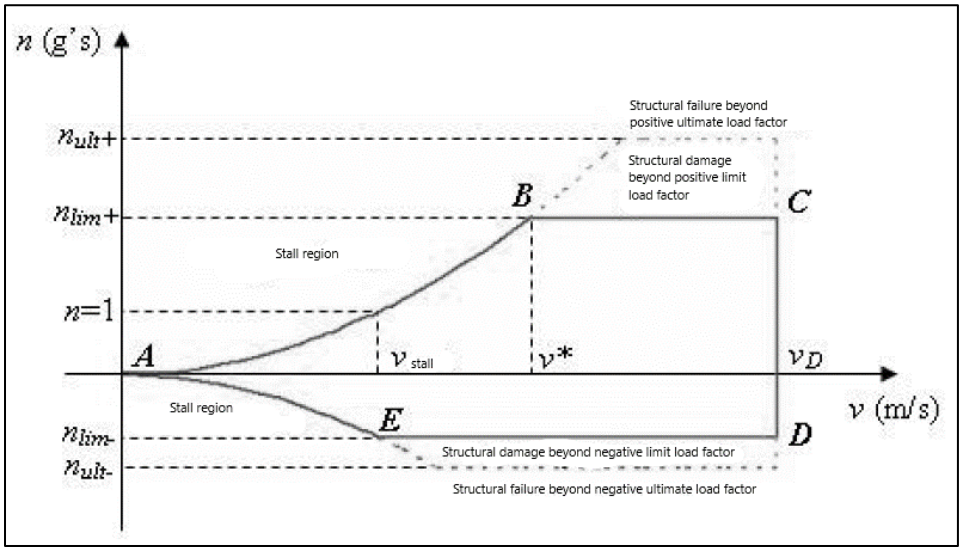

Figure 2.24 Flight envelope diagram [36]

The AB curve represented in the figure stands for the maximum load factor allowed by the maximum lift available at certain speeds, and point B is obtained from

$$n_{limit} = \frac{L_{max}}{W} = \frac{1/2\ \rho V^2 S C_{L_{max}}}{W} \quad (2.64)$$

Thus, if $C_{L_{max}}$ is exceeded at a certain speed (too high angle of attack), the aircraft will enter the stall condition and the air flow will detach from the upper surface of the wing.

Also important to note that for $n_{load} = 1$ the condition, $L = n_{load}\, W$, becomes $L = W$, which is the condition for a steady, level flight. The minimum speed allowed for this state is in fact

the stall speed, V_S. Hence by substituting $n_{limit} = 1$ in equation 2.64 and reformulating it in order to air speed, the result obtained is V_S.

The speed which intercepts the curve AB at point B, represented in the figure as V^*, is called the maneuver speed [36]. V^* defines the positive limit load factor value, n_{limit}, and if the speed increases beyond this point, the aircraft is only able to fly for values of $C_L < C_{L_{max}}$ in order not to exceed n_{limit} (as it can be observed from equation 2.64). To achieve it, the angle of attack which influences C_L is diminished as speed increases until V_{max}. Thus the limit load factor remains constant throughout the line BC. V^* can be written as

$$V^* = \sqrt{\frac{2Wn_{limit}}{\rho S C_{L_{max}}}} = V_S \sqrt{n_{limit}} \quad (2.65)$$

The curves AE and ED represent the maximum load factor allowed and the limit load factor, respectively, for negative $g's$.

Finally, the speed represented in the figure as V_D is the dive speed, limited by the line CD, and it is considered the critical speed to the aircraft structure. The dive speed must always be avoided due to the possibility of significant structural failure, and it is recommended that V_D should be 25% higher than the maximum allowed speed, V_{max} [36].

$$V_D = 1.25 V_{max} \quad (2.66)$$

Furthermore, it is interesting to highlight the influence of altitude, h, on stall speed, V_S, and maneuver speed, V^*, at which the aircraft is allowed to fly. Both V^* and V_S, as it can be observed in equation 2.65, are inversely proportional to air density. This means both increase as altitude increases, due to lesser ρ values [36].

So far the mission performance characteristic discussed considers the aircraft in full flight operation. However, the particulars for takeoff, in which the aircraft rolls at ground along the runaway, also need to be carefully studied, as they establish an acceleration performance problem of different features [35]. Determining how much distance is necessary for the aircraft to cover until it lifts into the air is a central requirement in liftoff performance analysis. In order to calculate the ground roll (or in other terms the necessary takeoff runway distance, S_{TO}), understanding the acting forces on the aircraft at ground is required. For a successful takeoff performance, in addition to the relation between lift and weight, the thrust force must overcome not only the drag, D, but also the friction force, R, resulting from the friction between the aircraft takeoff train and the ground, represented in Fig. 2.25 [35].

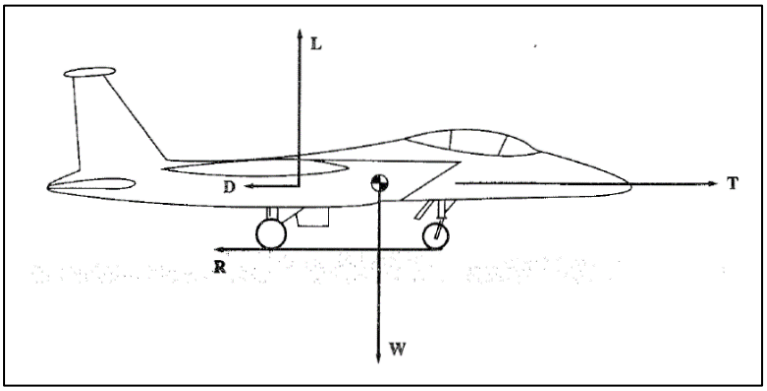

Figure 2.25 Forces acting on the aircraft during takeoff performance [35]

The friction force, R can be obtained from

$$R = \mu N \quad (2.67)$$

where μ is the coefficient of friction between the ground and the train wheels, and N is the normal reaction force exercised vertically by the ground on the aircraft. However, as the aircraft develops speed, the lift force, L, increases to overcome weight, W [36]. Therefore the normal reaction of the ground on the aircraft, N, tends to decrease during the takeoff duration and the equation may be reformulated as

$$R = \mu(W - L) \quad (2.68)$$

The coefficient of friction varies according to the type of ground characteristics. Example of typical μ values for specific ground surfaces is given below [35].

	μ_r(Typical Values)	
Surface	**Brakes off**	**Brakes on**
Dry concrete/asphalt	0.03–0.05	0.3–0.5
Wet concrete/asphalt	0.05	0.15–0.3
Icy concrete/asphalt	0.02	0.06–0.10
Hard turf	0.05	0.4
Firm dirt	0.04	0.3
Soft turf	0.07	0.2
Wet grass	0.08	0.2

Figure 2.26 Typical coefficient of friction for different ground surfaces [35]

Hence, and according to the motion equation given by the second law of Newton, where the product of mass and acceleration equals the resulting force, the overall relation between forces at takeoff stage is given by

$$F_R = ma = m\frac{dV}{dt} = T - D - \mu(W - L) \quad (2.69)$$

being a the acceleration of the aircraft (variation of speed during a certain amount of time, t) and m its mass.

The aircraft initiates its movement at ground and accelerates until it reaches the takeoff speed, V_{TO}, after rolling through the distance S_{TO} in a certain amount of time, t_{TO}. Reducing S_{TO} is primary objective in takeoff performance analysis, since it requires less costs related to runway length for the aircraft to liftoff. A simplified depiction of the aircraft ground roll is presented below.

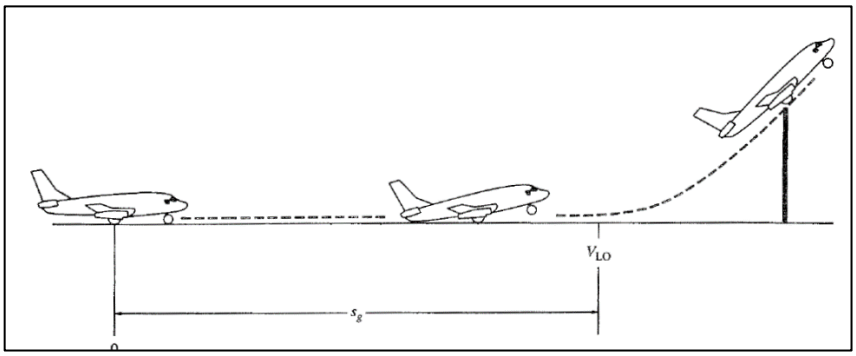

Figure 2.27 Ground roll [35]

To calculate the minimum runway distance, it is important to establish a relation which can provide the distance S_{TO} (represented in the figure as S_g), assuming a relation between the takeoff speed, the weight of the aircraft and the resulting actuating force. Thus performing a change of variable in equation 2.69 in order for it to be independent of time and dependent on the runway distance is required [36], and so

$$\frac{dV}{dt} = \frac{F_R}{m} (2.70)$$

$$dV = \frac{F_R}{m}\, dt \quad (2.70a)$$

$$\int_0^{V_{TO}} dV = \int_0^{t_{TO}} \frac{F_R}{m}\, dt \quad (2.70b)$$

$$V_{TO} = \frac{F_R}{m}\, t_{TO} \quad (2.70c)$$

$$t_{TO} = \frac{V_{TO}\, m}{F_R} \quad (2.70d)$$

Knowing also that takeoff speed is the variation of takeoff distance during takeoff time, then

$$V_{TO} = \frac{dS_{TO}}{dt_{TO}} \quad (2.71)$$

$$dS_{TO} = V_{TO}\, dt_{TO} \quad (2.71a)$$

$$\int_0^{S_{TO}} dS_{TO} = \int_0^{t_{TO}} V_{TO}\; dt_{TO} \quad (2.71b)$$

$$\int_0^{S_{TO}} dS_{TO} = \int_0^{t_{TO}} \left(\frac{F_R}{m}\, t_{TO}\right)\; dt_{TO} \quad (2.71c)$$

$$S_{TO} = \frac{F_R}{2\, m} t_{TO}^2 \quad (2.71d)$$

Substituting equation 2.75d on equation 2.76d the result is [36]

$$S_{TO} = \frac{F_R}{2\, m}\left(\frac{V_{TO}\, m}{F_R}\right)^2 \quad (2.71e)$$

$$S_{TO} = \frac{V_{TO}^2\, m}{2F_R} \quad (2.71f)$$

Hence, considering that mass is the ratio between weight and acceleration constant, $m = W/g$, and that F stand for the resulting forces acting on the aircraft during the takeoff phase, then [35]

$$S_{TO} = \frac{V_{TO}^2 W}{2\, g}\left[\frac{1}{[T_{TO} - D_{TO} - \mu(W - L)]}\right] \quad (2.72)$$

where T_{TO} and D_{TO} are the propeller thrust and drag at takeoff speed, respectively, and μ is assumed. D_{TO} is obtained according to a takeoff lift coefficient, $C_{L_{TO}}$, also assumed by the user.

Finally, considering that the takeoff speed must never be less than 20% of the stall speed, V_{TO} is given by

$$V_{TO} = 1.2\sqrt{\frac{2W}{\rho S C_{L_{max}}}} \quad (2.73)$$

where $C_{L_{max}}$ is achieved with flaps extended for takeoff. Substituting in equation 2.73, another possible way in which to formulate ground roll is

$$S_{TO} = \frac{1.21\, W/S}{g\rho C_{L_{max}}[T_{TO}/W - D_{TO}/W - \mu(1 - L/W)]} \quad (2.74)$$

Analyzing equation 2.74, the major design parameters that have an impact on takeoff ground roll are mainly the wing load, W/S, the thrust to weight ratio, T_{TO}/W, the maximum lift coefficient, $C_{L_{max}}$, and air density, ρ [35]. The wing load, W/S, is, by definition, the gross weight of an aircraft fully loaded divided by the wing area, in kg/m^2. Since wings generate lift, an aircraft with a small wing area in relation to its weight will need more speed in order to produce the required lift. Contrarily, a large wing area related to its mass will produce more lift for the given speed. Therefore an aircraft with lower wing load will be able to lift off at lower speeds, and requires less distance for the runway roll, S_{TO}. Or else, it is able to take off with a greater load which requires, however, higher speeds and therefore higher runway distance. Thus ground roll, S_{TO}, is directly proportional to W/S, i.e. $S_{TO} \propto W/S$.

Thrust to weight ratio, T_{TO}/W, is the amount of thrust produced in relation to the aircraft weight and indicates the capacity of the aircraft to overcome gravity and accelerate. If an engine produces less thrust than the airplane weighs, the airplane must also rely on aerodynamic lift to overcome its weight. A high thrust to weight ratio produces more acceleration and excess of thrust, and thus a higher rate of climb is achieved and requires less ground roll distance for takeoff. Hence S_{TO} is inversely proportional to thrust to weight ratio, i.e. $S_{TO} \propto \frac{1}{T/W}$. Significant to note that if the aircraft weight is, for example, duplicated, the wing load, W/S, is doubled whereas T/W is halved, increasing S_{TO} considerably. This means ground roll is extremely sensitive to the design parameter of weight, i.e. $S_{TO} \propto W^2$ [35].

Continuing the analysis of equation 2.74, if the aerodynamic lift produced is high, the aircraft will be able to produce higher lift values for less speed required, and consequently will be able to takeoff with less ground roll distance. So S_{TO} is inversely proportional to $C_{L_{max}}$, i.e. $S_{TO} \propto \frac{1}{C_{L_{max}}}$. Additionally, it is also inversely proportional to air density, not only by the explicit appearance of ρ in equation 2.74, but also on the predominant effect it has on thrust, T, as observed at the beginning of this sub-chapter (equation 2.45). Henceforward, $S_{TO} \propto \frac{1}{\rho^2}$. Since

air density decreases as altitude increases, airports located at higher altitudes will require longer runways [35].

In conclusion, S_{TO} is very sensitive not only to weight constraints, but also to altitude. Below is illustrated the relation between the runaway distance S_{TO}, altitude, h, and aircraft weight, W [36].

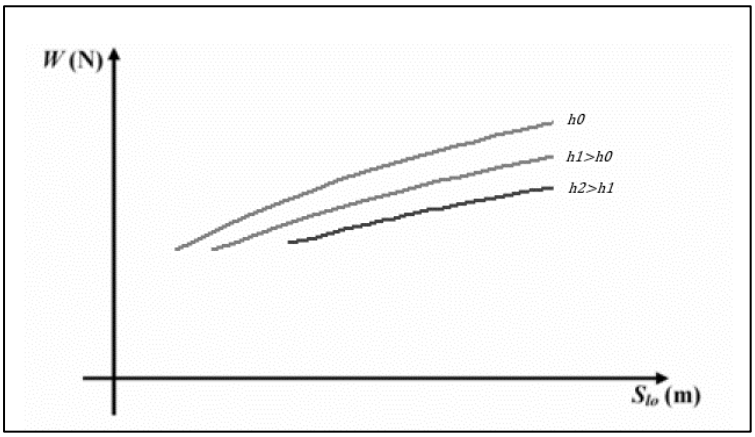

Figure 2.28 Relation between runway distance, altitude and weight [36]

Figure 2.28 demonstrates that for the same distance for ground roll, S_{TO}, the weight with which the aircraft is capable of lifting off will be less as altitude increases. In other terms, in order to be able to lift the same weight at higher altitudes the runway distance must increase. This illustrates the relations above exposed as $S_{TO} \propto \frac{1}{\rho^2}$ and $S_{TO} \propto W^2$.

Hence, similarly to the engine and propeller operating mechanisms, optimizing mission performance at the design stage involves a balance and weighting process of parameters that interrelate with one another.

3 Optimization Methodology

Optimizing an airframe design through a software that implements an optimization algorithm is the main focus of this dissertation. Modifications and implementations were made to an already existing optimization program [26], compiled in Intel Fortran. When entering certain design parameters, which are related to the performance of the engine, the program will then be able to calculate the objective function and proceed to the application of the optimization algorithm. Minimizing the mission energy required during flight operation is the objective function, and depending on the design variables and mission constraints set at the beginning, different solutions may be reached. When the optimum solution is achieved, a proper selection of the engine to match the airframe and propeller is required.

Hence one of the objectives of this dissertation was to modify the software, which was giving the optimum solution for one specific engine, and enable it to select an engine from an empirical data base. For that purpose a set of equations to calculate each engine specification as a function of independent design variables was obtained, based on empirical data from real engines. Afterwards, the equations obtained were introduced in the program, in order to calculate the engine specifications at each algorithm iteration. These design variables are initially set as input design parameters, to be optimized by the optimization software. Fig. 3.1 very briefly illustrates the overall process, with the addition modifications steps presented with dashed borders.

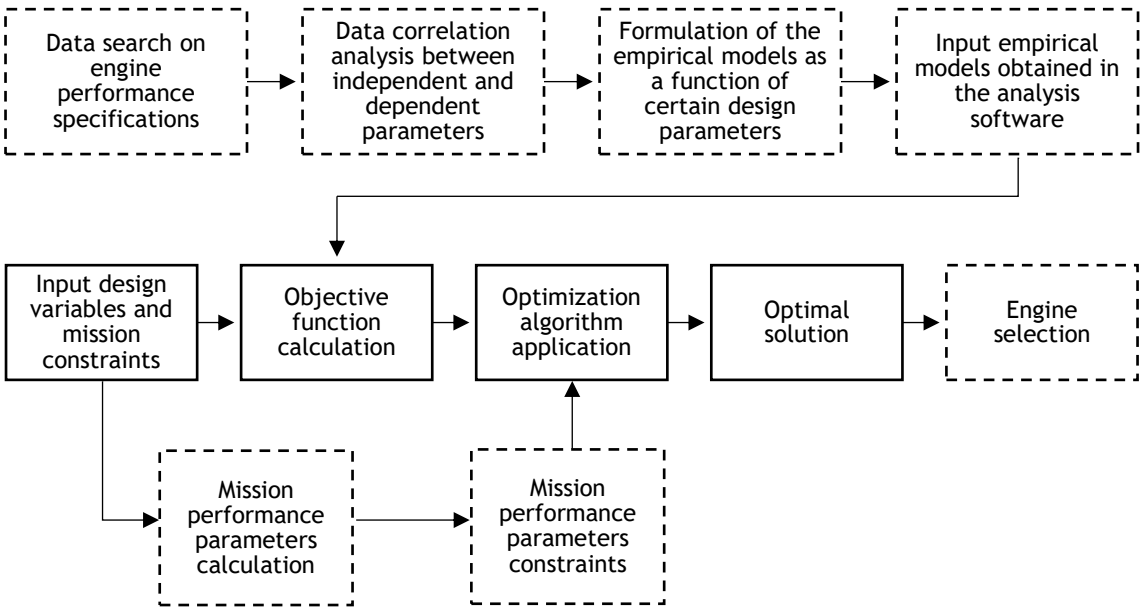

Figure 3.1 Brief introduction of the overall optimization process

The software modified in this dissertation already had constraints applied to the engine performance. Another aim of this thesis was to add the mission constraints to the software, through a process of iterative calculations latter described in section 3.6. Using the mathematical models of the propeller, the combustion engine and electric motor described previously in chapter 2, it is possible to calculate the objective function.

3.1 Objective function

The objective function in study is the minimization of the overall mission energy required, in Joule. In case of an electric motor this corresponds to the minimization of the product between electric power required, in W, and the average mission duration, in seconds. For an IC engine, it involves the product between the total fuel consumption fc, in g/s, and the average mission duration, in seconds. First, a brief explanation on how the software calculates the objective function must be given.

The optimization software, before modifications were made, was giving the optimum solution for one specific engine, whose performance parameters were defined initially by the user. For IC engines, parameters such as the rated power, bp_{max}, maximum engine speed at rated power, N_{max}, and specific fuel consumption at rated power, $bsfc_0$, are initially defined. For electric motors, the user sets the initial motor specifications by defining parameters such as the speed constant, K_v, torque constant, K_t (if not defined equals $0.95 \times K_v$), internal resistance, R, no load current, I_0, maximum allowed current, I_{max}, maximum allowed voltage, U_{max} , the battery cell internal resistance, R_U, and also the speed controller resistance, R_Ω. A speed controller resistance can vary the rotor resistance and therefore its current flux, changing the motor speed, as it is better clarified in section 1.4.4. This allows the calculation of the objective function for these specifications, before being submitted to the algorithm. With the initial specifications defined, the software proceeds to the calculation of the engine performance parameters, according to the mathematical models stated in chapter 2.

Assuming a mission with a specified number of segments [38] (for example a takeoff segment, a climbing segment, a cruise segment, a descending segment and a landing segment), the duration of the mission can be calculated through the sum of the time each segment takes to be completed. In the case of an IC engine, the aircraft weight in the following segment takes into account the loss in fuel weight, W_{fuel}, which decreases during mission.

For a proper matching of the propeller and engine, the power absorbed by the propeller must equal the engine shaft power, P_{shaft}. For combustion engines, the engine speed, N, is adjusted to match this condition through an iterative process, which given an assumed engine setting, δ, allows the calculation of the engine shaft power and the available power, P_A. For electric motors, the engine current, I, is adjusted to match this condition also through an iterative process, which given an assumed engine setting, δ, allows also the calculation of the motor

input voltage, motor speed, motor shaft power and propeller power, P_A. Then, for a minimum mission energy required (minimum fuel consumption or minimum electric power required), the propeller power, P_A, must assume a value as minimum as possible and consequently must equal the required power for leveled flight, P_R. The required power is calculated for each segment of the mission at certain air speeds, altitudes and temperature deviations from the ISA standard at sea level. Hence, at this stage the engine throttle, δ, is corrected and adjusted to match this condition of minimum consumption through an iterative process. This is one of the methods (in software it is designated as mode 2) in which it is possible to calculate the available power, P_A, given P_R and V. The iterative procedure is employed for each segment of the mission. Afterwards the mission energy consumed can be calculated [38]. For IC engines it is given, for each segment, by the total fuel consumed according to

$$W_{fuel_i}\,[N] = fc_i \Delta t_i = \left(bsfc \times P_{shaft} \times n_{engine} \times g\right)_i \times \Delta t_i \quad (3.1)$$

where n_{engine} is the number of engines, g the gravity acceleration constant in m/s^2, Δt_i the duration of the mission segment and $bsfc$ is the brake specific fuel consumption obtained from equation 2.8.

As for electric motors, the mission energy consumed for each mission segment is formulated as

$$E_i\,[J] = P_{ele_i} n_{engine} \Delta t_i = \left(U \times I + (\mathrm{R}_\Omega \times I^2 + R_U \times I^2)\right)_i \times n_{engine} \times \Delta t_i \quad (3.2)$$

where U is the input voltage, I is the input current. The electric power consumed, P_{ele}, takes into account energy losses due to the battery resistance, R_U, and motor speed controller resistance, R_Ω. Conclusively, the overall mission energy (the objective function) is given, for electric motors and IC engines respectively, by

$$E_m[J] = \sum_{i=1}^{k} E_i \quad (3.3)$$

$$W_{fuel}[N] = \sum_{i=1}^{k} W_{fuel_i} \quad (3.4)$$

where k is the total number of mission segments and E_i the energy required for each segment of the mission. With the objective function calculated, the algorithm is then applied according to the design engine and propeller input parameters, as well as the mission performance restrictions. The software applied the FFSQP subroutines to implement the optimization algorithm.

3.2 FFSQP subroutines

In this thesis, a gradient based algorithm (better accounted for in Section 1.4.2.1) was applied in the optimization procedure, through a set subroutines named FFSQP. FFSQP (FORTRAN Feasible Sequential Quadratic Programming) is a set of FORTRAN subroutines used for the minimization of the maximum of a set of smooth objective functions (in the context of this dissertation, the minimization of the maximum mission energy consumption), subject to general smooth constraints [39]. These set of constraints may be nonlinear or linear equality and inequality constraints, with certain boundaries limiting the design variables to be optimized. FFSQP applies the Sequential Quadratic Programming methodology for nonlinear optimization problems, which solves optimization problems in the form [39]

$$\min \quad \max_{i \in I}\{f_i(x_n)\} \quad set\ to \quad x \in X$$

where $f_i(x_n)$ is the objective function at each iteration and i is the iteration number, which belongs to the set of discrete variables $I = \{1,2, \dots, k\}$. X represents the totality of the feasible space, where a set of design variables, x, are constrained according to

$$lower\ boundary\ \leq x \leq upper\ boundary$$

and to a set of inequality constraints defined as

$$g_j(x_n) \leq\ reference\ constraint\ value,\ \ j = 1,2, \dots, m$$
$$\Leftrightarrow$$
$$g_j(x_n) -\ reference\ constraint\ value \leq 0$$

where m is the total number of mission constraints functions and the reference constraint value is the limitation set by the user for the mission parameters, which must not be exceeded. In this optimization problem, the SQP estimates the gradients of these functions by calculating the forward finite differences, presented in a very simplified manner in Fig.3.2. Δx is the algorithm increment set by the user.

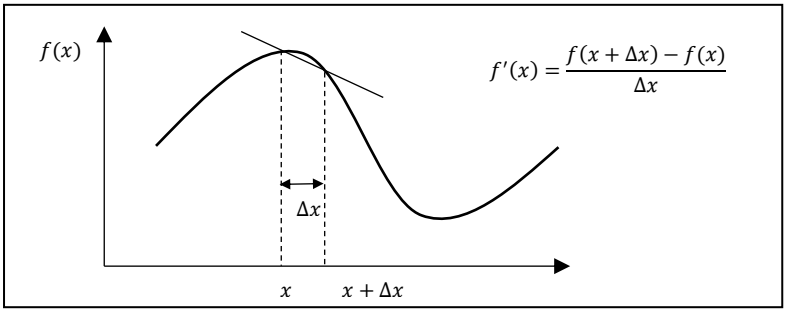

Figure 3.2 Simplified scheme of the forward finite differences method used to estimate the gradient at point x

At each iteration, the gradients of the functions enable the algorithm to find the direction in which to proceed, p_i. To proceed towards the minimum, the inner product between p_i and the gradients of the function at a certain iteration, $\nabla f(x_i)$, must be less than zero since the negative of a non-zero gradient is always a descent direction. In other terms

$$\langle p_i, \nabla f(x_i) \rangle < 0$$

indicates the descent direction of the objective function. Knowing the direction in which to proceed, the step length (α_i) is commuted. The algorithm obtains a satisfactory α_i if it reduces the value of the objective function, i.e.

$$f(x_i + p_i \alpha_i) < f(x_i)$$

While the algorithm increment, Δx, is a fixed step used to calculate the gradients, the step length, α_i, is an always changing step used to advance to the next x which minimizes the function. The computation of α_i is called line search, and the FFSQP subroutines can implement two different line search methods (monotone and non-monotone methods) [39]. If the condition above is satisfied, then the next x (design variable) value is updated to

$$x_{i+1} = x_i + p_i \alpha_i$$

and the algorithm initiates again its procedures, for a new updated design variable, and calculates the gradients according to the forward finite differences and the defined Δx. The optimum solution is achieved when the Hessian matrix of the objective function, $\nabla f(x_i)$, which contains the gradients of the functions at each iteration, converges to zero or to a very small tolerance value near zero, defined as ε. Fig.3.3 illustrates the overall SQP procedure, for a better understanding.

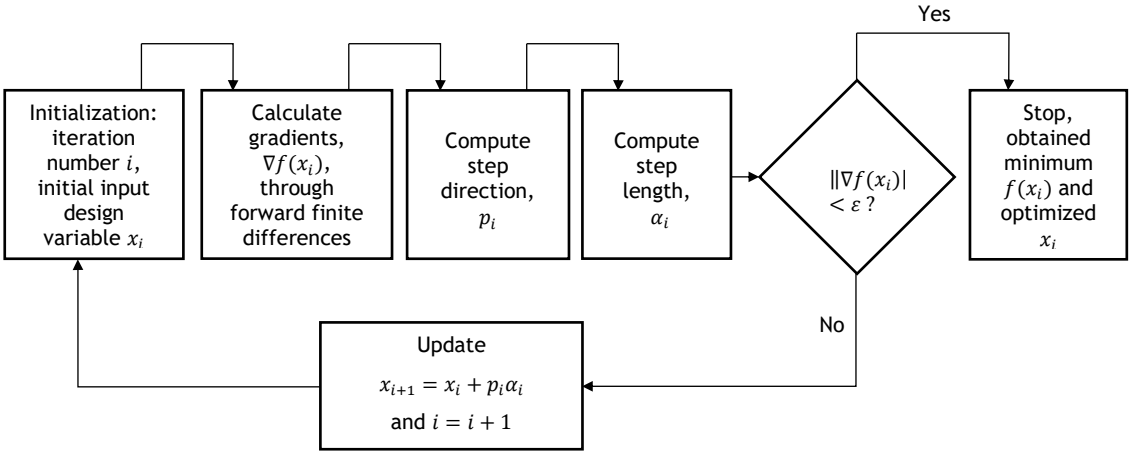

Figure 3.3 Sequential Quadratic Programming (SQP) optimization procedure

3.3 Engine performance parameters empirical study

The optimization software, before modifications were made, was giving the optimum solution for one specific engine, whose performance parameters were defined initially. In order for the software to be able to select from any engine from the data collected, there must exist a set of equations which can provide the values for these engine specifications as a function of certain design variables. Thus, performance data from real engines was collected and organized in a table format. With this empirical data, the relation between each parameter was analyzed, and charts were elaborated. Afterwards, the empirical models were obtained through a minimization of the sum of squared deviations of the predictions, which enables the minimization of the error associated with the coefficients. In other words, it minimizes the distance between the fitted line and all of the data points. Generally speaking, a model fits the data well if the differences between the data values and the values predicted by the model are as small as possible. The following sections better clarify this empirical study.

3.3.1 Empirical data collected on engine performance specifications

The IC engine specifications introduced originally into the optimization software for specific fuel consumption at full load, $bsfc_0$, maximum rated brake power, bp_{max}, rated speed, N_{max}, engine mass, M, minimum speed, N_{min}, and engine gear reduction, R_{gear}, corresponded to an engine defined initially by the user. Thus a search for data related to these engine parameters was made. The data was collected from diverse IC engines. In case of larger engines, it was collected from operator's manuals and data specifications sheets from Lycoming engines [40, 41, 42, 43, 44, 45, 46, 47], from Continental Motors [48, 49, 50, 51, 52], from Rotax engines [53, 54, 55, 56, 57, 58], from Limbach engines [59] and ULPower engines [60]. Otherwise, in the case of smaller engines like RC model airplanes, the data was collected from sales information provided by the manufactures, from O.S. engines [61], RCFG engines [62] and 3W engines [63]. Rated power, bp_{max}, rated speed, N_{max}, and especially the specific fuel consumption at full load/rated power, $bsfc_0$, may vary according to the type of IC engine, due to the different operating mechanisms that combustion engines present (briefly accounted for in section 1.4.3). Thus the models obtained are only an approximation, to use in the context of this specific optimization software.

The data for engine mass, M, rated power, bp_{max}, and the corresponding rated speed, N_{max}, were accessibly obtained for larger and smaller IC engines as they were explicitly specified by the manufacturer. However, the specific fuel consumption, $bsfc_0$, at bp_{max} and N_{max}, was not directly obtained as the data was not explicitly discriminated, and very hard to obtain in the case of smaller engines. Therefore the empirical data for $bsfc_0$ was obtained from charts available in manuals and specifications data sheets from large engines, which illustrated the variation of $bsfc$ in relation to engine speed, N, and engine power, bp. Also, some different charts represented the variation of $bsfc$ in relation to engine speed and available throttle, δ. Fig. 3.4 presents examples of these graphic representations.

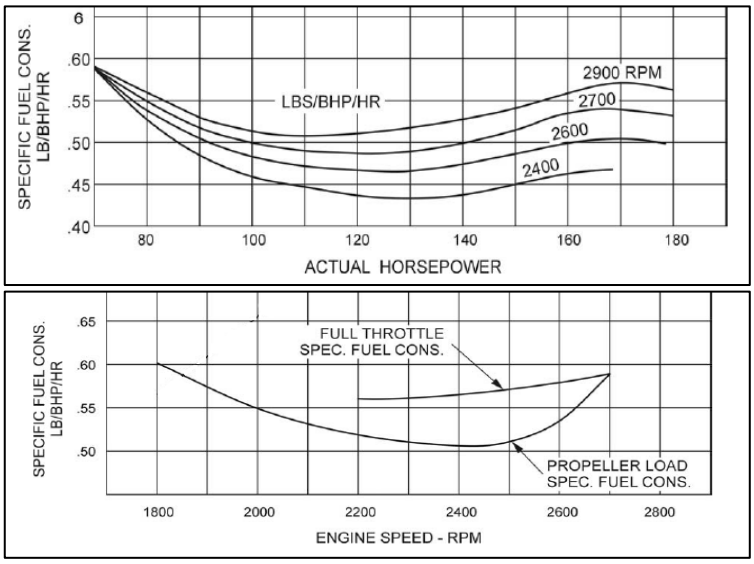

Figure 3.4 Typical specific fuel consumptions charts provided for Lycoming O-360 and HO-360 [47]

Specific fuel consumption at full load, $bsfc_0$, was obtained at each chart point which corresponded to the specific fuel consumption for rated power, bp_{max} (in some charts for full throttle), and rated speed, N_{max}, since $bsfc_0$ is achieved at these conditions. Furthermore, unit conversions were conveniently performed to kg/Ws. The empirical data collected for 197 engines is presented in table A-II in appendix A.

Regarding the electric motor specifications, among the original parameters introduced in the software for a fixed motor were the mass, M, motor no load current, I_0, maximum allowed current, I_{max}, speed constant, K_v, and motor resistance, R. The most accessible data was collected from small DC electric motors, powered by batteries (briefly accounted for in section 1.4.4) for small UAV's and RC models. Similarly to smaller IC combustion engines, the DC electric motor data was collected from sales information provided by the manufactures, from Turnigy, Propdrive, Keda, Scorpion and AXI electric motors, available in references [64, 65, 66]. The empirical data collected for 294 DC electric motors is presented in table B-II in appendix B.

3.3.2 Empirical correlation models for engine parameters

After the engine parameters data was collected, a study of the empirical correlation between dependent and independent variables was executed. The data was analyzed in Microsoft Excel, which performs linear regression (least square regression) and nonlinear regression through the add solver tool. By calculating the sum of the squared deviations between the real and the predicted value, i.e. $\sum_{i=1}^{k}(predicted\_value - real\_value)^2$, where k is the number of data elements, it is possible through the add solver tool to find the best fitting coefficients which minimize this squared sum. Afterwards, it was evaluated how close the data was to the fitted regression line created.

Hence, the regression tools in Excel perform the transformations and display in a chart the resulting modeling function and the coefficient of determination, R^2, which provides intuitive measure of how well the linear model fits a set of observations. Generally, the closer R^2 is to 100%, the better the model explains all the variability of the response data around its mean, providing a reasonable validation of the empirical model function. However, it is important to underline that the models created are approximations, always with a certain error associated with the function coefficients.

Therefore to obtain these empirical models, the correlation between the data parameters was investigated. It was necessary to obtain models for two IC engines parameters, $bsfc_0$ and mass, M, and three electric motors parameters, I_0, R and also M, as a function of certain input predictor/design variables.

The models obtained regarding the IC engine will be presented first. The empirical analysis revealed that the engine mass, M, was dependent on two independent parameters, bp_{max} and N_{max}, as it can be clearly observed in the tendencies illustrated in the charts below, with the respective model function and R^2 discriminated.

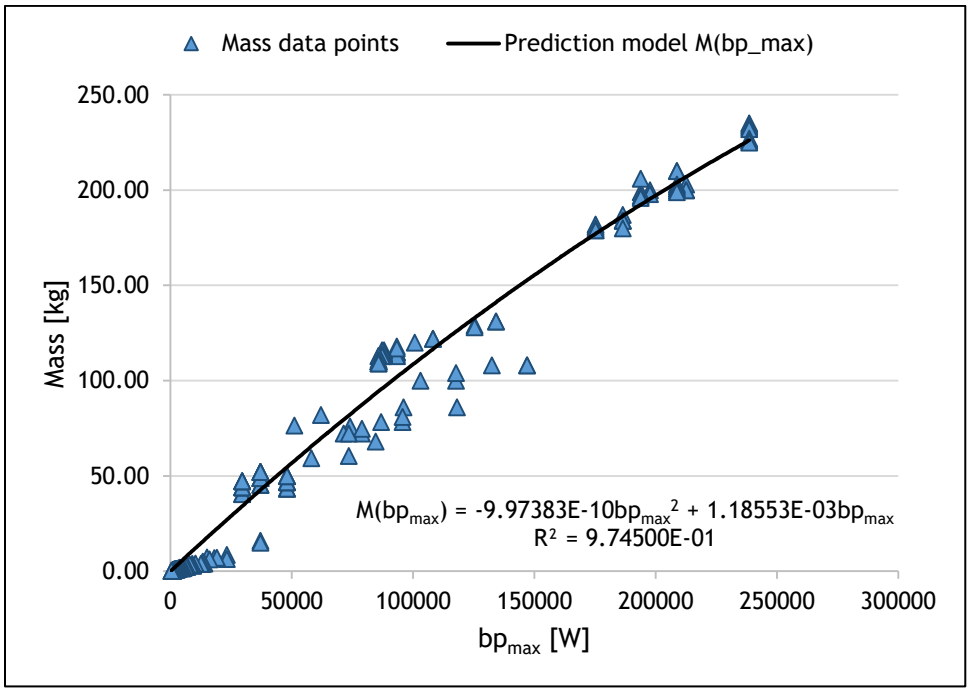

Figure 3.5 Engine mass relation with rated power, bp_{max}, for 197 IC engines

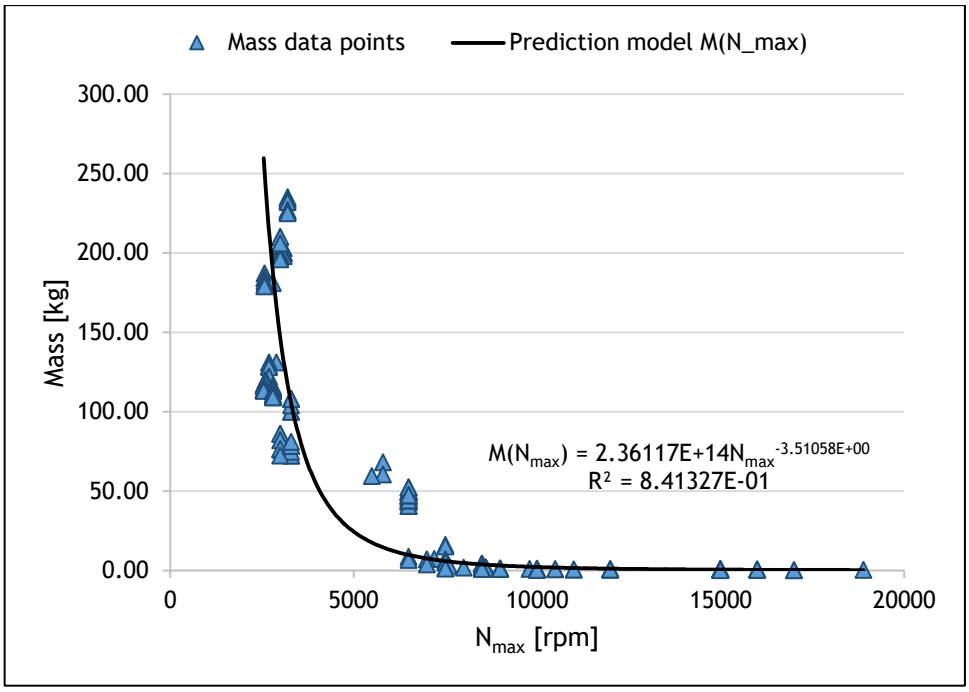

Figure 3.6 Engine mass relation with rated speed, N_{max}, for 197 IC engines

The charts presented in Fig. 3.5 and 3.6 illustrate that a proportional mass variation with rated power, and inversely proportional variation with speed exists. Hence there must also exist another model which considers both bp_{max} and N_{max} as inputs. Assuming a function in the form $M(bp_{max}, N_{max}) = \alpha_1 \times bp_{max}^{\alpha_2} \times N_{max}^{\alpha_3}$ and with the add solver tool, it was possible to obtain the best fitting coefficients, α_1, α_2 and α_3, which minimize best the sum of squared deviations between the predicted values and the actual data values. Hence one more mass empirical model for IC engines was obtained, and can be formulated as

$$M(bp_{max}, N_{max})\,[kg] = 0.12165 \times bp_{max}^{0.82408} \times N_{max}^{-0.33440} \quad (3.5)$$

where $\alpha_1 = 0.12165$, $\alpha_2 = 0.82408$ and $\alpha_3 = -0.33440$. After comparing the three possible models, it was proven that $M(bp_{max}, N_{max})$ presented the least squared deviation sum in relation to the other two models presented in Fig. 3.5 and 3.6, as it can be observed in table 3.1. It was therefore the best fitting model selected for the optimization software.

Table 3.1 Squared deviation sum for the three different mass empirical models analyzed

	$\boldsymbol{M(bp_{max})}$	$\boldsymbol{M(N_{max})}$	$\boldsymbol{M(bp_{max}, N_{max})}$
$\sum_{i=1}^{k}(predicted\_value - real\_value)^2$, for $k = 197$ IC engines	1.35793E+02	2.85043E+03	1.10533E+02

Below follows the chart which demonstrates graphically that the prediction model presented in equation 3.5 presents the minimum deviation from the real data values.

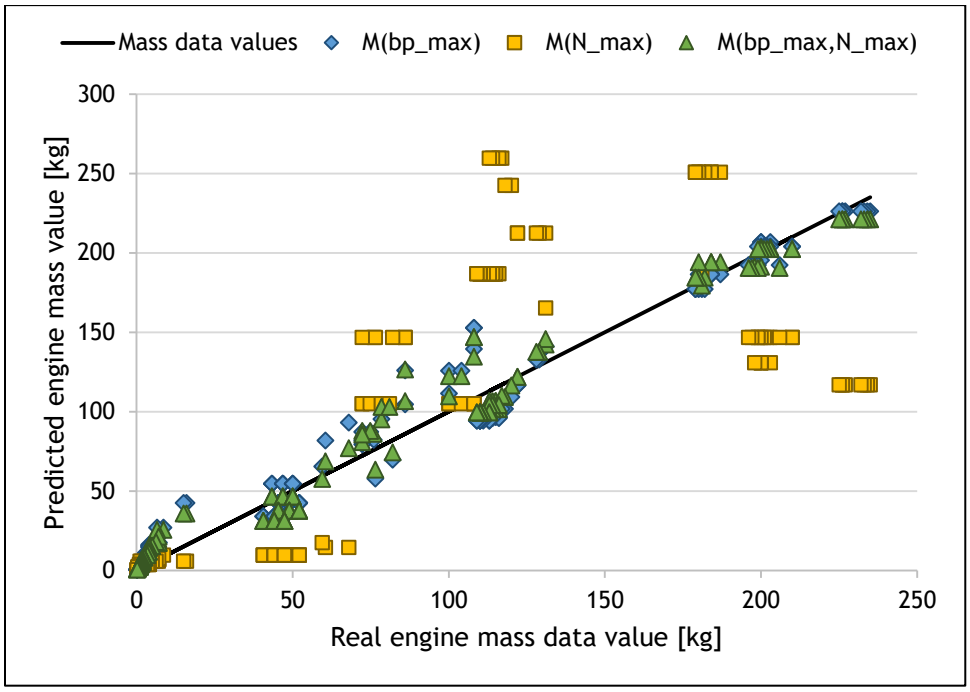

Figure 3.7 Deviation of the predicted engine mass values from the real data values

As for the specific fuel consumption, $bsfc_0$, the empirical analysis revealed that it was dependent on rated power, bp_{max}, as it is illustrated in Fig. 3.8. Not all engines displayed information regarding the specific fuel consumption, especially small UAV engines, and thus the analysis was performed for 118 larger IC engines.

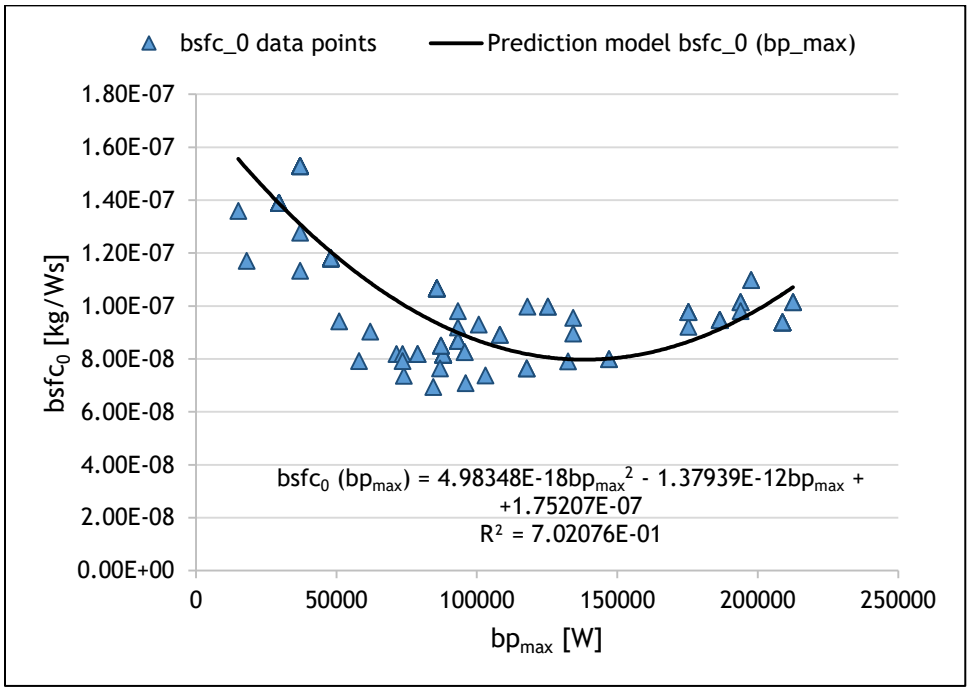

Figure 3.8 Engine maximum specific fuel consumption, $bsfc_0$, with rated power, bp_{max}, for 118 engines

Additionally, the relation between fc_0 with rated power was also studied, knowing that

$$bsfc_0\ [kg/Ws] = \frac{fc_0}{bp_{max}} \Leftrightarrow fc_0\ [kg/s] = bsfc_0 \times bp_{max} \quad (3.6)$$

The resulting proportional relation is presented in Fig. 3.9 below.

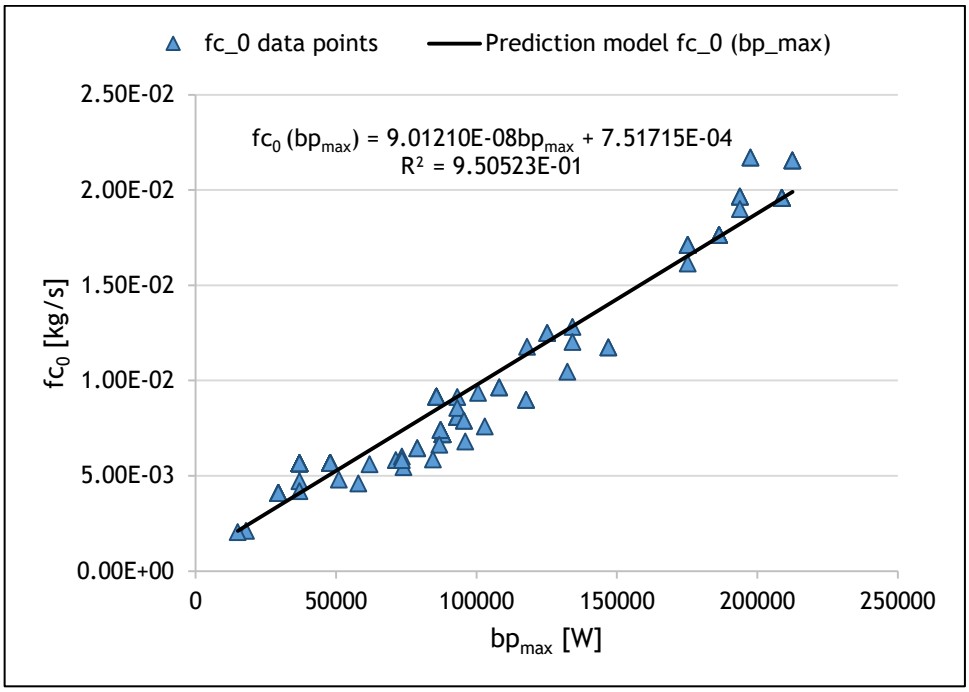

Figure 3.9 Engine maximum fuel consumption fc_0, with rated power, bp_{max}, for 118 IC engines

Hence fc_0, which intuitively increases with rated power, can be expressed by a linear function in the form $fc_0 = \beta_1 \times bp_{max} + \beta_2$ and consequently, another alternative function to express maximum specific fuel consumption, $bsfc_0'$, is obtained. Considering equation 3.6, $bsfc_0'$ is obtained by

$$fc_0\ [kg/s] = \beta_1 \times bp_{max} + \beta_2 \quad (3.7)$$

$$bsfc_0'\ [kg/Ws] = \frac{\beta_1 \times bp_{max}}{bp_{max}} + \frac{\beta_2}{bp_{max}} \quad (3.7a)$$

$$bsfc_0'\ [kg/Ws] = \beta_1 + \frac{\beta_2}{bp_{max}} \quad (3.7b)$$

Again, with the add solver tool it was possible to calculate the coefficients, β_1 and β_2, which better minimize the squared sum deviation. The obtained function is presented as

$$bsfc_0'(bp_{max})\ [kg/Ws] = 9.0121E-08 + \frac{7.5172E-04}{bp_{max}} \quad (3.8)$$

where $\beta_1 = 9.0121E-08$ and $\beta_2 = 7.5172E-04$. After comparing the two possible models, it was observed that the model presented in equation 3.8 provides the least squared sum of the deviation between the real and predicted values, as it is presented in table 3.2.

Table 3.2 Squared deviation sum for the two different $bsfc_0$ empirical models analyzed

	$\boldsymbol{bsfc_0(bp_{max})}$	$\boldsymbol{bsfc_0'(bp_{max})}$
$\sum_{i=1}^{k}(predicted\_value - real\_value)^2$, for $k = 118$ IC engines	1.23177E-07	4.58918E-10

Hence $bsfc'_0\ (bp_{max})$ was the best fitting model selected, used to assume the missing $bsfc_0$ data from the remaining small IC engines. Below is presented the deviation of these two models.

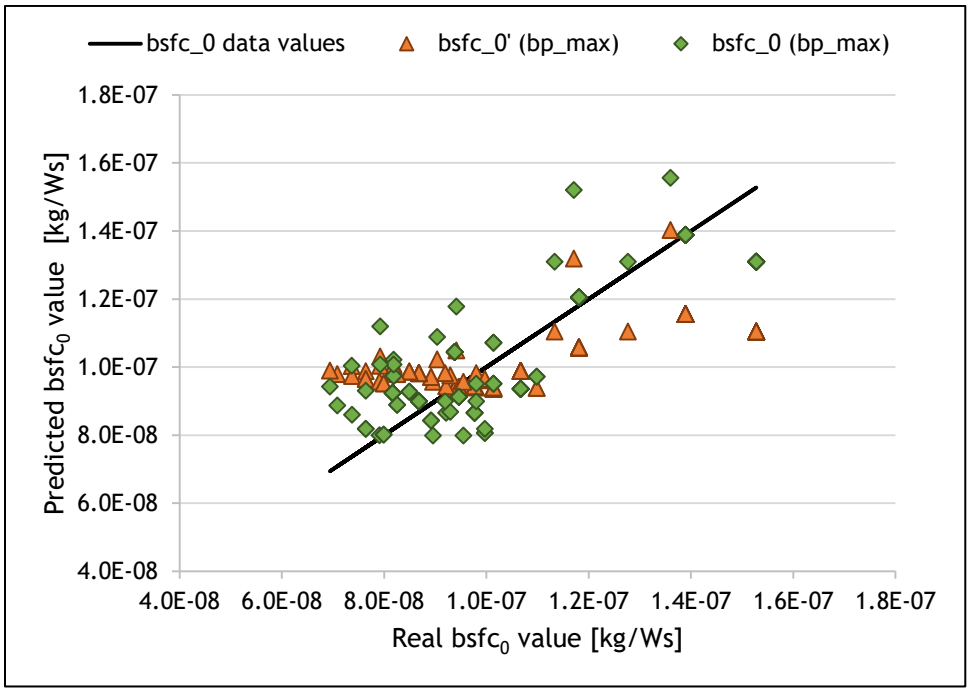

Figure 3.10 Deviation of the predicted $bsfc_0$ values from the real data values

In conclusion, the two empirical IC engine models selected for the optimization software, which best predict the output specifications in accordance with the design variables are

$$M(bp_{max}, N_{max})\ [kg] = 0.12165 \times bp_{max}^{0.82408} \times N_{max}^{-0.33440} \quad (3.5)$$

$$bsfc_0'(bp_{max})\ [kg/Ws] = 9.0121E-08 + \frac{7.5172E-04}{bp_{max}} \quad (3.8)$$

Concerning the electric motors, it was intended to find the best fitting models for motor mass, M, motor no load current, I_0 and motor resistance, R, as a function of certain input predictor/design variables. After analyzing the correlation between the motor parameters, it was observed that motor mass is dependent on two design variables, motor speed constant, K_v, and maximum allowed current, I_{max}. Below follow the charts which present these tendencies, with the respective model function and R^2 discriminated.

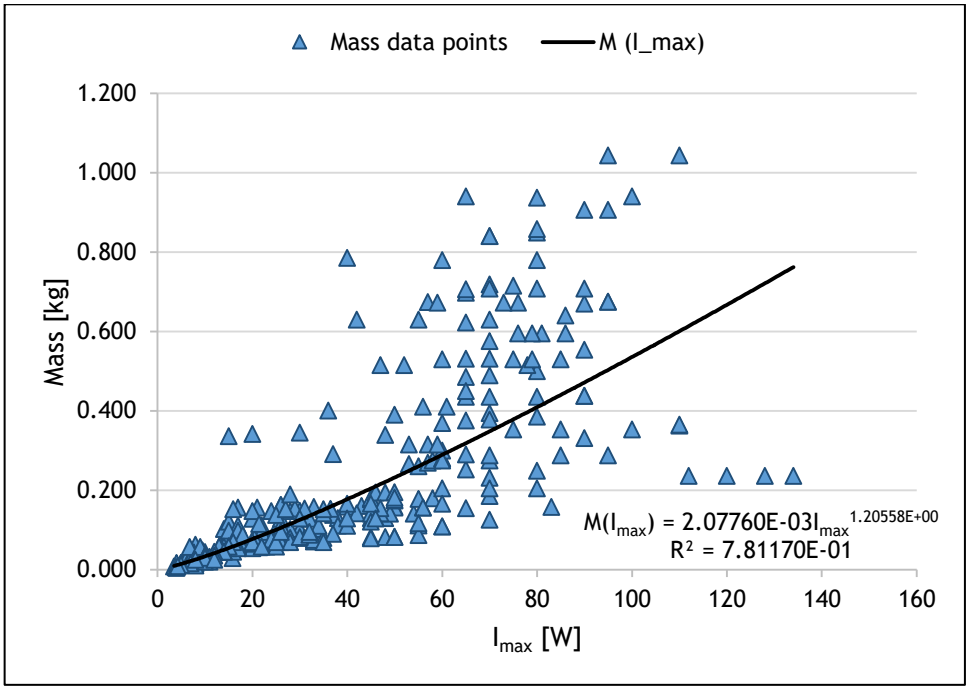

Figure 3.11 Motor mass relation with maximum allowed current, I_{max}, for 294 electric motors

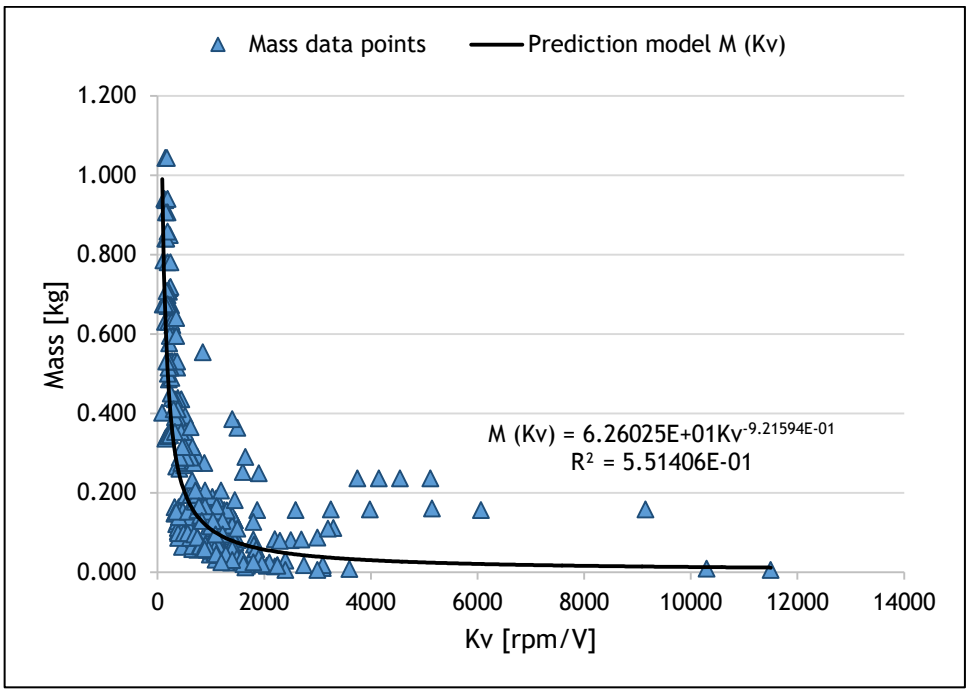

Figure 3.12 Motor mass relation with motor speed constant, Kv for 294 electric motors

Fig. 3.11 and 3.12 demonstrate that motor mass varies proportionally with I_{max}, and inversely with Kv. Thus there must also exist another motor mass empirical model which considers both Kv and I_{max} as input design variables. Similarly to the IC engine mass model described previously, it was possible to determine a function in the form $M\ (I_{max}, K_v) = \alpha_1 \times (I_{max})^{\alpha_2} \times Kv^{\alpha_3}$, by minimizing the squared sum deviation associated with the coefficients α_1, α_2 and α_3. The obtained function was then

$$M\ (I_{max}, K_v)\ [kg] = 0.4965 \times (I_{max})^{0.8265} \times Kv^{-0.6176} \quad (3.9)$$

where $\alpha_1 = 0.4965$, $\alpha_2 = 0.8265$and $\alpha_3 = -0.6176$. By comparing the three different models, it was concluded that the best fitting function which minimizes best the deviation is $M\ (I_{max}, Kv)$, as presented in table 3.3.

Table 3.3 Squared deviation sum for the three different motor mass empirical models analyzed

	$\boldsymbol{M(I_{max})}$	$\boldsymbol{M(Kv)}$	$\boldsymbol{M(I_{max}, Kv)}$
$\sum_{i=1}^{k}(predicted\_value - real\_value)^2$, for $k = 294$ electric motors	2.78018E-02	1.9934441E-02	4.80994E-03

Hence $M\ (I_{max}, K_v)$ was the model selected to use in the software, since it best predicts motor mass. Fig. 3.13 displays the graphical representation of the three models deviations, for a better comparison.

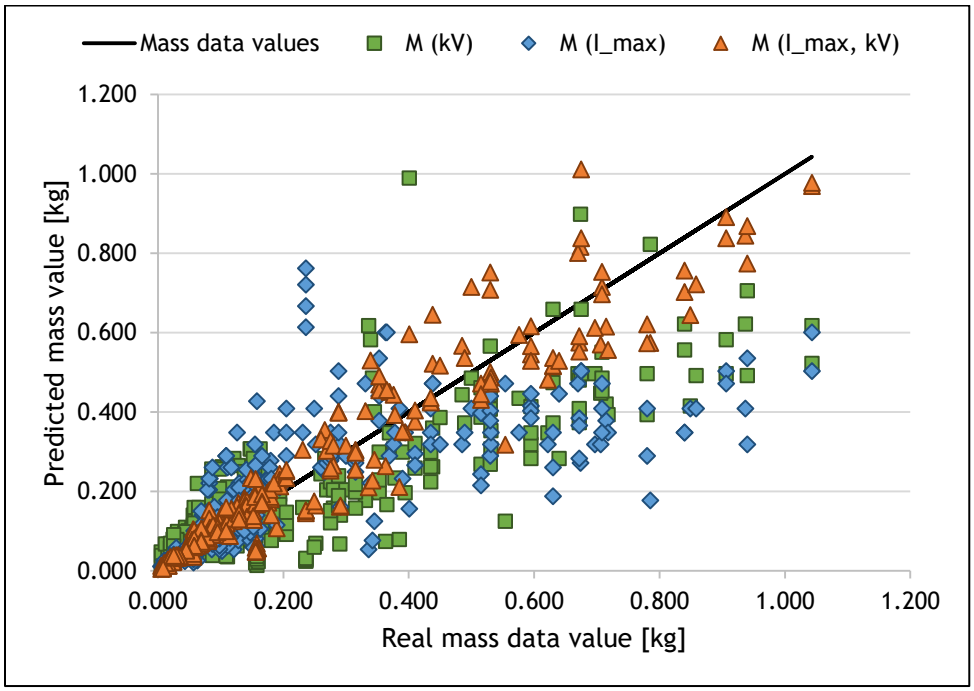

Figure 3.13 Deviation of the predicted motor mass values from the real data values

Another specification required in the software, as a function of a design variable, was motor electric resistance, R. After considering all the empirical relations between the motor parameters, it was observed that the only significant tendency was the relation between R and motor maximum allowed current, I_{max}, since all other design variables prove to be very unrelated to motor resistance. Hence only one model, $R\ (I_{max})$, evidenced a clear trend. Fig. 3.14 illustrates this relation, whereas Fig. 3.15 presents the deviation error of the predicted values, knowing that the model $R\ (I_{max})$ presented a squared deviation sum of 2.093463E-03.

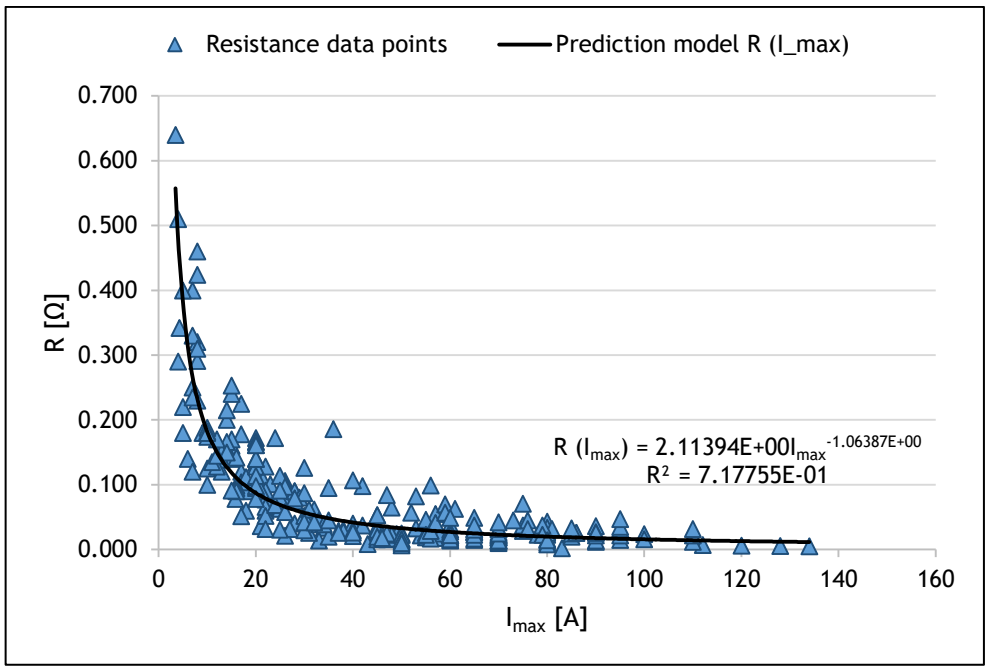

Figure 3.14 Motor resistance relation with maximum allowed current, I_{max}, for 265 electric motors

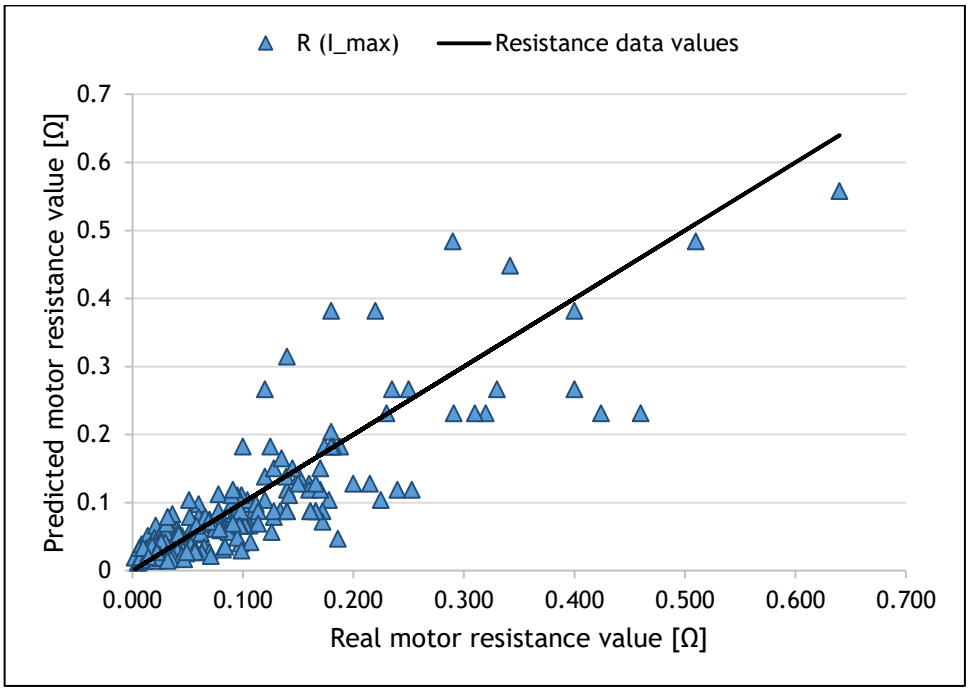

Figure 3.15 Deviation of the predicted motor resistance values from the real data values

Naturally, the error tends to propagate and increases for more ambitious predictions for resistance values larger and farther way from the data collected. Important to note that this model, translated by the function

$$R\ (I_{max})\ [\Omega] = 2.1139 \times I_{max}^{-1.0639} \quad (3.10)$$

was used to assume the motor resistance values of the remaining motors, since it was not always provided by the manufacture.

The last specification model required, as function of certain input design variables, was the motor no load current, I_0. After studying the various correlations between the parameters, for 158 electric motors, it was revealed that I_0 presented a significant inversely proportional tendency with motor resistance, R. This trend is in fact quite coherent, since I_0 is the required current to overcome motor internal resistance and will naturally vary according with it. Although motor resistance, R, is not directly an input design variable in the software, it can be calculated according to the input design variable I_{max} through the empirical model described previously, $R\ (I_{max})$, which, although is not 100% assertive, presents a reliable approximation. Hence, by logic, I_0 will also present a relation with motor maximum allowed current. In fact, a slight tendency with motor I_{max} was revealed, although not so suitable fitting as the relation between no load current and resistance. Below follow the charts which present these no load current empirical models, with the corresponding functions and R^2 discriminated, for 158 electric motors.

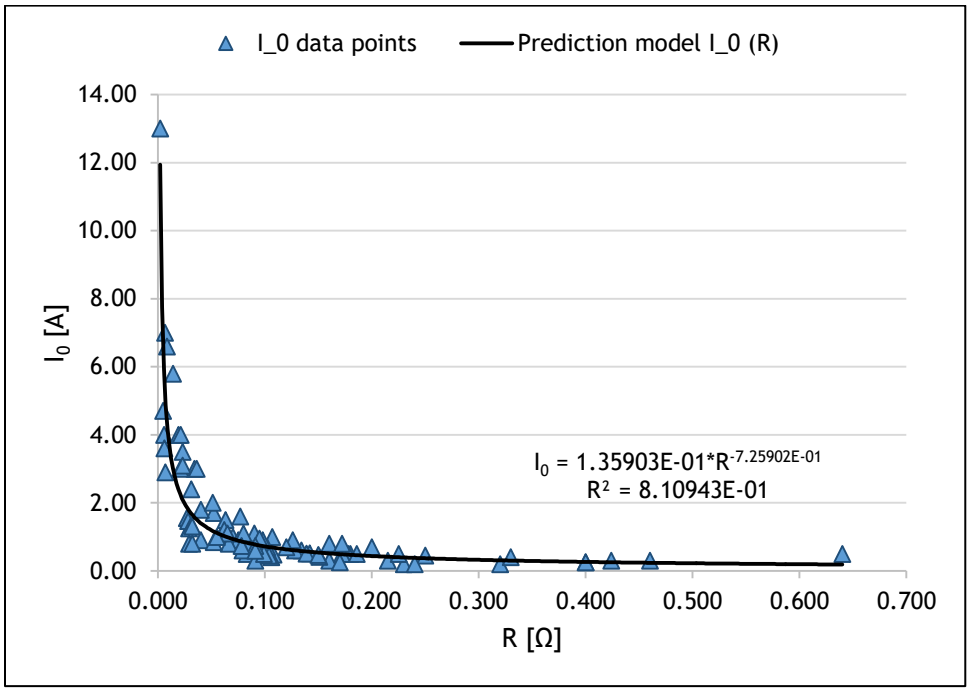

Figure 3.16 Motor no load current relation with motor resistance, R, for 158 electric motors

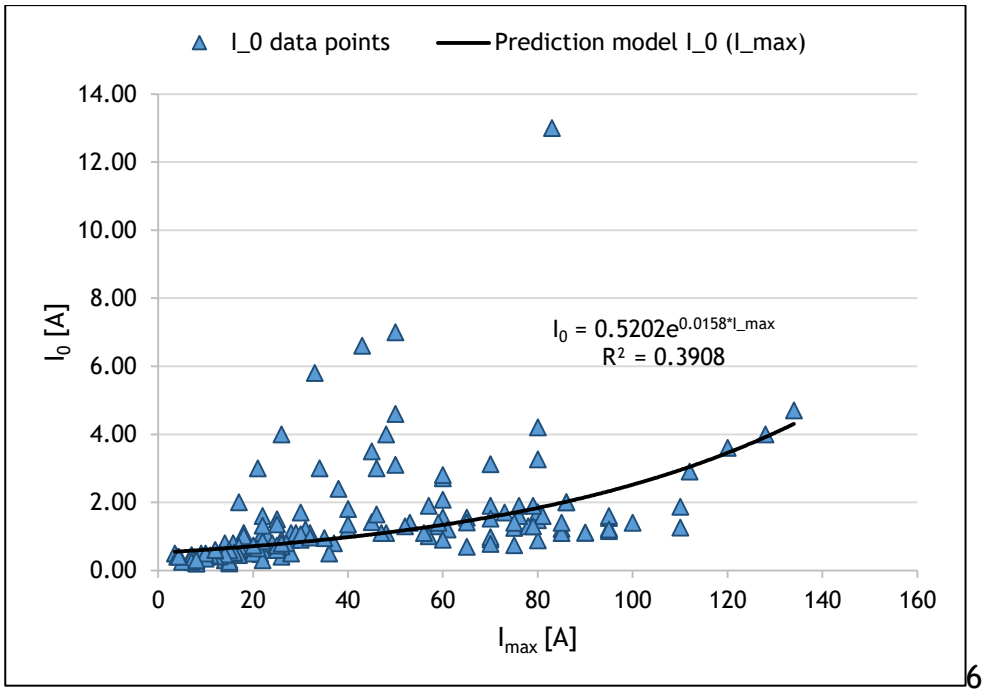

Figure 3.17 Motor no load current relation with maximum current, I_{max}, for 158 electric motors

Fig. 3.16 and 3.17 demonstrates that motor no load current, I_0, varies with motor resistance and maximum allowed current. Thus there must also exist another no load current empirical function which considers both R and I_{max} as inputs, in the form of $I_0(R, I_{max}) = \gamma_1 \times R^{\gamma_2} \times I_{max}^{\gamma_3}$. By minimizing the squared deviation sum associated with the coefficients γ_1, γ_2 and γ_3 through the add solver tool, the resulting function was

$$I_0\,(R, I_{max})\,[A] = 0.4999 \times R^{-0.8947} \times I_{max}^{-0.5047} \quad (3.11)$$

where $\gamma_1 = 0.4999$, $\gamma_2 = -0.8947$ and $\gamma_3 = -0.5047$. By comparing the three different models, it was concluded that the model $I_0\,(R, I_{max})$ presented the least deviation between the no load current predicted values and the real data values, and it was the selected function introduced in the software. Additionally, it was used to assume the values of the motor no load current values of the remaining motors, since it was not always provided by the manufacture. The squared deviations for the three models can be consulted in table 3.4 and visually confirmed in Fig. 3.18.

Table 3.4 Squared deviation sum for the three different motor I_0 empirical models analyzed

	$\boldsymbol{I_0(R)}$	$\boldsymbol{I_0(I_{max})}$	$\boldsymbol{I_0(R, I_{max})}$
$\sum_{i=1}^{k}(predicted\_value - real\_value)^2$, for $k = 158$ electric motors	4.86009E-01	1.97756E+00	3.12793E-01

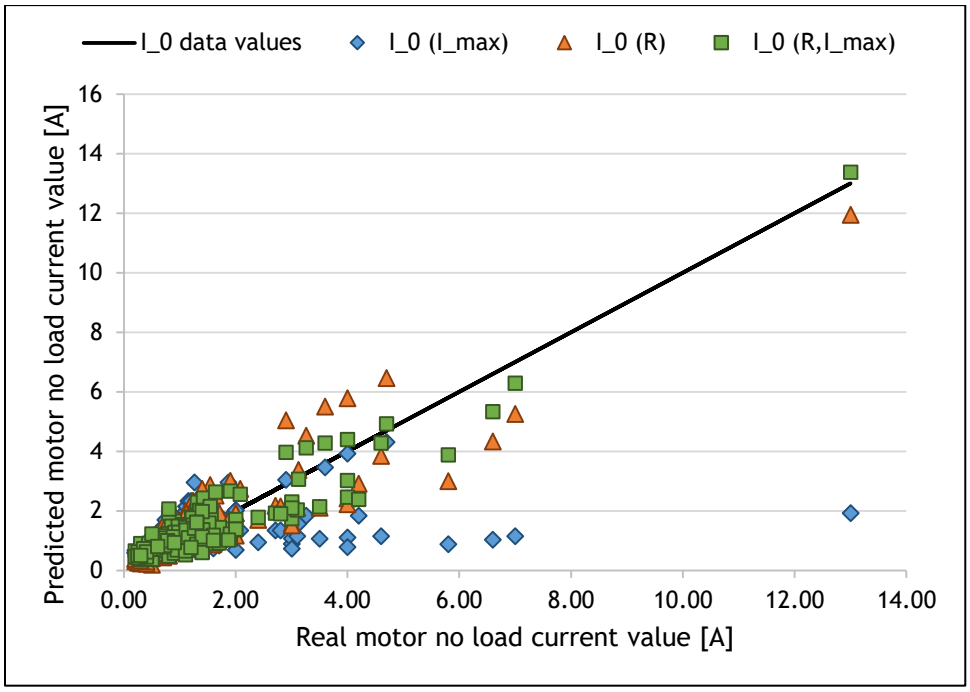

Figure 3.18 Deviation of the predicted motor no load current values from the real data values

In conclusion, the three motor empirical models selected for the optimization software, which best predict the output specifications in accordance with the design variables are

$$M\ (I_{max}, K_v)\ [kg] = 0.4965 \times (I_{max})^{0.8265} \times Kv^{-0.6176} \quad (3.9),$$

$$R\ (I_{max})\ [\Omega] = 2.1139 \times I_{max}^{-1.0639} \quad (3.10)$$

and

$$I_0\ (R, I_{max})\ [A] = \ 0.4999 \times R^{-0.8947} \times I_{max}^{-0.5047} \quad (3.11)$$

Therefore, the output specifications for IC engines are M and $bsfc_0$, and for electric motors M, R and I_0. More relevant still are the input design variables, which for IC engines are bp_{max} and N_{max}, and for electric motors I_{max}, and Kv.

These are the design variables which will be subjected to the constraints defined by the user (i.e. $lower \leq x \leq upper$, as referred in section 3.2). They will mold the feasible space and will take part in the iterations of the algorithm, returning for each iteration the output engine specifications required for the calculation of the objective function. When the algorithm finally converges to the minimum solution desired, the program will return the design variables of the last iteration, which match this optimum solution. Finally, with the virtual optimum values for the engine design parameters obtained, it is possible to select, from the data base created, an engine with the design variables as close as possible as the ones returned by the software.

3.4 Application of the empirical models by the software

After obtaining the empirical models for the IC engine and electric motor, the respective models equations were introduce into a subroutine of the software. For combustion engines, the user is allowed to input certain design values for bp_{max} and N_{max}. These inputs are then read by the software and used in the subroutine to calculate engine mass, M, and $bsfc_0$. Similarly, for electric motors the user is allowed to input certain design values for I_{max} and Kv, used in the subroutine to calculate M, R and I_0. Important to underline that the software gives the optimum solution for a certain mission, providing not only the optimized propeller diameter and pitch, but also the mission required maximum throttle, required maximum engine speed, and required maximum current. Consequently, in order to ensure that the inputted design variables are at least superior to the minimum required for the mission, the software ascertains that the overall maximum current and engine speed required for the mission, ${I_{max}}'$ and ${N_{max}}'$, must not exceed the inputted I_{max} and N_{max}. Fig. 3.19 illustrates an example of a simple mission (which is also inputted in the software by the user) where phase 1 represents takeoff, 2 the climbing stage, 3 the cruise flight, 4 the descending stage and 5 the landing stage. Each stage requires a minimum motor current (for electric motors only) and engine speed.

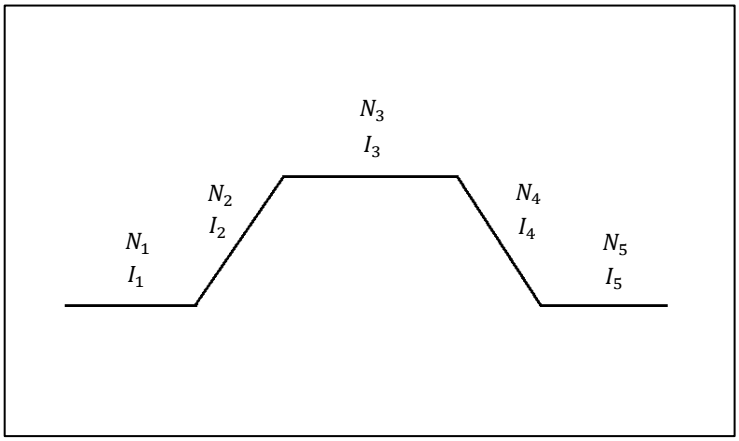

Figure 3.19 Required current and engine speed for different mission stages

Hence the overall maximum allowed current and rated engine speed for this particular mission, ${I_{max}}'$ and ${N_{max}}'$, matches the maximum among the different stage requirements and must not surpass the design variable defined by the user. In other words

$$ {I_{max}}' \, [A] = max(I_1, I_2, I_3, I_4, I_5) \quad (3.12) $$

$$ {N_{max}}' \, [rpm] = max(N_1, N_2, N_3, N_4, N_5) \quad (3.13) $$

$$ {I_{max}}' \leq I_{max} \quad (3.14) $$

$$ {N_{max}}' \leq N_{max} \quad (3.15) $$

Another important calculation performed throughout the optimization procedure is the aircraft weight update. Since the engine/motor empirical models return the motor weight as an output, during each iteration there must occur an update of the total aircraft weight, considering the new propeller mass and the new engine mass. Hence at an initial stage the software reads the information regarding the original propeller and engine masses, as well as all the aircraft masses (structure, systems, payload, and fuel or battery mass depending on the type of engine, given by M_{energy}). In other words

$$M_{aircraft}\,[kg] = M_{structure} + M_{systems} + M_{payload} + M_{energy} + M_{original\,prop} + M_{original\,eng} \quad (3.16)$$

Since the original propeller and engine are to be optimized and thus their weights change at each iteration of the algorithm, i, the software needs to update $M_{aicraft}$. Hence the propeller mass, M_{prop_i}, is updated at each iteration according to the new diameter value, D_i, and is given by

$$M_{prop_i}\,[kg] = M_{original\,prop} \times \left(\frac{D_i}{D_{original}}\right)^3 \quad (3.17)$$

where $D_{original}$ is the original propeller diameter. The engine mass, M_{engine_i}, is calculated according to the empirical models described previously in equations 3.6 and 3.10.

Thus, the updated aircraft weight is formulated by adding the increments which resulted from the difference between the updated masses and the original ones, i.e.

$$W_{aircraft_i}\,[N] = g \times \left[M_{aircraft} + (M_{engine_i} - M_{original\,eng}) + (M_{prop_i} - M_{original\,prop})\right] \quad (3.18)$$

However, the optimization procedure does not take into account the effects caused by the updated weight on the aircraft center of gravity, and therefore the optimized result is just an approximated estimation.

3.5 Engine selection

After the algorithm is applied and the optimum solution is achieved, the engine/motor which matches the specifications given by the empirical models is selected from the data tables. The selection is made based on the minimum squared deviation sum between the design specifications given by the empirical functions and the design specifications available in the data tables, represented with the subscript $data$. The design variables are the most important parameters to take into consideration when selecting an engine/motor. Therefore a larger weight was given to them when calculating the squared deviation sum. For IC engines, the design variables bp_{max} and N_{max} were given a weight of 40% each, in order to be the main influencers of the resulting squared error sum equation. N_{min} was given a weight of 10%, and

the outputs $bsfc_0$ and M were given a weight of 5% each. The position of the table line is given by the index j. For the IC engine selection, the squared deviation sum is given by

$$\sum_{1}^{k} error_{IC\ engine}(j)^2 = 0.4\left[\frac{bp_{max\ data}(j)}{bp_{max}} - 1\right]^2 + 0.4\left[\frac{N_{\underset{data}{max}}(j) * R_{gear}}{N_{max} * R_{gear}} - 1\right]^2 +$$

$$+ 0.1\left[\frac{N_{\underset{data}{min}}(j) \times R_{gear}}{N_{min} * R_{gear}} - 1\right]^2 + 0.05\left[\frac{bsfc_{0_{data}}(j)}{bsfc_0} - 1\right]^2 + 0.05\left[\frac{M_{data}(j)}{M} - 1\right]^2 \quad (3.19)$$

where k stands for the total number of data elements of the table. Some engines have a reduction gear which reduce the available rotational speed at the propeller. Hence, knowing the engine gear ration, the real rotational speed at the propeller shaft is obtained by the product between $N_{\underset{data}{max}}(j) \times R_{gear}$.

Likewise, for the electric motor selection, the design variables were given a larger weight. Kv and I_{max} were given a weight of 40% each. The output R was given a weight of 10%, and I_0 and M were given a weight of 5% each. The squared error sum is given by

$$\sum_{1}^{k} error_{Electric\ motor}(j)^2 = 0.4\left[\frac{I_{max\ data}(j)}{I_{max}} - 1\right]^2 + 0.4\left[\frac{Kv_{data}(j)}{Kv} - 1\right]^2 +$$

$$+ 0.1\left[\frac{R_{data}(j)}{R} - 1\right]^2 + 0.05\left[\frac{I_{0_{data}}(j)}{I_0} - 1\right]^2 + 0.05\left[\frac{M_{data}(j)}{M} - 1\right]^2 \quad (3.20)$$

After calculating the relative error for each element of the data table, the most suitable engine is the one whose index position in the table matches the index position of the minimum squared error sum value, since it deviates the least from the design specifications given by the empirical equations. In other words, the index corresponds to the location of the minimum value in the relative error vector, i.e.

$$min\ (squared\ error_1, squared\ error_2, \ldots\ldots, squared\ error_k) \quad (3.21)$$

where k stands for the total number of data elements of the table. These calculations are performed by a subroutine called after the implementation of the optimization algorithm, when the optimized design variables are obtained.

The software then displays a list with the 10 most similar engines/motors from the data base, which present the least squared deviation from the design variables given by the program. Preferably, the selected engine should be among the firsts of the list.

3.6 Mission performance parameters calculation

Another important objective of this dissertation was to add certain mission constraints in the analysis software, to be incorporated in the optimization algorithm. As it was stated before in section 3.2, the optimization algorithm subjects the objective function to a set of equality and inequality constraints, which defines the feasible space for the independent variables. The inequality constraints already available in the software were engine performance constraints, which limited not only the maximum allowed engine setting, δ_{max}, but also the maximum allowed current, I_{max}, or the maximum allowed engine speed, N_{max}, depending on the type of engine selected by the user (electric motor or IC engine).

Hence, a set of mission performance constraints was added. The user may define the limits for the feasible space, and how many constraints are to be active. The software then proceeds to calculate the mission parameter required and compares it to the constraint reference value initially defined. For that purpose, it was added into the software these parameters calculation, as well as the possibility for the user to select and define the algorithm mission constraints.

Most of the theoretical clarifications on the equations used for the parameters calculations, concerning mission performance, were already presented in section 2.4. Furthermore, the mission constraints were calculated for certain conditions of air speed, V, engine throttle, δ, altitude, h, and temperature deviation from standard sea level, dT. These later two conditions are defined also by the user. Thus, in order to influence the overall mission performance, the intended restrictions were applied to the takeoff runway distance, S_{TO}, maximum rate of climb, RC_{max}, maximum rate of climb angle, γ_{max}, maximum air speed, V_{max}, and minimum rate of climb for service ceiling, $RC_{sc_{min}}$ (a safety margin, in order not to reach a null value for excess of power available, ΔP). Regarding the performance for a level flight turn, the constraints added to the software limited the engine throttle required during a sustained turn, δ_{turn}, for certain conditions of altitude and limit load factor, also both defined initially by the user. Summarizing, the mission performance constrains can be modeled as

$$S_{TO} \leq S_{TO_{ref}} \quad at\ h_{TO} \quad (3.22)$$

$$\gamma_{max} \geq \gamma_{max_{ref}} \quad at\ h_{\gamma}\ and\ C_L * 1.44 \leq C_{L_{max}} \quad (3.23)$$

$$RC_{max} \geq RC_{max_{ref}} \quad at\ h_{RC}\ and\ C_L * 1.44 \leq C_{L_{max}} \quad (3.24)$$

$$V_{max} \geq V_{max_{ref}} \quad at\ h_{V_{max}} \quad (3.25)$$

$$RC_{sc_{min}} \geq 0.5\ [m/s] \quad at\ h_{sc}\ for\ C_L * 1.44 \leq C_{L_{max}} \quad (3.26)$$

$$\delta_{turn} \leq 1 \quad at\ h_{turn}\ and\ n_{limit} \quad (3.27)$$

where h_{TO} represents the takeoff speed altitude, h_{RC} the climb performance altitude, $h_{V_{max}}$ the maximum speed altitude, h_{sc} the service ceiling altitude and h_{turn} the altitude for a sustained turn, all set by the user. These maximum performance parameters calculation are performed by a subroutine named $PerformanceVariableCalculation()$.

Although this subroutine calculations for takeoff ground roll, S_{TO}, and engine throttle during a sustained turn, δ_{turn}, are fairly directly obtained through the application of the required equations presented in section 2.4, the remaining performance constraints concerning maximum speed, V_{max}, best rate of climb, RC_{max} and best rate of climb angle, γ_{max}, do not have a specific equation formulation. However, they are easily verified through graphical representations as a function of air speed, V. Hence, V_{max} is determined by the high speed intersection of the available power and required power curves represented in Fig. 2.17, whereas as γ_{max} and RC_{max}, according to Fig. 2.19, are determined at the maximum point of the parabolic curve. Since the speed at which these maximum conditions occur is not known, three iterations were performed in the software to match the desired maximum conditions. All iterations start initially at $1.2 \times V_s$ and continuously perform calculations for each speed, V, which increases according to a defined step value.

For maximum speed calculation, V_{max}, the iteration would ideally stop when the difference between available and required power, P_A and P_R, was null. Since this difference is never exactly equal to zero, the iteration was set to stop when the relative error of the difference between P_A and P_R was less than 0.1%. Hence the condition is formulated as

$$if\left(abs\left(\frac{P_A}{P_R} - 1\right) \leq 0.001\right)\ exit \quad (3.28)$$

and the returned speed value for this condition matches the maximum allowed speed, V_{max}. If this condition is not met, the subroutine would continuously calculate P_A and P_R until the available power was less than the required power, i.e. $P_A \leq P_R$. At this stage, the iteration would start again at the immediate preceding speed value, $V = V - step$, with an inferior step, $step = 0.5 * step$.

As for best rate of climb angle and best rate of climb, γ_{max} and RC_{max}, they both present the same type of parabolic curve when plotted as a function of V, so the same iterative process

was applied. The iteration would ideally stop when, as speed increases, the following value (RC_{i+1} or γ_{i+1}) would be less than the previous one (RC_i or γ_i), and the difference between them is null, since it matches the maximum point of the parabolic curve, before the descending phase. Since this difference is never exactly equal to zero, the iteration was set to stop when the relative error of the difference between the following value, $i+1$, and previous one, i, is less than 0.01%, with $i+1$ being less than the i, i.e. $RC_{i+1} \leq RC_i$ or $\gamma_{i+1} \leq \gamma_i$. Hence

$$if\left(abs\left(\frac{RC_i}{RC_{i+1}}-1\right)\leq 0.0001.AND.RC_i \geq RC_{i+1}\right)\ exit \quad (3.29)$$

$$if\left(abs\left(\frac{\gamma_i}{\gamma_{i+1}}-1\right)\leq 0.0001.AND.\gamma_i \geq \gamma_{i+1}\right)\ exit \quad (3.30)$$

and the returned RC_i and γ_i values for these conditions matches, respectively, the best rate of climb and best rate of climb angle, RC_{max} and γ_{max}. If these conditions are not met, the subroutine would continuously calculate RC and γ until the following value is less than the previous one, i.e. $RC_{i+1} \leq RC_i$ or $\gamma_{i+1} \leq \gamma_i$. In this case, and as stated before, the iteration would start again at the immediate preceding speed value, $V = V - step$, with an inferior step value, $step = 0.5 \times step$.

Thus, in order to perform these iterations, it was first necessary to elaborate another subroutine which calculated the stall speed (V_s), available and required power (P_A and P_R), and rate of climb and rate of climb angle (RC and γ), as a function of air speed, V, for certain altitude conditions. This subroutine, with certain inputs and outputs variables, is named $Required\_and\_Available\_Power(V, h, dT, P_R, P_A, RC, \gamma, V_S)$, and is called inside each iteration loop.

The inputs, in addition to the air speed, V, are the temperature deviation at sea level, dT, and the selected altitude, h, which are defined initially by the user and read by the software. Additionally, the aircraft in study has a weight, W, a wing area, S and a maximum lift coefficient, $C_{L_{max}}$, already defined in the software. Hence it is possible to apply the mission performance model presents in section 2.4 and calculate directly the required variables, namely P_R, for a certain airspeed V.

Having obtained the value for the required power, P_R, at a specific airspeed V, it is then necessary to obtained the available power, P_A, for the same airspeed value. As stated before, the software calculates the available power through a subroutine called $PowerAvailable(mode)$, which can employ two different calculation methods (mode 1 and 2). Mode 2 matches the propeller power to the engine shaft power, and then matches the available power to the required power so as to minimize the overall mission energy consumption.

However, for this mission parameters calculations, the available power is calculated not to equal the required power, but to obtain the P_A curve of Fig. 2.21. Hence the subroutine applies, for this case, mode 1 ($PowerAvailable(1)$) which only matches the propeller power to the engine shaft power, given an assumed engine throttle, δ, and speed, V. For mode 1 it was assumed that $\delta = 1$. With P_A calculated at each iteration, V_{max}, RC_{max} and γ_{max} can finally be calculated.

Additionally, as referred previously, this subroutine which determines the mission performance values for V_{max}, RC_{max} and γ_{max} also calculates, in a more direct manner, the takeoff ground roll, S_{TO}, and the engine throttle required during a sustained turn, δ_{turn}. δ_{turn} is obtained by using mode 2, at the maneuver speed, V^*, and the corresponding required power, P_R. This occurs since mode 1 does not calculate the engine setting, δ, but rather requires an assumption for it. Hence the required power is the input needed in mode 2, and not the engine throttle. In the case of a sustained turn, P_R is calculated at the maneuver speed, V^*, since it matches the operating limit speed for a sustained turn without having to decrease the lift coefficient.

Summarizing, the user selects the desired mission parameters that are to be constrained and activates them in the algorithm, defining the constraints reference values. Afterwards, the software calculates the parameters and the algorithm compares the calculated value to the defined reference value, at each iteration.

Thus, the optimum solution, given by the algorithm, matches a solution with an optimized set of design variables, and all mission constraints activated fall inside the feasible space.

4 Results

Two UAV's (unmanned aircrafts) were selected to be subjected to the optimization procedure, one powered by an IC engine and another by an electric motor. For both these two cases of study, the software employed the optimization algorithm which gives the optimized propeller diameter and pitch, as well as the optimized engine design variables, for a minimum energy consumption at a particular mission. Therefore it will be presented not only the resulting decrease in fuel/energy consumption and the engine selected, but also the manner in which the objective function and the design variables converged to the solution, according to the number of iterations performed by the algorithm.

4.1 LEEUAV

The LEEUAV is an unmanned aircraft which uses solar energy to power its electric motor. The following tables present the aircraft, motor, battery and propeller data, with the values for the drag polar vector C_{D_i} also discriminated, obtained through experimental data available in reference [67].

Table 4.1 LEEUAV data

AIRCRAFT NAME	Total Mass $[kg]$	Systems Mass $[kg]$	Solar System Mass$[kg]$	Structure Mass $[kg]$	Payload Mass$[kg]$
LEEUAV	5.506	0.458	0.801	2.624	0.200
	Wing Area $[m^2]$	Fuselage Cross Section Area $[m^2]$	Fuselage Wetted Area $[m^2]$	$C_{L_{max}}$	$C_{L_{TO}}$
	1.485	0.0144	0.2	1.5	0.8
	C_{D_1}	C_{D_2}	C_{D_3}	C_{D_4}	C_{D_5}
	0.0575979	-0.1338230	0.2420812	-0.1519270	0.4183674

Table 4.2 Original LEEUAV electric motor data

ENGINE NAME	$M\ [g]$	$Kv\ [rpm/V]$	$I_{max}\ [A]$	$R\ [\Omega]$	$I_0\ [A]$	$U_{max}\ [V]$	$R_\Omega\ [\Omega]$
Hyperion ZS3025-10	186	775	65	0.019	1.61	16.8	0.006

Table 4.3 LEEUAV battery data

BATERRY NAME	$U_{cell}\ [V]$	Number of cells	Battery Pack $U\ [V]$	Battery Pack $R_U\ [\Omega]$	Battery Pack $I_{max}\ [A]$	Battery Pack $M\ [g]$
SLS_APL_3SP1_10000mAH	4.20	3	12.60	0.003	150	750

Table 4.4 Original LEEUAV propeller data

PROPELLER	$M\ [g]$	$D\ [in]$	$p\ [\mathrm{in}]$
A general 2 blade propeller	72	19.09	15.43

The LEEUAV performance and design parameters were optimized for a certain mission inputted into the software. The mission waypoints defined initially are presented in table 4.5., whereas table 4.6 presents the loiter requirements.

Table 4.5 Mission waypoints

WAYPOINT	X POSITION $[m]$	Y POSITION $[m]$	ALTITUDE $[m]$	AIRSPEED $[m/s]$	WIND SPEED $[m/s]$	WIND DIRECTION $[°]$	TEMPERATURE DEVIATION $[K]$
1	0	0	400	0	0	0	15
2	-48.464	-18.877	400	8	0	0	15
3	-629.181	-10110.2	1000	10	1	45	0
4	-4663.59	-36866.7	1000	10	5	30	0
5	-510.147	-49438.3	300	8	0	0	5

Table 4.6 LEEUAV loiter requirements

LOITER	WAYPOINT	TIME [s]	AIRSPEED [m/s]	RADIUS [m]
1	4	1200	8	300

The aircraft lifts off at an altitude of 400 meters, and climbs until it reaches an altitude of 1000 meters. When the end of the mission approaches, it loiters before the landing stage (cruising for a certain amount of time over a small region) within a 300 meters radius, for about 20 minutes until landing. Hence the optimization was employed for this particular mission, whose performance constraints are presented in table 4.7. Table 4.8 presents fixed mission parameters.

Table 4.7 LEEUAV mission constraints, defined by the user.

MISSION CONSTRAINTS		
$V_{max}\ [m/s]$	$\geq$	15
$RC_{max}\ [m/s]$	$\geq$	2
$RC_{sc_{min}}\ [m/s]$	$\geq$	0.5
$\gamma_{max}\ [°]$	$\geq$	15
$S_{TO}\ [m]$	$\leq$	10
δ_{turn}	$\leq$	1

Table 4.8 LEEUAV mission parameters, defined by the user.

MISSION PARAMETERS	
$h_{TO}\ [m]$	500
$h_{RC}\ [m]$	500
$h_{\gamma}\ [m]$	500
$h_{turn}\ [m]$	500
$h_{V_{max}}\ [m]$	1000
$h_{sc}\ [m]$	2500
n_{limit}	1.5
$C_{L_{TO}}$	0.8
μ	0.05

As stated before, the algorithm implemented in the software will begin at a certain starting design value, x, and then searches for the minimum energy spent in the mission between a set of x values defined by an upper boundary and a lower boundary, i.e. $lower\ bound \leq x \leq upper\ bound$. Thus, the initial input value and respective boundaries for the propeller and motor design variables were defined, as presented in table 4.9 for an increment, Δx, of 0.00001, used in the calculations of the gradients through forward finite differences. The FFSQP algorithm will search for the best design variables between the defined boundaries, for a minimum mission energy consumption. The propeller initial input value is the original propeller diameter and pitch (19.09 x 15.3 in). I_{max} must not surpass $150\ A$ since it is the battery pack maximum allowed current.

Table 4.9 Design constraints for the LEEUAV

DESIGN VARIABLES (x)	INPUT VALUE	LOWER BOUND	UPPER BOUND
Propeller diameter, $D\ [m]$	0.484886	0.50	1.685
Propeller pitch, $p\ [m]$	0.391922	0.50	1.695
$Kv\ [rpm/V]$	775	100	2000
$I_{max}\ [A]$	65	20	150

Four different cases were analyzed. Case 0 presents the previous mission energy consumed with the LEEUAV original propeller and original motor. Case 1 presents the optimized solution after the optimization algorithm was employed, returning optimized values for the propeller and motor. These of course are virtual results, since there is no motor with exactly these design specifications values, or a propeller with the exact diameter and pitch as the optimized solution. Thus, after the software selects from the data base the motor with the most similar design variables as the virtual ones, case 2 analyzes if the solution remains similar with the motor and propeller selected, since the empirical motor models have an error associated with the functions coefficients and thus deviate slightly from the real data values. At last, another

interesting variant to analyze, in case 3, was to apply only the selected motor from case 1, and optimize the propeller to check if it would still recommend a similar diameter and pitch. If the results demonstrate decrease in mission energy consumed in relation to case 0, and consistent similar values between case 1, 2 and 3, the empirical motor models will prove satisfactory, even with some deviation associated with the real empirical approximations. Summarizing,

Table 4.10 LEEUAV cases of study

Case 0	Original LEEUAV propeller and motor
Case 1	Free propeller and motor
Case 2	Selected propeller and motor from case 1
Case 3	Free propeller for the selected motor from case 1

Table 4.11 presents the optimized solution, table 4.12 the mission performance parameters obtained for each case, and table 4.13 the motor selected from the virtual empirical results from case 1.

Table 4.11 LEEUAV mission solutions

	MISSION REQUIREMENTS				**PROPELLER AND MOTOR DESIGN VARIABLES**			
	Mission $E_m\ [J]$	**Mission required** δ_{max}	**Mission required** $I_{max}\ [A]$	**Mission Required** $N_{max}[rpm]$	**Propeller** $D\ [in]$	**Propeller** $p\ [in]$	Kv $[rpm/V]$	I_{max} $[A]$
Case 0	395814	0.286	31.248	2274.1	19.09	15.43	775	65
Case 1	302543	0.550	12.336	847.8	28.622	37.757	132.3	44.0
Case 2	309303	0.486	14.260	821.9	29.000	38.000	160.0	48.0
Case 3	308570	0.549	12.627	964.9	26.848	33.775	160.0	48.0

Table 4.12 LEEUAV mission performance solutions

	V_{max} $[m/s]$	RC_{max} $[m/s]$	γ_{max} [°]	$RC_{sc_{min}}$ $[m/s]$	S_g $[m]$	δ_{turn}
Case 0	18.530	2.640	16.010	2.370	2.320	0.255
Case 1	19.949	4.418	30.023	3.851	5.928	0.503
Case 2	20.990	5.040	33.590	4.670	5.140	0.439
Case 3	19.561	3.988	27.253	3.582	6.175	0.496

Table 4.13 Selected motor from the optimized empirical results from case 1

	Kv $[rpm/V]$	I_{max} $[A]$	M $[g]$	R $[\Omega]$	I_0 $[A]$
Empirical results from case 1	132.290	43.970	0.554	0.038	0.772
Selected motor: TURNIGY Multistar 9225-160KV	160	48	0.339	0.065	1.10

After the optimization algorithm was applied in case 1, the software returned a better solution with an optimized value of $28.622\ in$ propeller diameter (D), $37.757\ in$ pitch (p), $132.290\ rpm/V$ (Kv), and a maximum allowed current (I_{max}) of $43.970\ A$. Hence the total mission energy optimized in case 1 decreased around 23% compared to the original solution from case 0, from $395\,814\ J$ to $302\,543\ J$. Pitch assumes a high value since the approximated propeller model presented in Section 2.3 presents limitations when optimizing for low speeds. In other words, in order to sustain flight at low speeds the model tends to overestimates the pitch value and returns a high p/D.

Case 2 demonstrates that for the selected motor (TURNIGY Multistar 9225-160KV) and the selected propeller ($29\ x\ 38\ in$ is a more pragmatic value, since there is no propeller with exactly the same dimensions from case 1) the overall mission energy consumed, all mission requirements and mission performance parameters remained quite similar to the optimized solution. This validates that the empirical motor functions, although only general approximations, present satisfactory matches to the propeller selected, with a mission energy consumption of $309\,033\ J$.

Case 3 proves that inputting only the selected motor in the software and optimizing only the propeller dimensions, the optimization algorithm would still recommend a similar propeller, with a $26.848\ in$ diameter and a $33.775\ in$ pitch. Important to note that since the real motor selected has a Kv of $160\ rpm/V$, which is higher than the empirical result, the revolutions rate of the propeller is higher, and thus pitch will be lower since it does not need to compensate as much as the optimized pitch value from case 1. All mission performance constraints remain similar to case 2 and 1.

Regarding the mission performance results obtained, it is clear that there is an improvement in almost all parameters from case 0 (original propeller and motor) to case 1 (optimized solution), especially in the maximum rate of climb, RC_{max}, and maximum rate of climb angle, γ_{max}, since the propeller dimensions increased. Although the required takeoff distance, S_g, is greater when compared to the original motor, this is due to the fact that the aircraft became heavier with the new optimized propeller and motor. The original motor was particularly light, weighting only 186 g. All other mission performance parameters improved, while spending less energy during mission. Case 2 and 3 still present a similar solution to case 1.

Important also to illustrate, for case 1, the behavior of the objective function, E_m, and the design variables during the iteration process performed by the algorithm, in order to observed how the variable converged and stabilized before reaching the final solution. Fig. 4.2 illustrates the convergence of the objective function, E_m, and Fig. 4.3, 4.4 and 4.5 the convergence of the design variables, both according to the number of iterations performed by the algorithm.

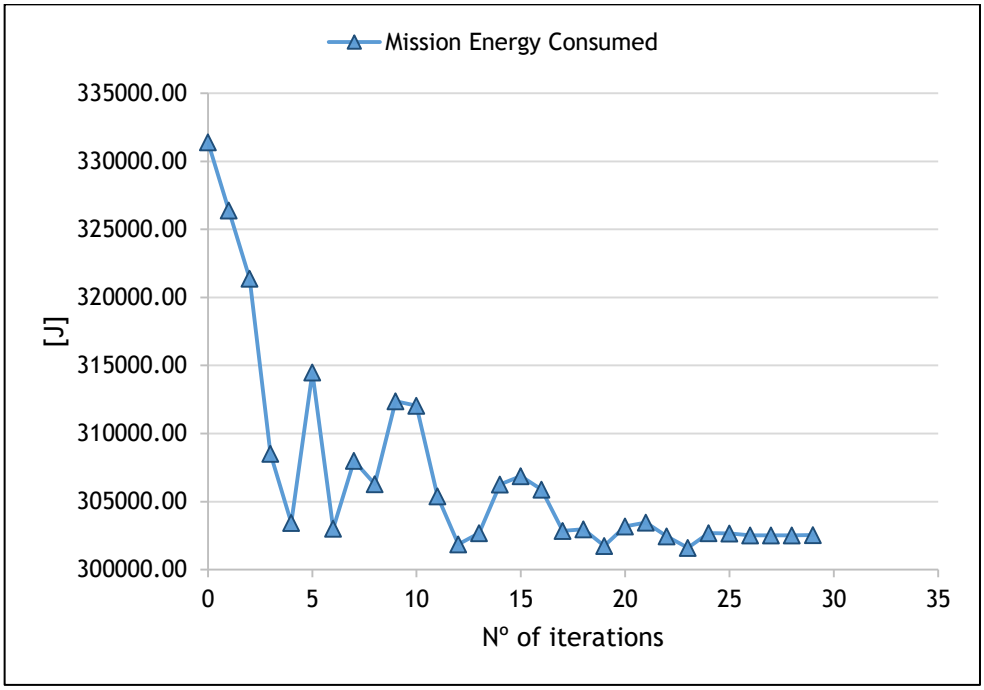

Figure 4.1 Convergence of the objective function, for case 1, into a stabilized solution for the LEEUAV according to the number of iterations

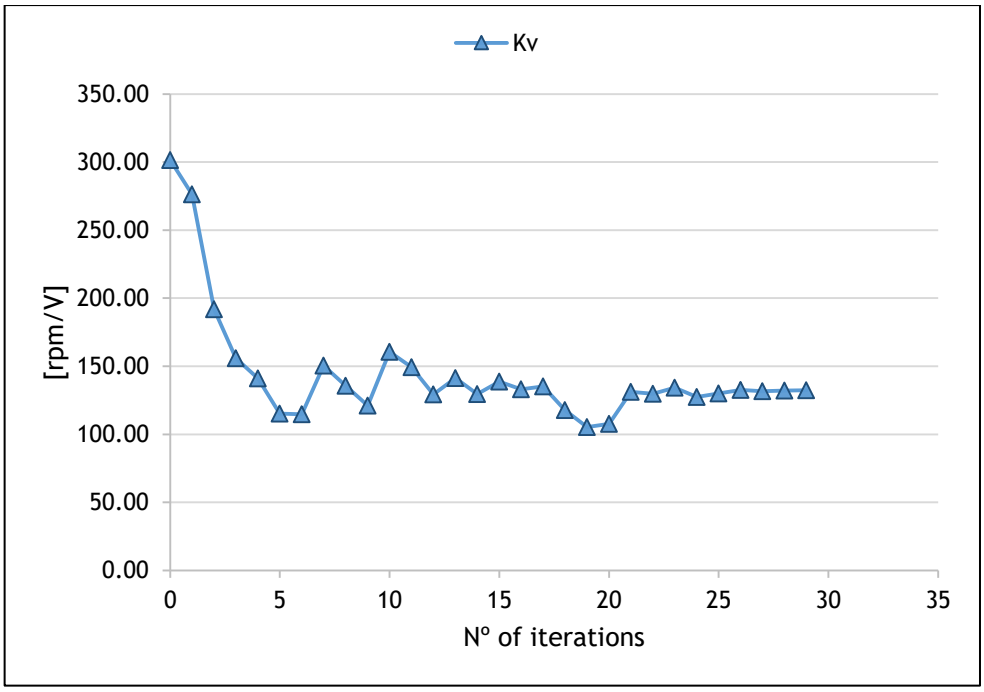

Figure 4.2 Convergence of Kv, for case 1, into a stabilized solution for the LEEUAV during the iteration process

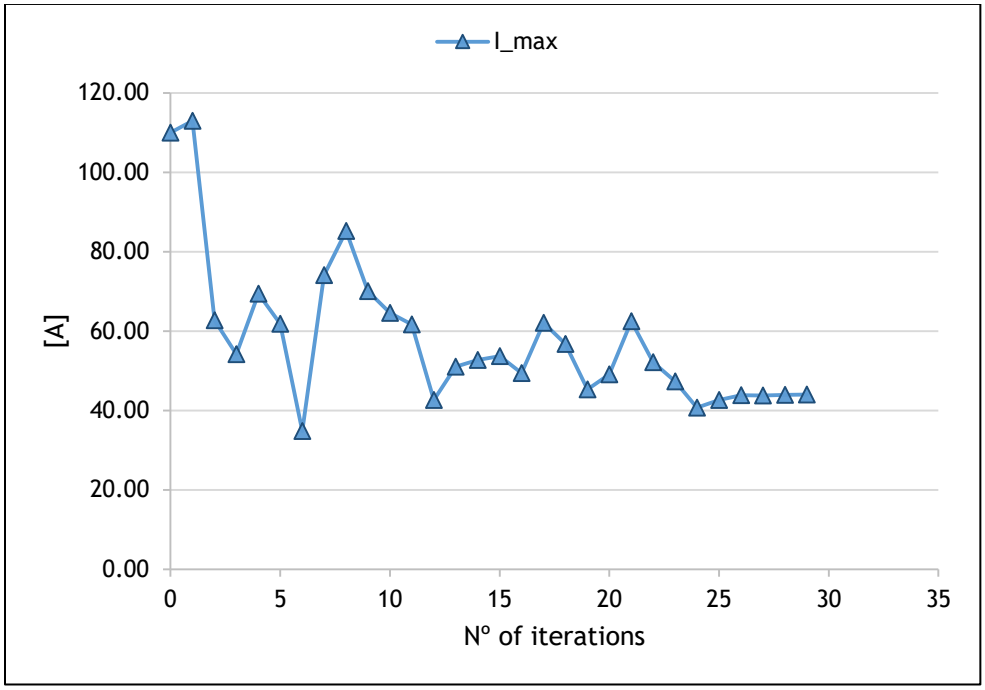

Figure 4.3 Convergence of I_{max}, for case 1, into a stabilized solution for the LEEUAV during the iteration process

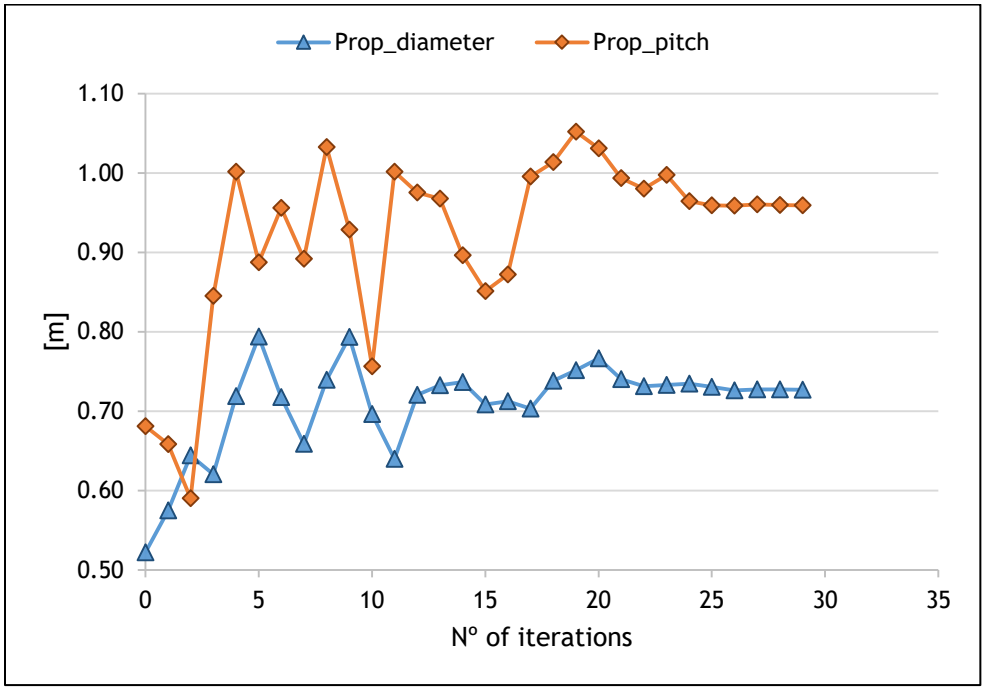

Figure 4.4 Convergence of the propeller design variables, for case 1, into a stabilized solution for the LEEUAV during the iteration process

In the first iterations, there is a much wide variation gap of the variable in relation to the variation gap in final iterations, where it stabilizes until the final solution is reached. This is

related to the gradient descent path stated in sections 1.4.2.1 and 3.2. In the search for the optimum minimum, and given a set of boundaries constraints for the design variables, x, the gradient of the objective function gives the direction in which the algorithm should progress. The higher the gradient value is, the faster the algorithm learns and progresses rapidly and in larger amounts through the variables, as it is demonstrated in the first iterations of Fig. 4.2, 4.3, 4.4 and 4.5. When it goes nearer to the intended solution, the gradients will assume smaller and smaller values to converge to the desired minimum. Thus as the final iteration approaches, the objective function and the design variables will stabilize as the gradients converge to zero, without compromising the feasible space set by the constraints. This feasible space compromises significantly the convergence of the gradients, as they restrict the gradients to converge sometimes not to zero, but to the possible minimum inside the feasible space of the design variables and mission performance parameters. Fig. 4.6 presents the gradient descent path of the objective function, scaled to the unit (fraction between the current gradient value and the initial gradient value).

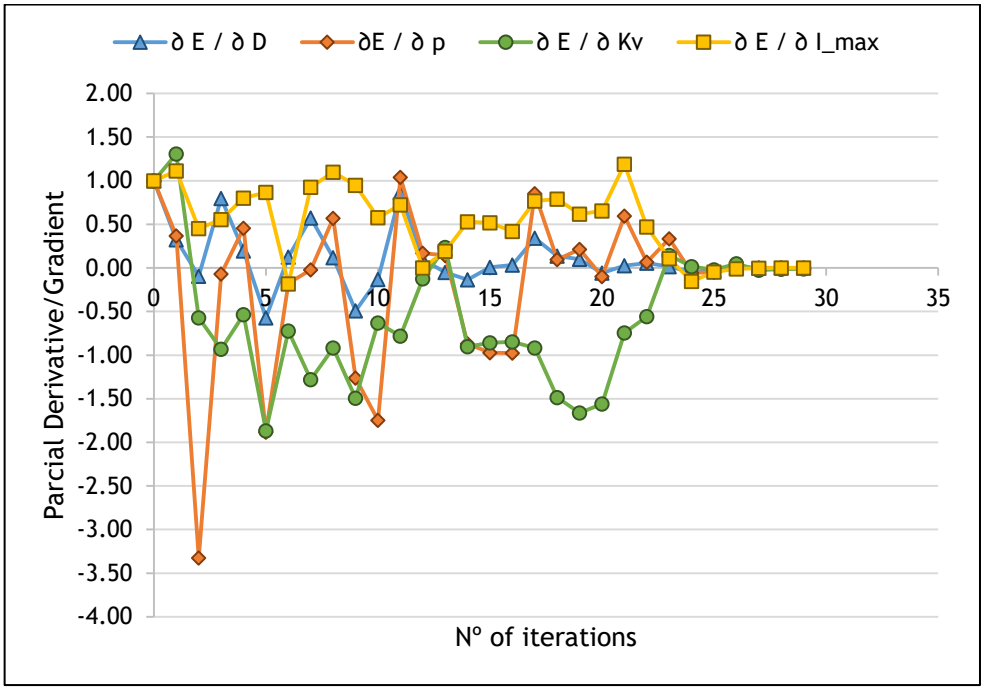

Figure 4.5 Gradient convergence to zero, for case 1

Hence the electric motor selected meets the objective, and minimizes the mission energy consumed, validating the practicality of the empirical motor models obtained.

4.2 HOJI UAV

The Hoji UAV is an unmanned aircraft powered by an IC engine. The aircraft data is displayed in table 4.14 below [68], where the drag polar vector C_{D_i} was assumed.

Table 4.14 HOJI data

AIRCRAFT NAME	Total Mass $[kg]$	Systems Mass $[kg]$	Fuel Mass$[kg]$	Structure Mass $[kg]$	Payload Mass $[kg]$
HOJI	570	154	130	137	150
	Wing Area $[m^2]$	**Fuselage Cross Section Area $[m^2]$**	**Fuselage Wetted Area $[m^2]$**	**$C_{L_{max}}$**	**$C_{L_{TO}}$**
	9.1	0.6	10.15	1.85	0.6
	C_{D_1}	**C_{D_2}**	**C_{D_3}**	**C_{D_4}**	
	0.0241	0.0181	0.0056	0.0092	

Unlike the LEEUAV, the Hoji did not have an original engine and propeller. Thus the objective was to find the propeller and engine which best minimized the total fuel weight consumed during mission. The mission requirements are presented in the tables below.

Table 4.15 HOJI mission waypoints

WAYPOINT	X POSITION $[m]$	Y POSITION $[m]$	ALTITUDE $[m]$	AIRSPEED $[m/s]$	WIND SPEED $[m/s]$	WIND DIRECTION [°]	TEMPERATURE DEVIATION $[K]$
1	0	0	0	0	0	0	0
2	500	0	0	30	0	0	0
3	50000	0	5000	36	0	0	0
4	60000	0	5000	36	0	0	0
5	80000	0	5000	36	0	0	0
6	500	0	0	50	0	0	0

Table 4.16 HOJI loiter requirements

LOITER	WAYPOINT	TIME [s]	AIRSPEED [m/s]	RADIUS [m]
1	4	54000	30	1000

These are the mission waypoints introduced in the software. The aircrafts lifts off at sea level, and climbs until it reaches an altitude of 5000 meters. Then, when it reaches the desired destination, it loiters for a recognition mission within a 1000 m radius for about 15 hours. Afterwards, it proceeds cruise until the landing stage. Hence the optimization was employed

for this particular mission, whose performance constraints and fixed parameters are presented in the tables below.

Table 4.17 Hoji mission constraints, defined by the user

MISSION CONSTRAINTS		
$V_{max}\ [m/s]$	$\geq$	45
$RC_{max}\ [m/s]$	$\geq$	6
$RC_{sc_{min}}\ [m/s]$	$\geq$	0.5
$\gamma_{max}\ [°]$	$\geq$	10
$S_{TO}\ [m]$	$\leq$	500
δ_{turn}	$\leq$	1

Table 4.18 Hoji mission parameters, defined by the user

MISSION PARAMETERS	
$h_{TO}\ [m]$	0
$h_{RC}\ [m]$	0
$h_{\gamma}\ [m]$	0
$h_{turn}\ [m]$	4000
$h_{V_{max}}\ [m]$	4000
$h_{sc}\ [m]$	6000
n_{limit}	1.5
$C_{L_{TO}}$	0.6
μ	0.05

As for the design variables constraints (already explained previously) the boundaries defined are presented in table 4.19 below, with an increment, Δx, of 0.00001.

Table 4.19 Design constraints for the Hoji UAV

DESIGN VARIABLES (x)	INPUT VALUE	LOWER BOUND	UPPER BOUND
Propeller diameter, $D\ [m]$	1.5	0.25	1.6
Propeller pitch, $p\ [m]$	1.5	0.1	2
$bp_{max}\ [W]$	73 500	0	200 000
$N_{max}\ [rpm]$	2600	2550	7000

Since very few engines from the data table have a N_{max} inferior to $2550\ rpm$, this was the lower bound inputted. Two different cases were analyzed. Case 1 is the optimized solution, which returns optimize values for D, p, bp_{max}, and N_{max}. Case 2 analyzes if the solution remains similar with the engine and propeller selected from case 1, since the empirical engine models

have an error associated with the functions coefficients and thus deviate slightly from the real data values. Summarizing,

Table 4.20 Hoji cases of study

Case 1	Free propeller and motor
Case 2	Selected propeller and motor

Table 4.21 presents the optimized solution, table 4.22 the mission performance parameters obtained for each case, and table 4.23 the engine selected from the virtual empirical results from case 1.

Table 4.21 Hoji mission solutions

	MISSION REQUIREMENTS			PROPELLER AND ENGINE DESIGN VARIABLES			
	Mission W_{fuel} $[N]$	Mission required δ_{max}	Mission Required $N_{max}[rpm]$	Propeller D $[in]$	Propeller p $[in]$	b_{max} $[W]$	N_{max} $[rpm]$
Case 1	2059.16	0.997	2521.8	61.080	52.412	93 899.9	2550
Case 2	1894.21	0.961	2508.3	61.000	52.000	845000	2400

Table 4.22 Hoji mission performance solutions

	V_{max} $[m/s]$	RC_{max} $[m/s]$	γ_{max} [°]	$RC_{sc_{min}}$ $[m/s]$	S_g $[m]$	δ_{turn}
Case 1	60.494	6.587	10.000	1.486	277.522	0.913
Case 2	55.38	5.74	10.26	1.49	247.29	0.88

Table 4.23 Selected engine from the optimized empirical results from case 1

	bp_{max} $[W]$	N_{max} $[rpm]$	M $[kg]$	$bsfc_0$ $[kg/Ws]$	R_{gear}
Empirical results from case 1	93899.91	2550	110.62	0.9813E-07	1.000
Selected engine: Rotax 914 UL/F	84500	5800*0.411 = 2384	68	0.6939E-07	0.411

Important to remind that since the selected engine as a reduction gear, which reduces the rotational speed that reaches the propeller shaft, the true available speed equals the product between the engine speed and gear ratio. After the optimization algorithm was applied, the software returned a solution with an optimized value of $61.080\,in$ propeller diameter (D), $52.412\,in$ pitch (p), $93899.91\,W$ of maximum power (bp_{max}), and a N_{max} of $2550\,rpm$. This solution matches a total mission fuel consumption of $2059.16\,N$. Although the N_{max} could be optimized to lower values, the lower boundary set at the beginning prevented the engine speed

to reach a more desirable solution, since there are few engines from the data base which have lower N_{max} values than 2550.

As is can be observed, the total mission fuel consumed in case 2 is noticeably less with the real engine, when compared to the virtual solution given by the empirical IC engine models in case 1. This happens since $bsfc_0$ empirical model presented in Fig. 3.10 tends to overestimate the resulting specific fuel consumption, and thus the $bsfc_0$ of the real engine data will be, most of the times, less than the virtual result. Hence while the Rotax engine has a $bsfc_0$ of $6.93900E-08\ kg/Ws$, the virtual result given by the empirical model, for a bp_{max} of $93\,899.9\ W$, indicated a $bsfc_0$ of $9.81300E-08\ kg/Ws$. Therefore the mission fuel consumed with the real engine would be considerably lower, since it requires less kg of fuel per Watt in one second. This deviation from the empirical model can be explained since the engine selected is recent, with new technologies which reduce the fuel consumption, compared to older engines from the data base. Furthermore, this empirical model is a simple approximation which translates $bsfc_0$ as dependent only of bp_{max}, whereas in reality it depends on much more factors (volume displacement, four or two stroke engines, carburetor or fuel injector engines, etc). Although the $bsfc_0$ overestimates the optimized result, it still minimizes the mission fuel consumed in satisfactory terms, validating the practicality of the empirical IC models obtained.

Regarding the mission performance parameters solution, it is possible to observed that the rate of climb angle, γ_{max}, imposed a tight bound on the result, preventing the mission solution from reaching a more optimized value. Additionally, the runway distance, S_g, is considerably lower for case 2 (selected engine and propeller) since the selected engine is much lighter than the empirical result. This is due to the fact, as explained before, that the Rotax engine has much more recent technology when compared to other engine data elements, and thus is lighter. At last, it is also interesting to note how altitude considerably affects the mission rate of climb at service ceiling, $RC_{sc_{min}}$, when compared to the maximum rate of climb at sea level, RC_{max}.

Both the N_{max} and the γ_{max} constraints imposed tight limits for the feasible space, and as a result the optimum solution obtained matches the most minimum possible fuel consumption, but only inside the boundaries set. Hence, since it is a local minimum and not the global one, the gradients of the objective function did not converge to zero, but to the minimum possible solution given the constraint limitations. The behavior of the objective function and the design variables, for case 1, during the iteration process performed by the algorithm is displayed in Fig. 4.8, 4.9, 4.10 and 4.11, in order to observed how the variable converged and stabilized before reaching the final solution. Most of the variable convergence process was already explained in the section 4.1.

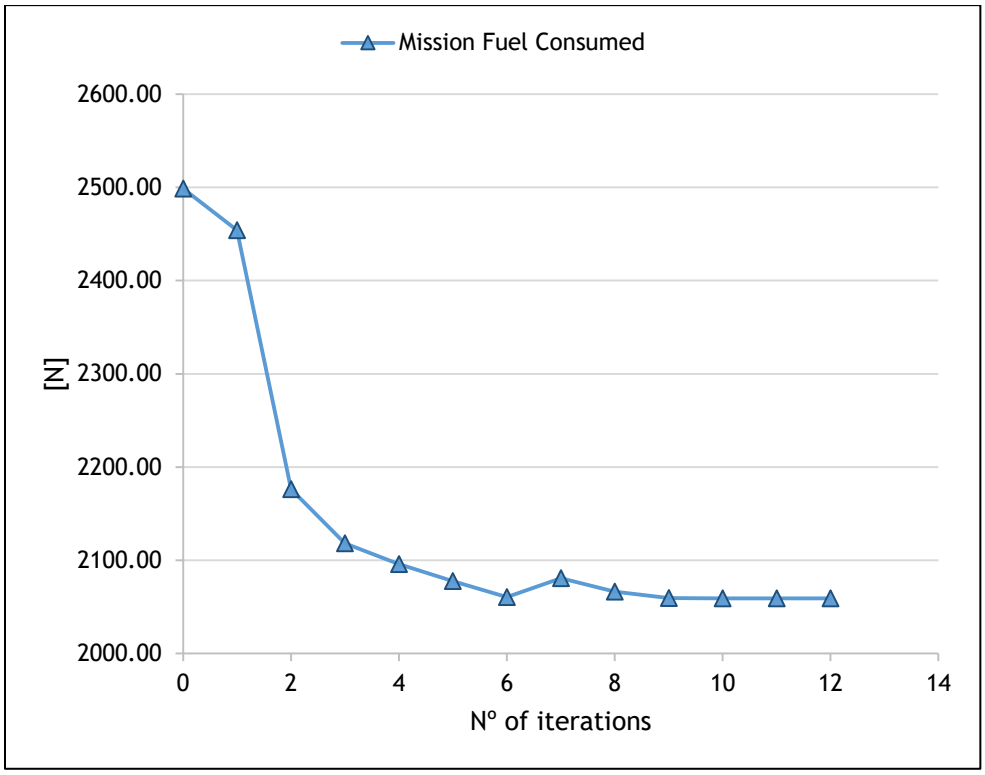

Figure 4.6 Convergence of the objective function, for case 1, into a stabilized solution for the Hoji during the iteration process

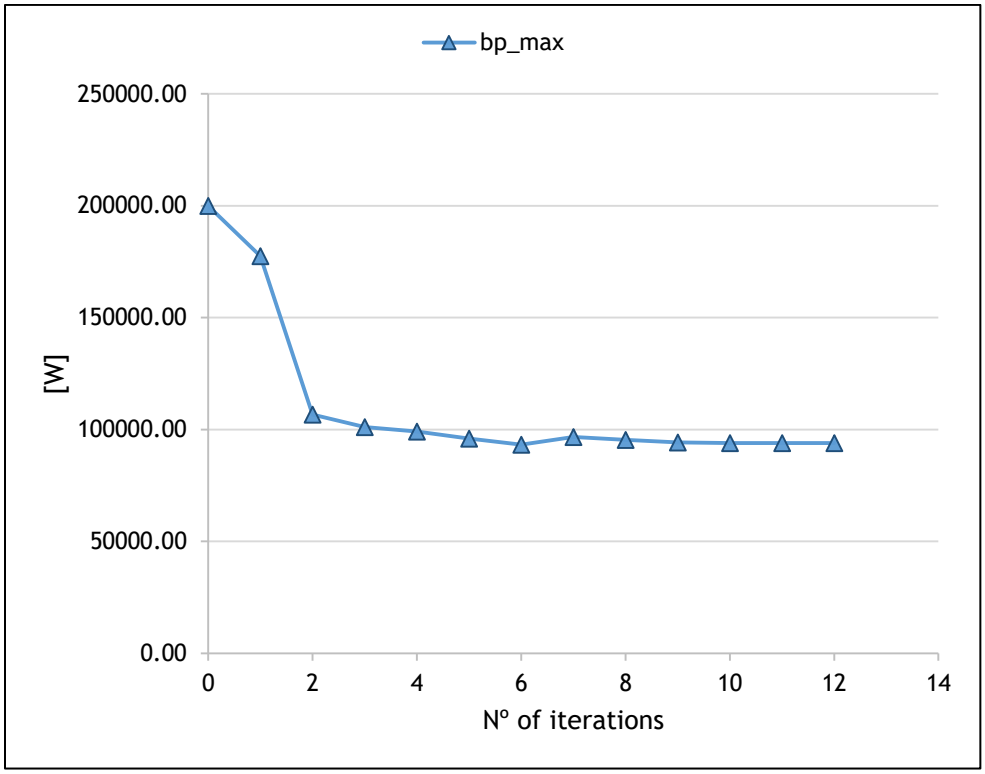

Figure 4.7 Convergence of bp_{max}, for case 1, into a stabilized solution for the Hoji during the iteration process

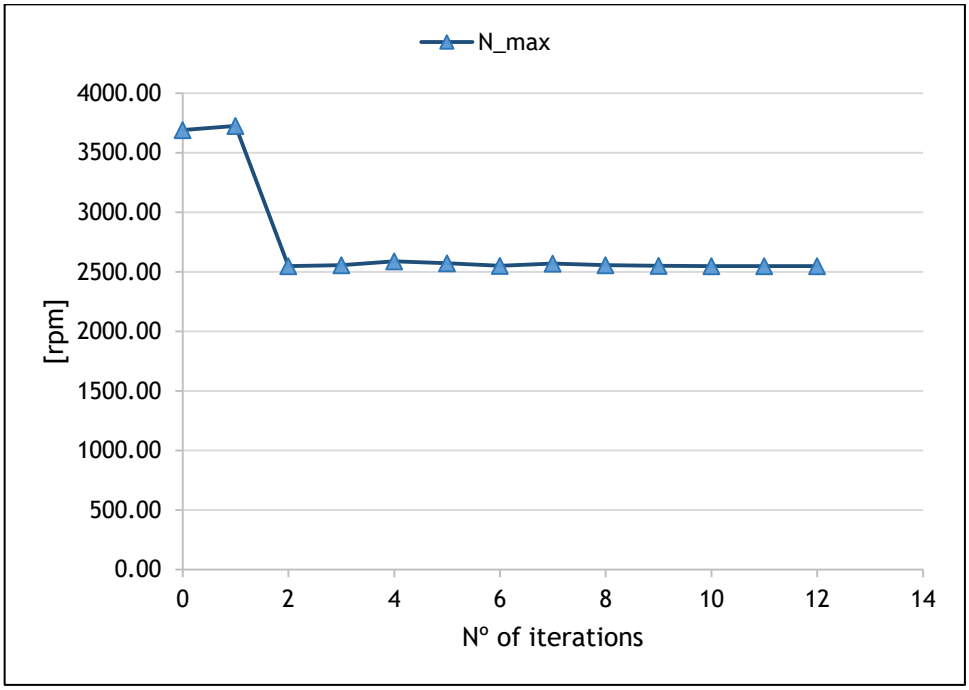

Figure 4.8 Convergence of N_{max}, for case 1, into a stabilized solution for the Hoji during the iteration process

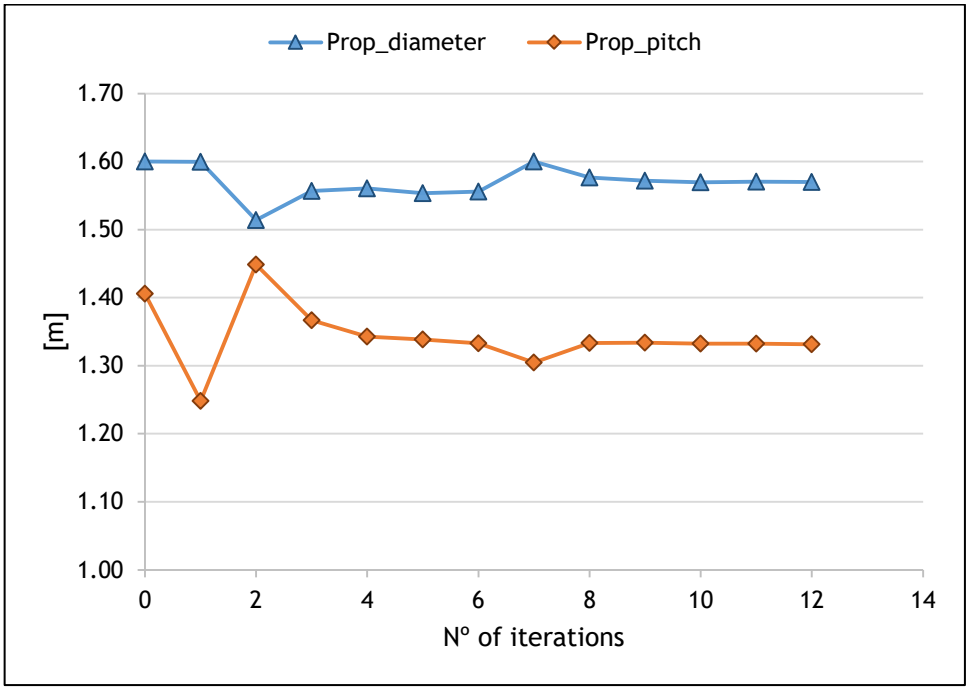

Figure 4.9 Convergence of the propeller design variables, for case 1, into a stabilized solution for the Hoji during the iteration process

The IC engine selected meets the objective, minimizing the mission fuel consumed and validating the practicality of the empirical engine models obtained, although these models presented not as good results as the electric motor empirical models.

5 Conclusions

One of the objectives established in this dissertation were the creation of two data bases, one with the IC engine specifications and another with the electric motor specifications, in order to develop empirical models as functions of certain design variables. These design variables were then introduced in the optimization software, to be optimized alongside the propeller and to match the most suitable propulsion system to the optimum solution obtained.

Both data bases were successfully created, and all empirical models obtained, although with a certain error associated with the coefficients of the functions. The specific fuel consumption model, specially, was the hardest to obtain since information regarding the engine specific consumption is not always available. Additionally, as stated before, the specific fuel consumption approximation was translated as being dependent only on engine rated power, when in reality it depends on many more factors. The remaining empirical models obtained provided, however, more reliable approximations.

The design variables selected to be introduced in the algorithm, which are the inputs of the empirical models, were bp_{max} and N_{max} for the IC engine, and I_{max} and Kv for the electric motor. After modifications were made to the software, the optimization algorithm started to optimize these design variables, and when the optimum solution was achieved, it selected from the data base the engine with the least deviations from the empirical models solution.

Regarding the mission performance calculations, another objective of this dissertation, they were successfully inputted into the software, and the algorithm was optimizing according to the feasible space defined not only by the propeller and engine boundaries, but also by the mission constraints the user may choose to define.

The results obtained confirmed the practicality of the engine empirical models, given good matches (although not perfect) to the optimum solution reached. The design variables and the objective function were converging correctly to a stabilized solution, and the gradients presented a descent until they also stabilized in the most minimum possible solution, considering the feasible space.

5.1 Future Works

For future studies related to this optimization software, it would be interesting to run the optimization with a different algorithm. Instead of a deterministic one, it would prove more challenging to implement a genetic algorithm to see what results it would generate in the search for the global minimum, and if they would deviate considerably or not from the previous results obtained with the FFSQP subroutines.

Furthermore, optimizing the mission trajectory to reach a certain destination and thus spending less resources, would also prove very ambitious, since until now the software only optimizes a certain mission trajectory inputted by the user.

It would also prove interesting and advisable to consider a reduction gear box not only in the IC engine models, but also in the electric motor models, and to additionally differentiate motor mass from gear box mass.

In conclusion, aircraft optimization certainly is an utmost challenging problem, which always presents trials and difficulties in which to improve. Further investigations in this field are always advantageous and relevant to the development of aircraft performance, and even the adversities may prove significant in leading optimization studies into progress and enhancement.

Bibliography

[1] W. W. Pulkrabek, Engineering Fundamentals of the Internal Combustion Engine, New Jersey: Pearson Education Limited, 1997.

[2] R. P. Liem, Multimission Fuel-Burn Minimization in Aircraft Design: A Surrogate-Modeling Approach, PhD Thesis, Toronto: University of Toronto Institute for Aerospace Studies, 2015.

[3] R. M. Hicks and C. A. Szelazek, "Airfoil Design by Numerical Optimization Using a Minicomputer," 1978.

[4] G. B. Consentino and T. L. Host, Numerical Optimization Design of Advanced Transonic Wing Configurations, California: National Aeronautics and Space Administration, 1984.

[5] J. S. Sobieski and R. T. Haftkat, "Multidisciplinary Aerospace Design Optimization: Survey of Recent Developments," in *34th Aerospace Sciences Meeting and Exhibit*, Nevada, 1995.

[6] N. E. Antoine and I. M. Kroo, "Aircraft Optimization for Minimal Environmental Impact," *Journal of Aircraft,* vol. 41, no. 4, p. 790, 2004.

[7] R. P. Liem, C. A. Mader, E. Lee and J. R. R. A. Martins, "Aerostructural design optimization of a 100-passenger regional jet with surrogate-based mission analysis," in *AIAA Aviation Technology, Integration, and Operations (ATIO) Conference*, Los Angeles, 2013.

[8] J. Arora, Introduction to Optimum Design, McGraw-Hill, New York, 1989.

[9] P. E. Gill, W. Murray and M. H. Wright, Practical optimization, London: Academic Press Inc, 1981.

[10] S. Koziel and X.-S. Yang, Computational Optimization, Methods and Algorithms, Springer-Verlag Berlin Heidelberg, 2011.

[11] D. H. Wolpert and W. G. Macready, "No free lunch theorems for optimization," *IEEE Transactions on Evolutionary Computation,* vol. 1, p. 67–82, 1997.

[12] X. S. Yang, Introduction to Computational Mathematics, Singapore: World Scientific Publishing, 2008.

[13] J. A. Nelder and R. Mead, "A simplex method for function optimization," *Computer Journal,* vol. 7, no. 4, p. 308–313, 1965.

[14] D. E. Goldberg, Genetic Algorithms in Search, Optimization and Machine Learning, Addison Wesley, 1989.

[15] A. I. J. Forrester and A. J. Keane, " Recent advances in surrogate-based optimization," *Progress in Aerospace Sciences,* vol. 45, pp. 50-79, 2009.

[16] R. M. Barker, M. G. Cox, A. B. Forbes and P. M. Harris, "Software Support for Metrology: Discrete Modelling and Experimental Data Analysis," National Physical Laboratory, UK, 2007.

[17] R. Fletcher and M. J. D. Powell, "A Rapidly Convergent Descent Method for Minimization," *The Computer Journal,* vol. 6, no. 2, p. 163–168, 1963.

[18] [Online]. Available: https://www.cs.ubc.ca/labs/lci/mlrg/slides/non_convex_optimization.pdf. [Accessed June 2018].

[19] [Online]. Available: http://adl.stanford.edu/aa222/Lecture_Notes_files/chapter3_gradient.pdf. [Accessed July 2018].

[20] G. Chiandussi, M. Codegone, S. Ferrero and F. E. Varesio, "Comparison of multi-objective optimization methodologies for engineering applications," *Computers and Mathematics with Applications,* vol. 63, no. 5, p. 912–942, 2012.

[21] R. Stone, Introduction to Internal Combustion Engines, Macmillan, 1992.

[22] V. Ganesan, IC Engines, Tata Mcgraw Hill Education Private Limited, 2012.

[23] C. Keyes, Electric Motors: Energy Efficiency Reference Guide, CEA Technologies Inc. (CEATI), 2007.

[24] D. L. Wall, Optimum Propeller Design for Electric UAVs, Master's Thesis, Auburn, Alabama: Auburn University, 2012.

[25] B. Roy and A. M. Pradeep. [Online]. Available: https://nptel.ac.in/courses/101101001/downloads/Intro-Propulsion-Lect-25.pdf. [Accessed January 2019].

[26] P. F. G. L. F. d. Albuquerque, Mission-Based MultidisciplinarDesign Optimization Methodologies for Unmanned Aerial Vehicles with Morphing Technologies, PhD Thesis, Covilhã: Universidade da Beira Interior, 2017.

[27] D. P. Raymer, Aircraft Design: A Conseptual Approach, Washington D.C.: American Institute of Aeronautics, Inc. , 1992.

[28] P. Buban and M. L. Schmitt , Understanding Electricity and Electronics, McGraw-Hill Inc., 1962.

[29] [Online]. Available: https://www.energy.gov/sites/prod/files/2014/04/f15/10097517.pdf. [Accessed August 2018].

[30] [Online]. Available: http://www.me.umn.edu/courses/me2011/arduino/technotes/dcmotors/motor-tutorial/. [Accessed July 2018].

[31] [Online]. Available: https://www.electric-skateboard.builders/t/how-does-the-torque-curve-change-with-voltage/25760/3. [Accessed July 2018].

[32] C. Burger, Propeller Performance Analysis and Multidisciplinary Optimization Using a Genetic Algorithm, Master's Thesis, Auburn, Alabama: Auburn University , 2007.

[33] [Online]. Available: http://webserver.dmt.upm.es/~isidoro/bk3/c17/Propellers.pdf. [Accessed September 2018].

[34] Airbus, Getting Grips with Aircraft Performance, Airbus, 2002.

[35] J. D. Anderson, Aircraft Performance and Design, Tata McGraw-Hill, 1999.

[36] L. E. M. J. Rodrigues, Fundamentos da Engenharia Aeronáutica - Aplicações ao Projeto SAE AeroDesign, São Paulo: Author's Edition , 2011.

[37] [Online]. Available: http://m.aircraftspruce.com/catalog/pdf/13-09981.pdf. [Accessed October 2018].

[38] L. Coelho, Mission Planner for Solar Powered Unmanned Aerial Vehicles, Master's Thesis, Covilhã: Universidade da beira Interior, 2019.

[39] J. L. Zhou, A. L. Tits and C. T. Lawrence, User's Guide for FFSQP Version 3.7: A FORTRAN Code for Solving Constrained Nonlinear (Minimax) Optimization Problems, Generating Iterates Satisfying All Inequality and Linear Constraints, University of Maryland.

[40] Lycoming, "AEIO-320, AEIO-360, AEIO-540 Series Operator's Manual," Lycoming, U.S.A., 2007.

[41] Lycoming, "GO-480, IGO-480, GSO-480 and IGSO-480 Series Operator's Manual," Lycoming, U.S.A., 2008.

[42] Lycoming, "O-235 and O-290 Series Operator's Manual," Lycoming, U.S.A., 2007.

[43] Lycoming, "O-320, IO-320, AIO-320, and LIO-320 series Operator's Manual," Lycoming, U.S.A., 1973.

[44] Lycoming, "O-540, IO-540 Series Operator's Manual," Lycoming, U.S.A., 2006.

[45] Lycoming, "TIO-540 Series Parallel Valve Cylinder Heads Operator's Manual," Lycomin, U.S.A., 2006.

[46] Lycoming, "TIO-540-AE2A Series," Lycoming, U.S.A., 2006.

[47] Lycoming, "O-360, HO-360, IO-360, AIO-360, HIO-360 & TIO-360 Series Operator's Manual," Lycoming, U.S.A., 2005.

[48] Continental Motors, Inc, "IO-470 Operator's Manual," Continental Motors, Inc, U.S.A., 2011.

[49] Continental Motors, Inc, "IO-520 Operator's Manual," Continental Motors, Inc, U.S.A., 1968.

[50] Continental Motors, Inc, "TSIO-360-F & FB Operator's Manual," Continental Motors, Inc, U.S.A., 1978.

[51] Continental Motors, Inc., "C-125, C-145, O-300 Maintenance and Operator's Manual," Continental Motor, Inc., U.S.A., 2011.

[52] Continental Motors, Inc., "IO-360-A, AB, C, CB, D, DB, ES, G, GB, H, HB, J, JB, K & KB Operator's Manual," Continental Motor, Inc., U.S.A., 2011.

[53] Rotax, "Rotax 447 UL SCDI, Rotax 503 UL DCDI, Rotax 582 UL DCDI Mod.99 Operator's Manual," Rotax, 2010.

[54] Rotax, "Operator's Manual for Rotax Engine Type 582 UL series," Rotax, 2018.

[55] Rotax, "Operator's Manual for Rotax Engine Type 912 series," Rotax, 2006.

[56] Rotax, "Operator's Manual for Rotax Engine Type 912 i series," Rotax, 2015.

[57] Rotax, "Operator's Manual for Rotax Engine Type 914 series," Rotax, 2015.

[58] Rotax, "Operator's Manual for Rotax Engine Type 915 i A series," Rotax, 2017.

[59] [Online]. Available: http://limflug.de/en/products/engines.php. [Accessed November 2018].

[60] [Online]. Available: http://ulpower.com/en/engines. [Accessed November 2018].

[61] [Online]. Available: https://www.osengines.com/. [Accessed May 2018].

[62] [Online]. Available: http://www.rcgfservice.com/. [Accessed May 2018].

[63] [Online]. Available: https://3w-modellmotoren.de/product-category/engines/?lang=en. [Accessed May 2018].

[64] [Online]. Available: https://hobbyking.com/pt_pt/power-systems/electric-motors.html. [Accessed April 2018].

[65] [Online]. Available: https://www.scorpionsystem.com/catalog/aeroplane/motors_1/. [Accessed November 2018].

[66] [Online]. Available: https://www.modelmotors.cz/e-shop/. [Accessed November 2018].

[67] A. S. Rodrigues, Airframe Assembly, Systems Integration and Flight Testing of a Long Endurance Electric UAV,Master's Thesis, Covilhã: Universidade da Beira Interior, 2017.

[68] R. Santos, H. Graça, A. Oliveira, P. Moutinho and D. Sousa, "Unmanned Aerial Vehicle Hoji_V2, Report," Universidade da Beira Interior, Covilhã, 2016.

Appendixes

Appendix A

Table A-I. Index of each IC engine name

INDEX	ENGINE NAME
1	LYCOMING GSO-480-B1B3
2	LYCOMING GSO-480-B1B6, -B1J6
3	LYCOMING GSO-480-B1A6, -B2D6
4	LYCOMING GSO-480-B1C6, -B2C6
5	LYCOMING GSO-480-B1F6
6	LYCOMING GSO-480-A1A6
7	LYCOMING GSO-480-B1E6, -B2H6
8	LYCOMING GSO-480-B1G6, -B2G6
9	LYCOMING GO-480-C2C6
10	LYCOMING GO-480-C2D6
11	LYCOMING GO-480-G2D6, -G2F6
12	LYCOMING GO-480-C1B6
13	LYCOMING GO-480-G1B6
14	LYCOMING GO-480-G1J6
15	LYCOMING GO-480-G1A6
16	LYCOMING GO-480-G1D6
17	LYCOMING GO-480-G1H6
18	LYCOMING GO-480-C1D6
19	LYCOMING GO-480-F6
20	LYCOMING GO-480-F1A6
21	LYCOMING GO-480-B1B
22	LYCOMING GO-480-B1C
23	LYCOMING GO-480-B, B1A6, -B1D
24	LYCOMING GO-480-D1A
25	LYCOMING O-540-A3D5
26	LYCOMING O-540-A1A, -A1A5, -A4A5
27	LYCOMING O-540-A1B5, -A1C5, -A4B5
28	LYCOMING O-540-A1D, -A4C5, -A1D5, -A45
29	LYCOMING O-540-A2B
30	LYCOMING O-540-F1B5
31	LYCOMING O-540-B2C5
32	LYCOMING O-540-B1D5
33	LYCOMING O-540-B1A5, -B2A5, -B4A5
34	LYCOMING O-540-B1B5, -B2B5, -B4B5
35	LYCOMING HO-360 -B1A, -B1B
36	LYCOMING O-360-C2B, -C2D
37	LYCOMING O-360-B2A, -B2C
38	LYCOMING O-360-D2A

39	CONTINENTAL MOTORS O-300-A,-B,-C & D
40	CONTINENTAL MOTORS O-C145
41	LYCOMING O-290-D2A,-D2B,-D2C
42	LYCOMING O-235 -J2A
43	LYCOMING O-235-G1
44	LYCOMING O-235-G2A
45	LYCOMING O-235-F2B
46	LYCOMING O-235 -F2A
47	LYCOMING O-235-F1B
48	LYCOMING O-290-D
49	CONTINENTAL MOTORS O-C125
50	LYCOMING O-235-M1
51	LYCOMING O-235-K2B
52	LYCOMING O-235 -L2A
53	LYCOMING O-235-K2A
54	LYCOMING O-235-L2C
55	LYCOMING O-235-K2C
56	LYCOMING O-235 -P2A
57	LYCOMING O-235-N2A
58	LYCOMING O-235-N2C
59	LYCOMING O-235-E1B
60	LYCOMING O-235-E2A
61	LYCOMING O-235-C2C
62	LYCOMING O-235 -H2C
63	LYCOMING O-235-C1
64	LYCOMING O-235-C1C
65	LYCOMING O-235-C2A
66	LYCOMING O-235-C2B
67	LYCOMING O-235-C
68	LYCOMING O-235-C1B
69	Limbach L 2400 DT.X
70	Limbach L 2400 DT/ET
71	Limbach L 2400 DF/EF
72	Limbach L 2400 EB
73	Limbach L 2000 EB
74	LIMBACH L 550 E
75	LIMBACH L 550 EF
76	LIMBACH L 275 EF
77	LIMBACH L 275 E
78	UL260i
79	UL260iS
80	UL260iSA
81	UL260iF
82	UL350i
83	UL350iS
84	UL350iSA

85	UL390i
86	UL390iS
87	UL390iSA
88	UL520i
89	UL520iS
90	UL520iSA
91	Rotax 914 UL/F
92	Rotax 912 ULS/S
93	Rotax 912 UL/A/F
94	ROTAX
95	ROTAX
96	ROTAX
97	ROTAX
98	ROTAX
99	ROTAX
100	ROTAX
101	ROTAX
102	ROTAX
103	ROTAX
104	ROTAX
105	ROTAX
106	ROTAX
107	ROTAX
108	ROTAX
109	ROTAX
110	ROTAX
111	ROTAX
112	ROTAX
113	ROTAX
114	ROTAX
115	ROTAX
116	ROTAX
117	ROTAX
118	ROTAX
119	ROTAX
120	ROTAX
121	ROTAX
122	ROTAX
123	ROTAX
124	ROTAX
125	ROTAX
126	ROTAX
127	3W 342i B2
128	3W 342i B2 TS
129	3W 275Xi B2R TS
130	3W 220i B4

131	3W 170Xi B2 TS
132	3W 170Xi B2
133	3W 210Xi B2 TS
134	3W 157Xi B2 TS
135	3W 157Xi B2
136	3W 140i B4
137	RCGF 120cc-T
138	3W 112i B4
139	3W 110i B2
140	3W 110i R2
141	3W 85Xi TS
142	3W 85Xi
143	3W 80Xi TS
144	3W 80Xi
145	RCGF 70cc-T
146	RCGF 60cc
147	3W 70i B2
148	RCGF 60cc-T
149	RCGF 56cc
150	O.S. ENGINES GT60
151	3W 55Xi
152	3W 55i
153	3W 56i B2
154	RCGF 40cc-T
155	RCGF 50cc-T
156	RCGF 40cc-TS
157	RCGF 35cc RE
158	RCGF 32cc
159	O.S. ENGINES GT33
160	O.S. ENGINES GF40
161	RCGF 30cc-T
162	3W 28i CS
163	3W 28i
164	O.S. ENGINES 1.20 AX
165	RCGF 26cc BM
166	O.S. ENGINES 95 AX
167	RCGF 20cc SBM
168	RCGF 20cc RE
169	RCGF 21cc-T
170	O.S. ENGINES GF30
171	O.S. ENGINES GT22
172	O.S. ENGINES FS155-a
173	O.S. ENGINES GT15
174	O.S. ENGINES 75 AX
175	RCGF 15cc BM
176	O.S. ENGINES GGT15

177	O.S. ENGINES FS-120 III-P
178	O.S. ENGINES FT-160
179	RCGF 10cc RE
180	RCGF 10cc
181	O.S. ENGINES 65 AX
182	O.S. ENGINES 55 AX ABL
183	O.S. ENGINES FS-95V
184	O.S. ENGINES 46 AX II ABL
185	O.S. ENGINES GGT10
186	O.S. ENGINES 35AX
187	O.S. ENGINES MAX-46LA-S
188	O.S. ENGINES FSa-72II
189	O.S. ENGINES FS72-a
190	O.S. ENGINES FS-62V
191	O.S. ENGINES MAX-40LA-S
192	O.S. ENGINES FS56-a
193	O.S. ENGINES FSa-56II
194	O.S. ENGINES 25FX
195	O.S. ENGINES MAX-25LA-S
196	O.S. ENGINES MAX-15LA-S
197	O.S. ENGINES 15LA

Table A-II. IC engine specifications data table

index	bp_{max} $[W]$	N_{max} $[rpm]$	N_{min} $[rpm]$	R_{gear}	$bsfc_0$ $[kg/Ws]$	M $[kg]$
1	238612.1	3200	700	1	1.39E-07	235
2	238612.1	3200	700	1	1.39E-07	234
3	238612.1	3200	700	1	1.39E-07	233
4	238612.1	3200	700	1	1.39E-07	232
5	238612.1	3200	700	1	1.39E-07	227
6	238612.1	3200	700	1	1.39E-07	226
7	238612.1	3200	700	1	1.39E-07	226
8	238612.1	3200	700	1	1.39E-07	225
9	212513.9	3100	700	1	1.01E-07	203
10	212513.9	3100	700	1	1.01E-07	200
11	212513.9	3100	700	1	1.01E-07	200
12	208785.6	3000	700	1	9.38E-08	210
13	208785.6	3000	700	1	9.38E-08	210
14	208785.6	3000	700	1	9.38E-08	203
15	208785.6	3000	700	1	9.38E-08	202
16	208785.6	3000	700	1	9.38E-08	201
17	208785.6	3000	700	1	9.38E-08	200
18	208785.6	3000	700	1	9.38E-08	199
19	197600.6	3100	700	1	1.10E-07	200
20	197600.6	3100	700	1	1.10E-07	198

21	193872.3	3000	700	1	1.01E-07	199
22	193872.3	3000	700	1	1.01E-07	197
23	193872.3	3000	700	1	1.01E-07	196
24	193872.3	3000	700	1	9.80E-08	206
25	186415.7	2575	700	1	9.46E-08	187
26	186415.7	2575	700	1	9.46E-08	184
27	186415.7	2575	700	1	9.46E-08	184
28	186415.7	2575	700	1	9.46E-08	184
29	186415.7	2575	700	1	9.46E-08	180
30	175230.7	2800	700	1	9.21E-08	181
31	175230.7	2575	700	1	9.77E-08	182
32	175230.7	2575	700	1	9.77E-08	180
33	175230.7	2575	700	1	9.77E-08	179
34	175230.7	2575	700	1	9.77E-08	179
35	134219.3	2900	700	1	9.55E-08	131
36	134219.3	2700	700	1	8.96E-08	131
37	125271.3	2700	700	1	9.97E-08	129
38	125271.3	2700	700	1	9.97E-08	128
39	108121.1	2700	700	1	8.91E-08	122
40	108121.1	2700	700	1	8.91E-08	122
41	100664.5	2600	700	1	9.29E-08	120
42	93207.84	2800	700	1	8.68E-08	115
43	93207.84	2800	700	1	8.68E-08	115
44	93207.84	2800	700	1	8.68E-08	115
45	93207.84	2800	700	1	8.68E-08	114
46	93207.84	2800	700	1	8.68E-08	113
47	93207.84	2800	700	1	8.68E-08	113
48	93207.84	2600	700	1	9.80E-08	118
49	93207.84	2550	700	1	9.19E-08	117
50	87988.2	2800	700	1	8.16E-08	116
51	87988.2	2800	700	1	8.16E-08	115
52	87988.2	2800	700	1	8.16E-08	114
53	87988.2	2800	700	1	8.16E-08	114
54	87988.2	2800	700	1	8.16E-08	114
55	87988.2	2800	700	1	8.16E-08	113
56	87242.54	2550	700	1	8.49E-08	116
57	87242.54	2550	700	1	8.49E-08	114
58	87242.54	2550	700	1	8.49E-08	113
59	85751.21	2800	700	1	1.07E-07	113
60	85751.21	2800	700	1	1.07E-07	113
61	85751.21	2800	700	1	1.07E-07	111
62	85751.21	2800	700	1	1.07E-07	110
63	85751.21	2800	700	1	1.07E-07	110
64	85751.21	2800	700	1	1.07E-07	110
65	85751.21	2800	700	1	1.07E-07	110
66	85751.21	2800	700	1	1.07E-07	110

67	85751.21	2800	700	1	1.07E-07	109
68	85751.21	2800	700	1	1.07E-07	109
69	118000	3000	1000	1	9.97E-08	86
70	96000	3000	1000	1	7.08E-08	86
71	74000	3000	1000	1	7.36E-08	76
72	62000	3000	1000	1	9.03E-08	82
73	51000	3000	1000	1	9.41E-08	76.5
74	37000	7500	1000	1	1.28E-07	16
75	37000	7500	1000	1	1.13E-07	15
76	18000	7500	1000	1	1.17E-07	7
77	15000	7200	1000	1	1.36E-07	7.2
78	71300	3300	750	1	8.18E-08	72.3
79	78900	3300	750	1	8.18E-08	72.3
80	78900	3300	750	1	8.18E-08	74.8
81	73500	3000	750	1	8.18E-08	72.3
82	86800	3300	750	1	7.64E-08	78.4
83	95600	3300	750	1	8.25E-08	78.4
84	95600	3300	750	1	8.25E-08	81
85	103000	3300	750	1	7.37E-08	100
86	117700	3300	750	1	7.64E-08	100
87	117700	3300	750	1	7.64E-08	104
88	132400	3300	750	1	7.91E-08	108
89	147000	3300	750	1	7.99E-08	108
90	147000	3300	750	1	7.99E-08	108
91	84500	5800	1500	0.4115	6.94E-08	68
92	73500	5800	1500	0.4115	7.92E-08	60.5
93	58000	5500	1500	0.4405	7.92E-08	59.4
94	48000	6500	2500	0.5	1.18E-07	43.3
95	48000	6500	2500	0.45	1.18E-07	43.3
96	48000	6500	2500	0.39	1.18E-07	43.3
97	48000	6500	2500	0.38	1.18E-07	46.8
98	48000	6500	2500	0.33	1.18E-07	46.8
99	48000	6500	2500	0.29	1.18E-07	46.8
100	48000	6500	2500	0.25	1.18E-07	46.8
101	48000	6500	2500	0.38	1.18E-07	50
102	48000	6500	2500	0.33	1.18E-07	50
103	48000	6500	2500	0.29	1.18E-07	50
104	48000	6500	2500	0.25	1.18E-07	50
105	37000	6500	2500	0.5	1.53E-07	45.4
106	37000	6500	2500	0.45	1.53E-07	45.4
107	37000	6500	2500	0.39	1.53E-07	45.4
108	37000	6500	2500	0.38	1.53E-07	48.9
109	37000	6500	2500	0.33	1.53E-07	48.9
110	37000	6500	2500	0.29	1.53E-07	48.9
111	37000	6500	2500	0.25	1.53E-07	48.9
112	37000	6500	2500	0.38	1.53E-07	52.1

113	37000	6500	2500	0.33	1.53E-07	52.1
114	37000	6500	2500	0.29	1.53E-07	52.1
115	37000	6500	2500	0.25	1.53E-07	52.1
116	29500	6500	2500	0.5	1.39E-07	40.6
117	29500	6500	2500	0.45	1.39E-07	40.6
118	29500	6500	2500	0.39	1.39E-07	40.6
119	29500	6500	2500	0.38	1.39E-07	44.1
120	29500	6500	2500	0.33	1.39E-07	44.1
121	29500	6500	2500	0.29	1.39E-07	44.1
122	29500	6500	2500	0.25	1.39E-07	44.1
123	29500	6500	2500	0.38	1.39E-07	47.3
124	29500	6500	2500	0.33	1.39E-07	47.3
125	29500	6500	2500	0.29	1.39E-07	47.3
126	29500	6500	2500	0.25	1.39E-07	47.3
127	23160	6500	700	1	1.23E-07	8.57
128	23160	6500	700	1	1.23E-07	6.5
129	19120	7000	700	1	1.29E-07	7.03
130	16030	7500	700	1	1.37E-07	6.2
131	13970	8500	700	1	1.44E-07	4.11
132	13300	8500	700	1	1.47E-07	3.93
133	13230	7500	700	1	1.47E-07	5
134	12860	8500	700	1	1.49E-07	4.11
135	12500	8500	700	1	1.50E-07	3.93
136	10300	8500	700	1	1.63E-07	4
137	9321	7600	700	1	1.71E-07	2.93
138	8970	7000	700	1	1.74E-07	3.87
139	8680	8500	700	1	1.77E-07	3.05
140	7830	8500	700	1	1.86E-07	3.49
141	6910	8500	700	1	1.99E-07	2.39
142	6760	8500	700	1	2.01E-07	2.4
143	6400	8500	700	1	2.08E-07	2.5
144	6250	8500	700	1	2.10E-07	2.38
145	5518	8600	700	1	2.26E-07	1.81
146	5100	8500	700	1	2.38E-07	1.62
147	4850	8500	700	1	2.45E-07	1.95
148	4700	8600	700	1	2.50E-07	1.86
149	4500	7500	700	1	2.57E-07	1.54
150	4474	8000	700	1	2.58E-07	1.68
151	4010	8500	700	1	2.78E-07	1.79
152	3820	8500	700	1	2.87E-07	1.94
153	3800	8500	700	1	2.88E-07	1.85
154	3580	8600	700	1	3.00E-07	1.54
155	3510	8600	700	1	3.04E-07	1.73
156	3430	8600	700	1	3.09E-07	1.32
157	3057	9000	700	1	3.36E-07	1.15
158	2900	9000	700	1	3.49E-07	1.16

159	2871	9000	700	1	3.52E-07	0.98
160	2796	8600	700	1	3.59E-07	1.38
161	2759	7500	700	1	3.63E-07	1.15
162	2650	8500	700	1	3.74E-07	1.21
163	2500	8500	700	1	3.91E-07	1.21
164	2312	9000	700	1	4.15E-07	0.89
165	2200	9800	700	1	4.32E-07	0.94
166	2133	15000	700	1	4.43E-07	0.75
167	2100	10500	700	1	4.48E-07	0.84
168	2100	10500	700	1	4.48E-07	0.8
169	2088	8500	700	1	4.50E-07	0.92
170	2058	9000	700	1	4.55E-07	1.2
171	1983	9000	700	1	4.69E-07	1
172	1909	10000	700	1	4.84E-07	0.9
173	1767	15000	700	1	5.16E-07	0.9
174	1767	15000	700	1	5.16E-07	0.75
175	1760	15000	700	1	5.17E-07	0.77
176	1730	15000	700	1	5.25E-07	0.79
177	1544	12000	700	1	5.77E-07	1
178	1491	10000	700	1	5.94E-07	1.1
179	1400	12000	700	1	6.27E-07	0.62
180	1400	12000	700	1	6.27E-07	0.57
181	1290	16000	700	1	6.73E-07	0.5
182	1253	16000	700	1	6.90E-07	0.53
183	1253	10000	700	1	6.90E-07	0.65
184	1215	16000	700	1	7.09E-07	0.49
185	1178	10000	700	1	7.28E-07	0.56
186	954	16000	700	1	8.78E-07	0.36
187	910	15000	700	1	9.16E-07	0.26
188	880	12000	700	1	9.44E-07	0.53
189	880	11000	700	1	9.44E-07	0.53
190	805	11000	700	1	1.02E-06	0.49
191	753	15000	700	1	1.09E-06	0.27
192	738	10000	700	1	1.11E-06	0.46
193	738	10000	700	1	1.11E-06	0.39
194	626	18900	700	1	1.29E-06	0.31
195	455	15000	700	1	1.74E-06	0.19
196	313	17000	700	1	2.49E-06	0.13
197	298	17000	700	1	2.61E-06	0.14

Appendix B

Table B-I. Index of each electric motor name

INDEX	MOTOR NAME
1	TURNIGY Park250 - 1680kv
2	TURNIGY Park250 - 2050kv
3	TURNIGY Park250 - 2200kv
4	TURNIGY Park300 - 1380kv
5	TURNIGY Park300 - 1600kv
6	TURNIGY Park450 - 890kv
7	TURNIGY Park450 - 1050kv
8	TURNIGY Park450 - 1200kv
9	TURNIGY Park480 - 850kv
10	TURNIGY Park480 1020kv
11	TURNIGY Park480 - 1320kv
12	TURNIGY D2836/8 - 1100KV
13	TURNIGY D2836/9 - 950KV
14	TURNIGY D2836/11 - 750KV
15	TURNIGY D3530/14 - 1100KV
16	TURNIGY D3536/5 - 1450KV
17	TURNIGY D3536/6 - 1250KV
18	TURNIGY D3536/8 - 1000KV
19	TURNIGY D3536/9 - 910KV
20	TURNIGY D3542/4 - 1450KV
21	TURNIGY D3542/5 - 1250KV
22	TURNIGY D3542/6 - 1000KV
23	TURNIGY D3548/4 - 1100KV
24	TURNIGY D3548/6 - 790KV
25	TURNIGY RotoMax 1.20
26	TURNIGY RotoMax 1.40
27	TURNIGY RotoMax 1.60
28	TURNIGY TrackStar 3.5T 9150KV
29	TURNIGY TrackStar 5.5T 6069KV
30	TURNIGY TrackStar 6.5T 5150KV
31	TURNIGY TrackStar 8.5T 3983KV
32	TURNIGY TrackStar 10.5T 3250KV
33	TURNIGY TrackStar 13.5T 2590KV
34	TURNIGY TrackStar 17.5T 1870KV
35	TURNIGY TrackStar SCT 4T 5120KV
36	TURNIGY TrackStar SCT 4.5T 4550KV
37	TURNIGY TrackStar SCT 5T 4150KV
38	TURNIGY TrackStar SCT 5.5T 3750KV
39	TURNIGY Multistar V-Spec 1104-3600KV CW
40	TURNIGY Multistar V-Spec 1304-3100KV CW

41	TURNIGY MultiStar V-Spec 1808-2400KV CW
42	TURNIGY Multistar 2312-460Kv HV
43	TURNIGY Multistar 2810-750kv CCW
44	TURNIGY Multistar 3508-380KV
45	TURNIGY Multistar 3508-580KV
46	TURNIGY Multistar 3508-700KV
47	TURNIGY Multistar 3510-350kv
48	TURNIGY Multistar 3525-650Kv
49	TURNIGY Multistar 3525-850Kv
50	TURNIGY Multistar 4010-375KV
51	TURNIGY Multistar 4010-485KV
52	TURNIGY Multistar 4010-580KV
53	TURNIGY Multistar 4014-320KV
54	TURNIGY Multistar 4014-400KV
55	TURNIGY Multistar 4108-380KV
56	TURNIGY Multistar 4108-480KV
57	TURNIGY Multistar 4108-600KV
58	TURNIGY Multistar 4112-320KV
59	TURNIGY Multistar 4112-400KV
60	TURNIGY Multistar 4112-485KV
61	TURNIGY Multistar 4114-320KV
62	TURNIGY Multistar 4220-650Kv
63	TURNIGY Multistar 4220-880Kv
64	TURNIGY Multistar 4225-390Kv
65	TURNIGY Multistar 4225-610Kv
66	TURNIGY Multistar 4230-630Kv
67	TURNIGY Multistar 4822-390Kv
68	TURNIGY Multistar 4822-490Kv
69	TURNIGY Multistar 4822-570Kv
70	TURNIGY Multistar 4822-690Kv
71	TURNIGY Multistar 4230-400Kv
72	TURNIGY Multistar 4830-420Kv
73	TURNIGY Multistar 4830-480Kv
74	TURNIGY Multistar 5130-350Kv
75	TURNIGY Multistar 5130-570Kv
76	TURNIGY Multistar 9225-90KV
77	TURNIGY Multistar 9225-160KV
78	TURNIGY Multistar 9235-100KV
79	TURNIGY SK3 - 2118-2250KV
80	TURNIGY SK3 - 2118-2750KV
81	TURNIGY SK3 - 2118-3100KV
82	TURNIGY SK3 - 2122-1570KV
83	TURNIGY SK3 - 2122-2100KV
84	TURNIGY SK3 - 2822-1090kv
85	TURNIGY SK3 - 2822-1275kv
86	TURNIGY SK3 - 2822-1740kv

87	TURNIGY SK3 - 2826-980kv
88	TURNIGY SK3 - 2826-1130kv
89	TURNIGY SK3 - 2826-1240kv
90	TURNIGY SK3 - 2830-920kv
91	TURNIGY SK3 - 2830-1020kv
92	TURNIGY SK3 - 2830-1130kv
93	TURNIGY SK3 - 2836-1040kv
94	TURNIGY SK3 - 2836-1500kV
95	TURNIGY SK3 - 2836-2500kv
96	TURNIGY SK3 - 3516-3300kv
97	TURNIGY SK3 - 3530-1150kv
98	TURNIGY SK3 - 3530-1340kv
99	TURNIGY SK3 - 3530-1460kv
100	TURNIGY SK3 - 3536-1050kv
101	TURNIGY SK3 - 3536-1200kv
102	TURNIGY SK3 - 3536-1400kv
103	TURNIGY SK3 - 3542-800kv
104	TURNIGY SK3 - 3542-1000kv
105	TURNIGY SK3 - 3542-1185kv
106	TURNIGY SK3 - 3542-1250kv
107	TURNIGY SK3 - 3548-700kv
108	TURNIGY SK3 - 3548-840kv
109	TURNIGY SK3 - 3548- 1050kv
110	TURNIGY SK3 - 3659-1600KV
111	TURNIGY SK3 - 3659-1900kv
112	TURNIGY SK3 - 3850 - 3.5 960kv
113	TURNIGY SK3 - 3850 - 3.5 1400kv
114	TURNIGY SK3 - 3858 - 4.6 840kv
115	TURNIGY SK3 - 3858 - 4.6 1120kv
116	TURNIGY SK3 - 3968-1500KV
117	TURNIGY SK3 - 3994-850kv
118	TURNIGY SK3 - 4240-530kv
119	TURNIGY SK3 - 4240-620KV
120	TURNIGY SK3 - 4240-740KV
121	TURNIGY SK3 - 4250-350kv
122	TURNIGY SK3 - 4250-410KV
123	TURNIGY SK3 - 4250-500KV
124	TURNIGY SK3 - 4956-520KV
125	TURNIGY SK3 - 5045-450KV
126	TURNIGY SK3 - 5045-500KV
127	TURNIGY SK3 - 5045-660KV
128	TURNIGY SK3 - 5055-280kv
129	TURNIGY SK3 - 5055-320kv
130	TURNIGY SK3 - 5055-430kv
131	TURNIGY SK3 - 5065-236kv
132	TURNIGY SK3 - 5065-275kv

133	TURNIGY SK3 - 5065-320kv
134	TURNIGY SK3 - 6354-215kv
135	TURNIGY SK3 - 6354-260kv
136	TURNIGY SK3 - 6364-190kv
137	TURNIGY SK3 - 6364-213kv
138	TURNIGY SK3 - 6364-245kv
139	TURNIGY SK3 - 6374-149KV
140	TURNIGY SK3 - 6374-168KV
141	TURNIGY SK3 - 6374-192kv
142	TURNIGY SK8 - 5045-150KV
143	TURNIGY SK8 5045-195KV
144	TURNIGY SK8 - 5045-240KV
145	TURNIGY SK8 - 6354-140KV
146	TURNIGY SK8 - 6354-200KV
147	TURNIGY SK8 - 6354-260KV
148	TURNIGY SK8 - 6364-110KV
149	TURNIGY SK8 - 6364-190KV
150	TURNIGY SK8 - 6364-245KV
151	TURNIGY SK8 - 6374-130KV
152	TURNIGY SK8 - 6374-149KV
153	TURNIGY SK8 - 6374-192KV
154	PROPDRIVE v2 2628 1000KV (Short Shaft Version)
155	PROPDRIVE v2 2826 1000KV
156	PROPDRIVE v2 2826 1000KV (Short Shaft Version)
157	PROPDRIVE V2 2826 1100kv
158	PROPDRIVE v2 2826 1100KV (Short Shaft Version)
159	PROPDRIVE v2 2826 1200KV
160	PROPDRIVE v2 2826 1200KV (Short Shaft Version)
161	PROPDRIVE v2 2826 1350KV
162	PROPDRIVE v2 2830 800KV
163	PROPDRIVE v2 2830 800KV (Short Shaft Version)
164	PROPDRIVE v2 2830 1000KV
165	PROPDRIVE v2 2830 1100KV
166	PROPDRIVE v2 2830 1200KV
167	PROPDRIVE v2 2836 1200KV
168	PROPDRIVE v2 2836 1400KV
169	PROPDRIVE v2 2836 1800KV
170	PROPDRIVE v2 2836 2200KV
171	PROPDRIVE v2 2836 2300KV (Short Shaft Version)
172	PROPDRIVE v2 2836 2700KV
173	PROPDRIVE v2 3530 1400KV
174	PROPDRIVE v2 3536 1400KV
175	PROPDRIVE v2 3536 1800KV

176	PROPDRIVE v2 3542 1000KV
177	PROPDRIVE v2 3542 1250KV
178	PROPDRIVE v2 3548 900KV
179	PROPDRIVE v2 3548 1100KV
180	PROPDRIVE v2 4238 750KV
181	PROPDRIVE v2 4248 650KV
182	PROPDRIVE v2 4258 500KV
183	PROPDRIVE v2 5050 580KV
184	PROPDRIVE v2 5060 380KV
185	PROPDRIVE v2 5060 270KV
186	PROPDRIVE NTM 13-12 2400KV / 40W
187	PROPDRIVE NTM 13-12 3000KV / 28W
188	PROPDRIVE NTM 28-26 1000KV / 235W (short shaft version)
189	PROPDRIVE NTM 28-26 1100kv / 252w
190	PROPDRIVE NTM 28-26 1100kv / 252w (short shaft version)
191	PROPDRIVE NTM 28-26A 1200kv / 286w
192	PROPDRIVE NTM 28-26A 1200kv / 286w (short shaft version)
193	PROPDRIVE NTM 28-30S 800KV / 300W (short shaft version)
194	PROPDRIVE NTM 28-36 750KV / 265W
195	PROPDRIVE NTM 28-36 3000KV / 755W
196	PROPDRIVE NTM 35-30 1100kv / 380w
197	PROPDRIVE NTM 35-36A 1400Kv / 550W
198	PROPDRIVE NTM EF-1 3842-1300KV / 930W (v2)
199	KEDA 23-28S 1480KV
200	KEDA 25-29 1250Kv
201	KEDA 27-28 1070Kv
202	KEDA 27-28 1130KV
203	KEDA 28-30 920KV
204	KEDA 33-28L 1000Kv
205	KEDA 36-30L 1000Kv
206	KEDA 36-30M 1100Kv
207	KEDA 36-36 1000Kv
208	KEDA 36-42M 930Kv
209	KEDA 36-48 1030Kv
210	KEDA 43-62 1650Kv
211	KEDA 49-55 750Kv
212	KEDA 49-64 330Kv
213	KEDA 56-63 195KV
214	KEDA 63-64 190KV
215	SCORPION S-1805-2250KV
216	SCORPION S-1804-1650KV
217	SCORPION SII-2215-1400KV (V2)
218	SCORPION SII-2212-1400kv (V2)

219	SCORPION SII-2215-1810KV (V2)
220	SCORPION SII-2215-1127KV (V2)
221	SCORPION SII-2215-900KV (V2)
222	SCORPION SII-2212-1850KV (V2)
223	SCORPION SII-2212-1070KV (V2)
224	SCORPION SII-2212-960KV (V2)
225	SCORPION SII-2212-885KV (V2)
226	SCORPION SII-2208-1280KV (V2)
227	SCORPION SII-2208-1100KV (V2)
228	SCORPION SII-2205-1490KV (V2)
229	SCORPION SII-2205-1585KV (V2)
230	SCORPION SII-2205-1900KV (V2)
231	SCORPION S-2503-1960KV (F3P Special)
232	SCORPION S-2503-1610KV (F3P Special)
233	SCORPION SII-3032-880KV (V2)
234	SCORPION SII-3032-690KV (V2)
235	SCORPION SII-3026-1190KV (V2)
236	SCORPION SII-3026-890KV (V2)
237	SCORPION SII-3026-710KV (V2)
238	SCORPION SII-3020-1110KV (V2)
239	SCORPION SII-3020-890KV (V2)
240	SCORPION SII-3020-780KV (V2)
241	SCORPION SII-3014-1220KV (V2)
242	SCORPION SII-3014-1040KV (V2)
243	SCORPION SII-3014-830KV (V2)
244	SCORPION SII-3008-1220KV (V2)
245	SCORPION SII-3008-1090KV (V2)
246	SCORPION SII-4035-450KV
247	SCORPION SII-4035-380KV
248	SCORPION SII-4035-330KV
249	SCORPION SII-4035-250KV
250	SCORPION SII-4020-630KV
251	SCORPION SII-4020-540KV
252	SCORPION SII-4025-520KV
253	SCORPION SII-4025-440KV
254	SCORPION SII-4025-330KV
255	SCORPION SII-4020-420KV
256	SCORPION S-5028-220KV (F3A Limited Series)
257	SCORPION SII-5535-190KV
258	SCORPION SII-5535-160KV
259	SCORPION SII-5525-195KV
260	SCORPION SII-5525-210KV
261	SCORPION SII-5525-170KV
262	SCORPION SII-6530-150KV
263	SCORPION SII-6530-180KV
264	AXI 4120/14 GOLD LINE V2

265	AXI 4120/18 GOLD LINE V2
266	AXI 4120/20 GOLD LINE V2
267	AXI 4130/16 GOLD LINE V2
268	AXI 4130/20 GOLD LINE V2
269	AXI 5320/18 GOLD LINE V2
270	AXI 5320/28 GOLD LINE V2
271	AXI 5320/34 GOLD LINE V2
272	AXI 5325/18 GOLD LINE V2
273	AXI 5325/20 GOLD LINE V2
274	AXI 5325/24 GOLD LINE V2
275	AXI 5325/16 GOLD LINE V2
276	AXI 5320/18 3D Extreme KV370 V2
277	AXI 5330/18 GOLD LINE V2
278	AXI 5330/24 GOLD LINE V2
279	AXI 5330/F3A GOLD LINE V2
280	AXI 5325/16 3D Extreme KV350 V2
281	AXI 8112/10 V2
282	AXI 8112/14 V2
283	AXI 8120/8 V2
284	AXI 8120/10 V2
285	TURNIGY AX-2804C 1400KV
286	TURNIGY DT38 620kv
287	TURNIGY 480S BL 1500kv
288	TURNIGY 480S BL 3200kv
289	TURNIGY 1015 11500kv
290	TURNIGY 1220 10300kv
291	TURNIGY 3020 1200kv
292	TURNIGY 3020 1800kv
293	TURNIGY 3648 1450kv
294	TURNIGY XK4074-B-1400KV

Table B-II. Motor specifications data table

index	Kv $[rpm/V]$	I_{max} $[A]$	U_{max} $[V]$	R $[\Omega]$	I_0 $[A]$	M $[kg]$
1	1680	8	7	0.32	0.2	0.016
2	2050	8	7	0.23	0.2	0.016
3	2200	7	7	0.25	0.45	0.014
4	1380	7	11	0.33	0.4	0.024
5	1600	9	11	0.18	0.5	0.025
6	890	14	11	0.2	0.7	0.067
7	1050	18	11	0.09	0.9	0.066
8	1200	18	11	0.06	1.1	0.066

9	850	28	11	0.09	0.9	0.08
10	1020	22	11	0.06	1.1	0.081
11	1320	28	11	0.04	0.9	0.08
12	1100	18	15	0.107	1	0.07
13	950	23	15	0.07	1	0.07
14	750	14	11	0.16	0.8	0.067
15	1100	22	15	0.077	1.6	0.073
16	1450	45	15	0.023	3.5	0.13
17	1250	34	15	0.034	3	0.102
18	1000	30	15	0.052	1.7	0.102
19	910	25	15	0.063	1.5	0.102
20	1450	48	15	0.019	4	0.13
21	1250	46	15	0.021	3	0.13
22	1000	38	15	0.031	2.4	0.13
23	1100	50	19	0.023	3.1	0.159
24	790	40	19	0.04	1.8	0.159
25	280	65	30	0.027	1.55	0.622
26	228	75	37	0.029	1.25	0.715
27	231	80	37	0.028	1.47	0.849
28	9150	83	7.4	0.0021	13	0.158
29	6069	50	7.4	0.0065	7	0.156
30	5150	43	7.4	0.0085	6.6	0.16
31	3983	33	11.1	0.0141	5.8	0.158
32	3250	26	11.1	0.0213	4	0.158
33	2590	21	14.8	0.0363	3	0.156
34	1870	17	14.8	0.0513	2	0.156
35	5120	134	7.4	0.0049	4.7	0.236
36	4550	128	7.4	0.0057	4	0.236
37	4150	120	11.1	0.0061	3.6	0.236
38	3750	112	11.1	0.0069	2.9	0.236
39	3600	3.5	8	0.64	0.5	0.008
40	3100	8	8	0.46	0.3	0.01
41	2400	15.8	11.08	0.078	0.8	0.029
42	460	8	22.5	0.424	0.3	0.063
43	750	21.5	14.88	0.108	0.48	0.056
44	380	14	22.86	0.215	0.3	0.102
45	580	26	13.08	0.106	0.4	0.102
46	700	28	12.86	0.083	0.5	0.102
47	350	15	25	0.16	0.3	0.121
48	650	17	15	0.178	0.5	0.058
49	850	23	10.87	0.101	0.6	0.058
50	375	20	22.5	0.134	0.6	0.128
51	485	26	19.23	0.085	0.8	0.128
52	580	32	17.19	0.062	1.1	0.128
53	320	26	27.69	0.102	0.7	0.163
54	400	26	28.85	0.075	0.9	0.163

55	380	17	21.18	0.225	0.5	0.111
56	480	22	17.27	0.128	0.6	0.111
57	600	26	15.38	0.098	0.9	0.111
58	320	20	33	0.172	0.5	0.147
59	400	24	28.33	0.172	0.8	0.147
60	485	28	25	0.09	1.1	0.147
61	320	30	22	0.126	0.9	0.148
62	650	17	15	0.12	0.7	0.065
63	880	22	11	0.066	0.8	0.065
64	390	15	22	0.24	0.2	0.086
65	610	22	15	0.091	0.3	0.086
66	630	37	14.86	0.029	0.8	0.138
67	390	15	20	0.17	0.25	0.098
68	490	17	22	0.104	0.45	0.098
69	570	21	14.76	0.092	0.65	0.098
70	690	22	14.55	0.052	0.85	0.095
71	400	25	22	0.079	0.6	0.138
72	420	29	22.41	0.08	1.1	0.154
73	480	31	21.94	0.062	1.2	0.154
74	350	16	25	0.099	0.5	0.152
75	570	27	14.81	0.032	0.8	0.152
76	90	36	45	0.186	0.5	0.401
77	160	48	35	0.065	1.1	0.339
78	100	57	45	0.055	1	0.674
79	2250	4	11	0.29	0.752	0.017
80	2750	5	11	0.22	0.86	0.017
81	3100	5	7	0.18	1.029	0.017
82	1570	6	11	0.14	1.175	0.025
83	2100	7	11	0.12	1.248	0.024
84	1090	7	11	0.235	0.684	0.031
85	1275	8	11.5	0.291	0.528	0.03
86	1740	10	11	0.125	1.005	0.032
87	980	10	11	0.174	0.748	0.044
88	1130	13	11	0.12	0.913	0.044
89	1240	16	11	0.095	1.013	0.045
90	920	16	11	0.09	1.064	0.057
91	1020	18	9.39	0.112	0.824	0.055
92	1130	20	11	0.095	0.906	0.058
93	1040	28	11	0.075	0.944	0.08
94	1500	31	11	0.026	2.314	0.08
95	2500	35	11	0.02	2.752	0.08
96	3300	55	15	0.019	2.294	0.111
97	1150	24	15	0.069	1.099	0.076
98	1340	33	11.94	0.039	1.56	0.071
99	1460	33	11	0.045	1.372	0.075
100	1050	34	15	0.039	1.536	0.11

101	1200	38	15	0.028	1.954	0.111
102	1400	40	15	0.021	2.463	0.11
103	800	42	19	0.037	1.448	0.142
104	1000	45	15	0.031	1.638	0.141
105	1185	49	15	0.024	1.973	0.141
106	1250	54	15	0.022	2.03	0.141
107	700	45	19	0.035	1.469	0.177
108	840	50	15	0.025	1.883	0.174
109	1050	50	15	0.016	2.807	0.176
110	1600	65	26	0.015	2.605	0.252
111	1900	80	22.13	0.011	3.096	0.249
112	960	35	15	0.045	1.332	0.142
113	1400	47	15	0.016	2.896	0.142
114	840	45	19	0.031	1.638	0.18
115	1120	58	15	0.021	2.042	0.18
116	1500	110	30	0.012	2.439	0.363
117	850	90	43	0.012	2.699	0.554
118	530	46	19	0.023	2.116	0.194
119	620	48	19	0.017	2.714	0.194
120	740	50	19	0.013	3.38	0.195
121	350	53	19	0.033	1.426	0.266
122	410	55	19	0.026	1.732	0.26
123	500	57	19	0.018	2.364	0.269
124	520	70	45	0.0214	1.826	0.394
125	450	58	26	0.025	1.747	0.275
126	500	60	26	0.022	1.925	0.28
127	660	60	19	0.014	2.885	0.28
128	280	60	37	0.031	1.417	0.369
129	320	65	37	0.027	1.539	0.376
130	430	70	30	0.019	2.031	0.378
131	236	60	37	0.019	2.195	0.53
132	275	65	37	0.017	2.329	0.531
133	320	70	37	0.014	2.669	0.531
134	215	65	37	0.032	1.322	0.485
135	260	70	37	0.023	1.712	0.489
136	190	65	37	0.028	1.49	0.697
137	213	65	37	0.023	1.777	0.706
138	245	70	37	0.018	2.131	0.718
139	149	70	44	0.021	1.857	0.84
140	168	70	44	0.019	2.031	0.84
141	192	80	44	0.016	2.214	0.858
142	150	15	45	0.253	0.436	0.336
143	195	20	45	0.128	0.694	0.342
144	240	30	45	0.087	0.798	0.345
145	140	42	45	0.098	0.606	0.63
146	200	55	45	0.046	1.04	0.63

147	260	70	45	0.027	1.483	0.63
148	110	40	45	0.107	0.574	0.785
149	190	60	45	0.038	1.181	0.78
150	245	80	45	0.023	1.6	0.78
151	130	65	45	0.049	0.903	0.94
152	149	80	45	0.043	0.914	0.937
153	192	100	45	0.024	1.376	0.94
154	1000	14	17	0.166	0.658	0.058
155	1000	15	17	0.14	0.74	0.059
156	1000	20	17	0.166	0.55	0.06
157	1100	20	17	0.14	0.64	0.059
158	1100	20	17	0.14	0.64	0.06
159	1200	20	17	0.166	0.55	0.059
160	1200	20	17	0.114	0.769	0.06
161	1350	20	17	0.098	0.881	0.058
162	800	20	17	0.161	0.565	0.065
163	800	20	17	0.161	0.565	0.069
164	1000	25	17	0.114	0.687	0.069
165	1100	26	17	0.097	0.779	0.069
166	1200	28	17	0.079	0.901	0.069
167	1200	48	14.8	0.023	2.071	0.082
168	1400	45	14.8	0.053	1.014	0.082
169	1800	30	17	0.03	2.07	0.082
170	2200	50	14.8	0.023	2.029	0.083
171	2300	45	17	0.053	1.014	0.079
172	2700	50	14.8	0.016	2.807	0.082
173	1400	37	17	0.026	2.116	0.09
174	1400	45	17	0.016	2.96	0.121
175	1800	70	17	0.01	3.606	0.126
176	1000	47	17	0.025	1.942	0.155
177	1250	56	17	0.017	2.511	0.156
178	900	55	17	0.023	1.933	0.178
179	1100	70	14.8	0.014	2.669	0.185
180	750	56	17	0.029	1.557	0.156
181	650	70	21	0.023	1.712	0.231
182	500	60	25.9	0.028	1.552	0.3
183	580	90	22.2	0.014	2.351	0.331
184	380	90	36	0.022	1.569	0.438
185	270	90	29.6	0.036	1.01	0.438
186	2400	4	11	0.4837	0.476	0.005
187	3000	3.9	8	0.4969	0.47	0.0056
188	1000	15	15	0.1185	0.859	0.054
189	1100	20	15	0.0873	0.977	0.057
190	1100	20	15	0.0873	0.977	0.054
191	1200	17	15	0.1038	0.908	0.0576
192	1200	17	15	0.1038	0.908	0.0536

193	800	20	23	0.0873	0.977	0.065
194	750	18	15	0.0976	0.932	0.087
195	3000	55	15	0.0298	1.535	0.087
196	1100	32	15	0.0529	1.205	0.088
197	1400	55	15	0.0298	1.535	0.117
198	1300	65	15	0.0249	1.654	0.155
199	1480	11	11	0.1649	0.748	0.032
200	1250	14	11	0.1276	0.833	0.046
201	1070	9.5	11	0.1927	0.7	0.048
202	1130	7.7	11	0.241	0.637	0.043
203	920	6.8	11	0.275	0.603	0.057
204	1000	9	11	0.2041	0.683	0.057
205	1000	20.5	15	0.085	0.988	0.078
206	1100	36.5	15	0.046	1.278	0.153
207	1000	21.4	12	0.0812	1.007	0.115
208	930	35	15	0.0481	1.254	0.152
209	1030	28	15	0.061	1.135	0.1895
210	1650	65	22	0.0249	1.654	0.29
211	750	37	15	0.0454	1.286	0.291
212	330	50	22	0.0329	1.471	0.39
213	195	80	22	0.02	1.815	0.5
214	190	90	37	0.0176	1.914	0.67
215	2250	7	6.4	0.4	0.25	0.016
216	1650	5	6.4	0.4	0.25	0.012
217	1400	35	14.8	0.095	0.95	0.069
218	1400	25	14.8	0.091	0.73	0.058
219	1810	25	11.1	0.031	1.35	0.069
220	1127	20	11.1	0.078	0.73	0.069
221	900	16	14.8	0.142	0.52	0.069
222	1850	22	11.1	0.032	1.31	0.058
223	1070	15	11.1	0.091	0.59	0.058
224	960	13	14.8	0.139	0.51	0.058
225	885	13	14.8	0.151	0.41	0.058
226	1280	14	11.1	0.15	0.47	0.045
227	1100	12	11.1	0.17	0.41	0.045
228	1490	10	11.1	0.188	0.42	0.035
229	1585	10	11.1	0.182	0.47	0.035
230	1900	12	11.1	0.128	0.58	0.035
231	1960	11	7.27	0.135	0.44	0.02
232	1610	10	7.2	0.18	0.35	0.02
233	880	70	17.5	0.012	3.12	0.275
234	690	60	17.5	0.022	2.71	0.275
235	1190	80	17.5	0.008	3.26	0.205
236	890	70	14.8	0.014	1.9	0.205
237	710	60	18.5	0.022	1.56	0.205
238	1110	60	14.8	0.016	2.08	0.166

239	890	45	18.5	0.02	1.42	0.166
240	780	40	18.5	0.03	1.21	0.166
241	1220	46	14.8	0.018	1.64	0.129
242	1040	40	14.8	0.0263	1.35	0.129
243	830	30	14.8	0.042	1.06	0.129
244	1220	32	14.8	0.042	0.97	0.095
245	1090	26	14.8	0.058	0.79	0.095
246	450	80	29.6	0.026	1.71	0.435
247	380	70	29.6	0.025	1.52	0.435
248	330	65	37	0.031	1.41	0.435
249	250	65	44.4	0.037	0.69	0.45
250	630	95	25.2	0.015	1.54	0.288
251	540	85	25.2	0.02	1.22	0.288
252	520	100	25.2	0.016	1.4	0.353
253	440	85	25.9	0.025	1.1	0.353
254	330	75	29.6	0.037	0.74	0.353
255	420	70	22.2	0.032	0.91	0.288
256	220	70	34.8	0.032	0.98	0.576
257	190	95	44.4	0.022	1.24	0.906
258	160	90	44.4	0.027	1.11	0.906
259	195	80	37	0.034	0.88	0.708
260	210	90	36.9	0.026	1.11	0.708
261	170	70	37	0.042	0.78	0.708
262	150	95	44.4	0.032	1.15	1.043
263	180	110	44.5	0.022	1.26	1.043
264	660	57	17.81	0.041	1.9	0.315
265	515	59	25.42	0.07	1.3	0.315
266	465	53	21.89	0.082	1.4	0.315
267	385	61	29.18	0.063	1.2	0.41
268	305	56	29.46	0.099	1.1	0.41
269	370	78	23.72	0.023	1.3	0.515
270	249	52	30.77	0.057	1.3	0.515
271	206	47	39.36	0.084	1.1	0.515
272	308	81	30.12	0.032	1.6	0.595
273	280	79	30.76	0.037	1.9	0.595
274	232	76	37.5	0.045	1.6	0.595
275	350	86	30.81	0.026	2	0.595
276	370	79	24.05	0.023	1.3	0.53
277	259	76	37.76	0.032	1.9	0.672
278	197	59	37.63	0.057	1.4	0.672
279	235	73	38.08	0.045	1.7	0.672
280	350	86	31.4	0.026	2	0.64
281	215	85	32.94	0.033	1.4	0.53
282	165	75	40	0.071	1.4	0.53
283	190	95	42.11	0.035	1.6	0.675
284	140	95	44.21	0.047	1.2	0.675

285	1400	10	8	0.1	0.5	0.03
286	620	110	18.5	0.032	1.87	0.365
287	1500	60	14.8	0.0493	0.9	0.109
288	3200	60	11.1	0.0223	2.8	0.109
289	11500	4	3.7	0.51	0.4	0.0051
290	10300	4.3	3.7	0.342	0.4	0.0084
291	1200	8	11.1	0.31	0.3	0.025
292	1800	12	11.1	0.145	0.6	0.025
293	1450	50	32	0.01	4.6	0.181
294	1400	80	22.2	0.0147	4.2	0.385